Chapter 5

Generation of Long Bunches in the LHC

Whereas the benefits of different kinds of long and flat bunches have been discussed with respect to the strong incoherent beam-beam limit, this chapter is devoted to the creation of these bunches by means of longitudinal RF manipulations as introduced in Chapter 3.

The generation of the beam for the nominal LHC scheme and especially its bunch pattern defines the initial conditions for the long bunch creation. It is therefore described in the first part of this chapter. Secondly, schemes to combine several, nearly nominal LHC bunches to long and flat bunches are examined. It is shown that the straightforward approach to confine the long bunches between barrier buckets has inherent disadvantages.

An RF manipulation scheme based on well-proven RF gymnastics, namely batch compression and bunch pair merging, is proposed and worked out in detail in the last part of this chapter. The discussion of high intensity effects will be addressed in a separate chapter.

5.1 Generation of the nominal and ultimate LHC beam

The parameters of the proton beam and its final parameters during injection into the LHC at an energy of 450 GeV strongly depend on the parameters of the upstream accelerators in the injector chain. Before entering the LHC, the protons have to pass through a linear accelerator and three synchrotrons of different size and properties. Albeit extensive upgrades have been carried out [145, 146, 147, 148], these accelerators have intrinsic limitations like direct space charge in the low energy regime, which cannot be circumvented. Basic parameters like injection and ejection energy or the circumference require unreasonable effort or are even impossible to be implemented at existing accelerators. Furthermore, the beam structure delivered by an accelerator depends on the parameters of the various subsystems with which it is equipped, e.g. the frequency of the RF system that defines the possible bunch spacings which can be accelerated.

A brief overview on the different accelerators in the LHC injector chain is given in the subsequent sections. Their fundamental limitations will also be introduced to sketch their basic capabilities of delivering modified beam parameters so that the bunches at the SPS ejection could be used as an starting point for the generation of long and flat bunches in the LHC.

5.1.1 Proton injectors for the LHC

Before injection into one of the two LHC rings, the particles coming from a linear accelerator (Linac2) are accelerated in three circular accelerators, namely the Proton Synchrotron Booster (PSB), the Proton Synchrotron (PS) and the Super Proton Synchrotron (SPS). The proton injector chain is sketched in Fig. 5.1. A non-exhaustive list of the relevant parameters of the

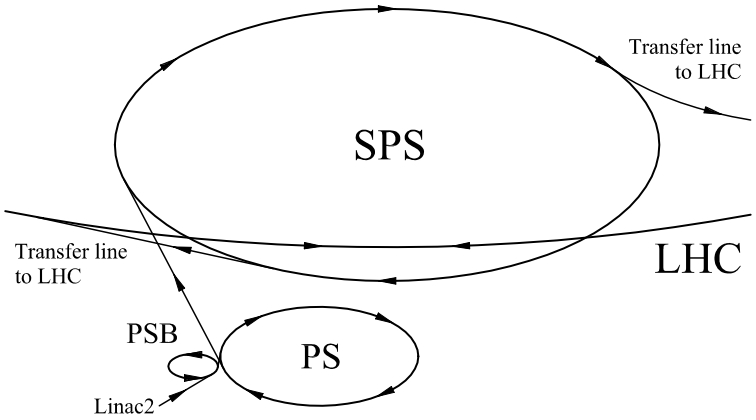

Fig. 5.1: Sketch of the proton injector chain of the LHC: the protons are pre-accelerated in Linac2 up to a kinetic energy of 50 MeV. The PSB boosts their kinetic energy to 1.4 GeV for injection into the PS. After extensive RF manipulations and acceleration to a total energy of 26 GeV, they are transferred to the SPS which finally accelerates the beam to the LHC injection energy of 450 GeV. Note that PSB and PS are sketched four times too large compared to SPS and LHC. The PSB is made up of four rings which are not shown in the sketch. Note that the LHC consists of two storage rings for the counter-rotating proton beams.

circular accelerators relevant for proton injection into the LHC is compiled in Tab. 5.1.

Linear Accelerator (Linac2)

The linear accelerator Linac2 mainly consists of three cavity sections with Alvarez structures working at 202.5 MHz. It accelerates the beam from a kinetic energy of 750 keV to 50 MeV [149]. Linac2 is fed by radio frequency quadrupole (RFQ), a special cavity type which can perform bunching, acceleration and transverse focusing of low energy beams simultaneously. The maximum output current has been optimized to 190 mA to fulfill the intensity requirements of the LHC beam and to deliver at least 180 mA to the PSB.

Proton Synchrotron Booster (PSB)

The PSB is a synchrotron which actually consists of four identical rings stacked on top of each other [150, 151]. It was originally installed to overcome the space charge limitation imposed by direct injection from the linac to the PS. Since then its ejection energy has been upgraded twice from to 800 MeV via 1 GeV to finally 1.4 GeV, in order to push the space charge limitation during transfer from the PSB to the PS. The second upgrade to 1.4 GeV was implemented especially for the production of the ultimate beam for the LHC which would have an excessive space charge induced betatron tune shift ΔQ at 1 GeV. With its four rings, the PSB accelerates four times the intensity per ring in one cycle. In the case of the nominal and ultimate LHC beams, the PSB provides one bunch per ring using RF operating on the first harmonic of the revolution frequency [152, 153, 154]. To optimize the ratio of peak to average intensity,

Machine:		PSB (four rings)	PS	SPS
Circumference, $2\pi R$	[m]	157.1	628.3	6911.5
(normalized to PS)		1/4	1	11
Injection energy, $E_{\rm inj}$	[GeV]	$0.05 + E_0$	$1.4 + E_0$	26.0
Ejection energy, $E_{\rm ej}$	[GeV]	$1.4 + E_0$	26.0	450
Filling scheme		1 bunch	2 PSB batches	2/3/4 PS bats.
Number of bunches, n_b		1	$4 + 2 \longrightarrow 72$	144/216/288
Bunch spacing, t_b	[ns]		$327 \longrightarrow 25$	25
RF harmonics, h		1+2	$7 \rightarrow 21 \rightarrow 84$	4620
Fund. RF frequencies, $f_{\rm RF}$	[MHz]	0.6–1.7	3.1/9.3–10/40	200.4
Long. emittance at inj.	[eVs]			0.35
Long. emittance at ej.	[eVs]	1	0.35	0.70
Nominal scheme:				
Beam int. at inj., $N_{\rm tot}$		$1.87 \cdot 10^{12}$ /rg. $I_L = 180\,{\rm mA}$	$9.66 \cdot 10^{12}$	$1.66/2.48/3.31 \cdot 10^{13}$
Beam int. at ejection, $N_{\rm tot}$		$1.63 \cdot 10^{12}$ /rg.	$8.28 \cdot 10^{12}$	$1.66/2.48/3.31 \cdot 10^{13}$
Ultimate scheme:				
Beam int. at inj., $N_{\rm tot}$		$2.76 \cdot 10^{12}$ /rg. $I_L = 180\,{\rm mA}$	$1.43 \cdot 10^{12}$	$2.45/3.67/4.90 \cdot 10^{13}$
Beam int. at ejection, $N_{\rm tot}$		$2.41 \cdot 10^{12}$ /rg.	$1.22 \cdot 10^{13}$	$2.45/3.67/4.90 \cdot 10^{13}$

Tab. 5.1: Relevant parameters of the circular accelerators in the LHC injector chain.

a second harmonic RF system is used to flatten the bunches and thus to decrease the peak intensity [155, 156]. For the LHC beam each PSB bunch has an intensity of some $1.6 \cdot 10^{12}$ protons, slightly more than twelve times the intensity of an LHC bunch because of losses during transfer and capture in the PS. The transfer between the four rings of the PSB and the PS is sketched in Fig. 5.2. During the first transfer, bunches from all four booster rings are stringed

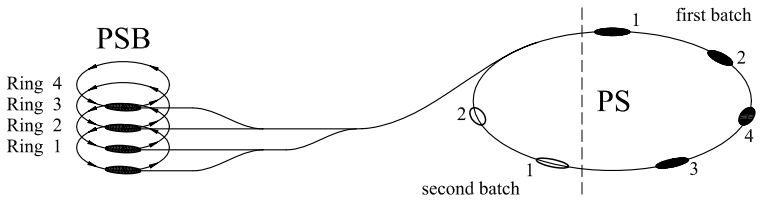

Fig. 5.2: Double batch transfer scheme from PSB to PS. For the injection into the PS all four booster rings are used, each delivering one bunch. The second injection is performed with two booster bunches only.

up in the PS. One PSB machine cycle later (corresponding to 1.2 s), half of the rings are used to deliver two more bunches. Finally, six of seven PS buckets are populated. The empty bucket is needed for the transfer from the PS to the SPS to preserve a gap for the beam ejection.

Proton Synchrotron (PS)

The PS is a combined function alternating gradient synchrotron which accelerates the proton beam to a total energy of up to 26 GeV [157, 158, 159]. However, acceleration is not the only function of the PS in the LHC injector chain [160]. It also has to prepare the bunch structure for the LHC: bunches with an intensity of slightly more than $1.15 \cdot 10^{11}$ protons with a bunch spacing of 25 ns. Successive longitudinal splitting procedures are performed to meet these requirements.

The longitudinal emittance at ejection from the PS must be around 0.35 eVs, much below the final nominal emittance of 2.5 eVs in the LHC, to fit the bunches into the rather small buckets of the 200 MHz RF system in the SPS.

As the six bunches coming from the PSB are injected at $h = 7$, the bunch spacing at final energy would be some 300 ns, and the longitudinal emittance would be much too large to capture these bunches in the SPS. Therefore each bunch is split into twelve equal fractions, which reduces the longitudinal emittance per bunch to a value that is acceptable for the SPS. The bunch spacing is also divided by twelve to the nominal LHC parameter of 25 ns. The splitting factor can be decomposed to $12 = 3 \cdot 2 \cdot 2$, so that one triple-splitting and two bunch pair splittings are performed (see Sec. 3.2.2). To keep the RF frequencies during acceleration within the capabilities of the main RF system in the PS (2.8 to 10 MHz) [161, 162], the triple splitting is initiated during the injection flat-bottom at 1.4 GeV [163]. Thereafter the beam is accelerated on $h = 21$ and subsequently the bunches are split twice to $h = 42$ and finally to $h = 84$. The RF gymnastics for the preparation of the LHC beam in the PS is illustrated in Fig. 5.3. Finally one ends with a batch of 72 bunches and, as the empty bucket splits exactly

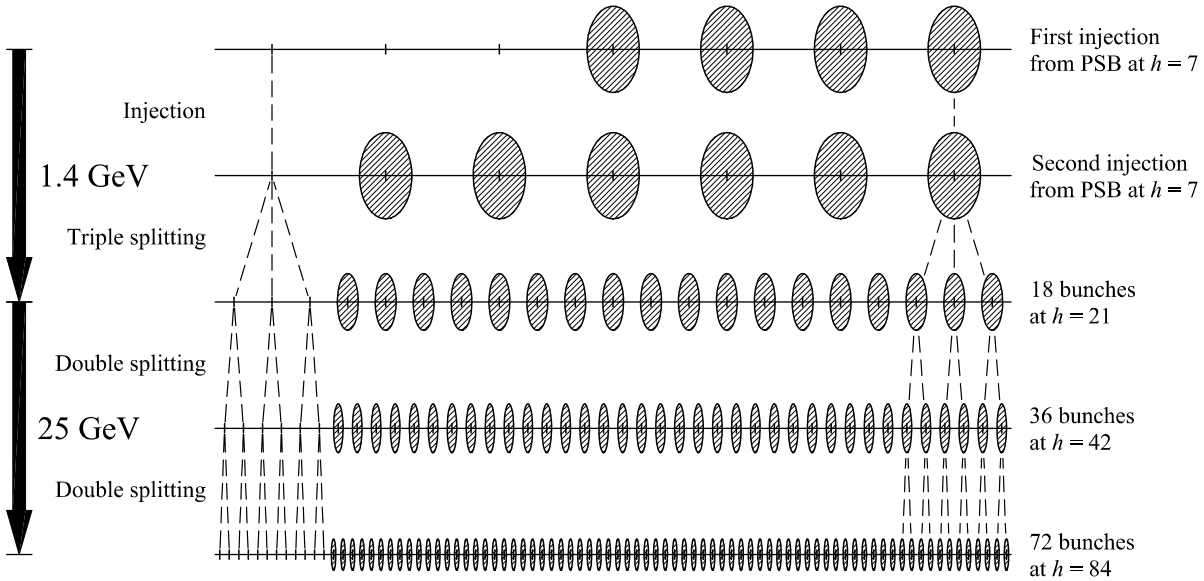

Fig. 5.3: Acceleration and bunch splitting scheme of the nominal LHC beam in the PS. Starting from $4 + 2$ bunches from the PSB each of them is split twelve times in total so that on ends up with a batch of 72 bunches at $h = 84$ with 25 ns. The empty bucket is also multiplied, and the gap is therefore 12 bunch positions long.

like the bunches, a gap of 12 non-populated buckets. This gap is sufficiently long to allow the extraction kicker magnet to be switched on without perturbing the beam.

However, the bunches after the last double bunch splitting are held with some 100 kV at 40 MHz, where their bunch length of 12 ns is still too long to fit into the SPS 200 MHz buckets. Since the voltage required in the PS to shorten them adiabatically would be unreasonably large, a non-adiabatic rotation (see Sec. 3.3.1) of the bunches in the longitudinal phase space is used for bunch compression before extraction [164, 165]. By rapidly switching the RF amplitude at 40 MHz ($h = 84$) to 300 kV and additionally applying some 600 kV at 80 MHz ($h = 168$), the bunch length is reduced to 4 ns [166] after some 600 turns in the PS, well below the bucket length of 5 ns in the SPS. Fast extraction delivers the batch of 72 bunches to matched 200 MHz buckets in the SPS.

Super Proton Synchrotron (SPS)

The batches coming from the PS are accumulated and accelerated in the SPS up to the injection energy of the LHC at 450 GeV. As mentioned in App. A, the SPS is a separated function alternating gradient synchrotron [167] equipped with a special traveling wave RF system for acceleration. Its circumference of 6.9 km is exactly eleven times as long as the circumference of the PS. However, eleven PS batches consisting of 72 bunches cannot be accelerated in the SPS because the total beam intensity is presently limited to some $5 \cdot 10^{13}$ by the maximum power that can be transferred to the proton beam during its passage through the RF cavities.

Two, three or four PS batches are therefore accumulated at flat-bottom in the SPS, corresponding to an intensity of 1.7, 2.5 or $3.3 \cdot 10^{13}$ protons (see Tab. 5.1). No special RF gymnastics during the injection procedure is necessary, as the beam is prepared by the PS to fit in matched 200 MHz buckets. It is worth noting that the whole intensity is confined within 2/11, 3/11 or 4/11 of the circumference, and that the RF power must be delivered to the beam within this fraction of the revolution period during each turn.

After an injection flat-bottom of some 3.6/7.2/10.8 s, the beam is accelerated to 450 GeV within some 8.3 s and ejected to the LHC. During acceleration the bunch emittance is intentionally blown-up to twice its initial value to avoid longitudinal instabilities. This blow-up in effective longitudinal emittance is achieved by either introducing noise to the RF amplitude at 200 MHz or by an additional RF amplitude at 800 MHz, the fourth harmonic of the fundamental RF system [168]. The bunches with nominal intensity have a longitudinal emittance below 0.6 eVs at extraction from the SPS [169].

Large Hadron Collider (LHC)

Each of the LHC rings will be filled by 12 injections at 450 GeV. The two rings will be equipped with a superconducting RF system consisting of eight cavities per ring that are capable to deliver up to 16 MV to the beam [170]. As the 400.8 MHz buckets in the LHC cannot be exactly matched to the bunch length to energy spread ratio of the injected bunches, a longitudinal emittance blow-up of some 25 % to 0.8 eVs hast to be accepted. On the one hand, the maximum voltage of the 200.4 MHz RF system is not enough to match the beam to the LHC buckets, and on the other hand, the RF voltage in the LHC cannot be lowered because of insufficient bucket area. A detailed analysis of the injection procedure can be found in [118].

After injection, the two beams are accelerated to the collision energy of 7 TeV. As longitudinal instabilities are expected during acceleration for low-emittance bunches, the longitudinal emittance is again intentionally blown up to 1 ... 1.5 eVs. Due to the long ramping time of 20 min that is limited by the ramp rate of the superconducting magnets, acceleration takes place at a moderate rate of 485 keV/turn.

The expected final bunch parameters at 7 TeV, which are the basis for the RF gymnastics for long and flat bunches, are presented in Fig. 5.4 and Tab. 5.2. The longitudinal emittance of the bunches will be deliberately blown up to 2.5 eVs during acceleration to prevent from unwanted emittance dilution due to intra-beam scattering at collision energy. However, 1 eVs at the end of the acceleration cycle should be within reach.

It should be mentioned that synchrotron radiation can be neglected for the calculation of the nominal bunch parameters. Although it is important for the heat load on the superconducting magnets, the average energy loss as calculated in Sec. 2.8 is with 6.71 keV per turn negligible compared to the external RF voltage of 16 MV. The resulting synchronous phase angle becomes $\phi_0 = (180 - 0.024)^0$.

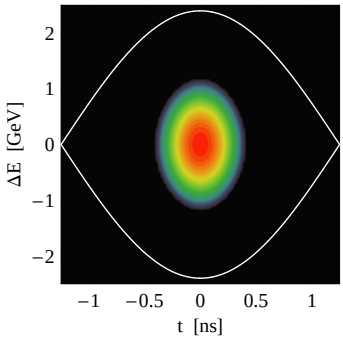

Fig. 5.4: LHC bunch at 7 TeV energy with $\varepsilon_l = 1.5\,\text{eVs}$.

	Small emittance	Nominal
Bucket area, A	7.62 eVs	
Bucket length	0.748 m (2.5 ns)	
Bucket height	2.4 GeV	
Long. emittance, ε_l	1.0 eVs	2.5 eVs
Bunch length	0.20 m (0.66 ns)	0.32 m (1.08 ns)
Energy spread	0.97 GeV	1.51 GeV
(relative)	$(0.13 \cdot 10^{-3})$	$(0.22 \cdot 10^{-3})$
Peak current (par.)	42.3 A	26.5 A

Tab. 5.2: Relevant parameters of a nominal LHC bucket and bunch with a longitudinal emittance of 1.0 or 2.5 eVs.

Nominal bunch pattern in the LHC

For the filling of one LHC ring, twelve SPS cycles containing three or four PS batches each will be required. At a bunch spacing of 25 ns the LHC has 3564 possible bunch positions, but not all of these bunch positions can be populated by a bunch, as there are several restriction imposed by the injector chain as presented above and by the LHC itself [171, 172]:

Firstly, the transfer of multiple batches from PS to SPS demands for a gap of at least 8 bunch positions as the SPS injection kicker magnet needs to be switched on between subsequent batches. It should be mentioned that the gap between two batches in the SPS is shorter than the extraction kicker gap in PS. Secondly, a gap of 38 or 39 empty bunch positions, depending on the number of PS batches delivered from the PS, must be provided for the injection kicker magnet in the LHC. The largest gap in the LHC bunch pattern assigns the time for the so-called beam dump kicker. As this kicker magnet must be activated at the collision energy of 7 TeV, its rise time is significantly longer than those of the kicker magnets considered above. At least 119 bunch positions (3 μs) must be kept free from particles to allow save abort of beam at full energy to the dump.

Various bunch patterns for the different operation modes, i.e. different bunch spacing or ions instead of proton beams, have been analyzed. As an example for a standard bunch pattern, the nominal filling scheme for high luminosity operation with 25 ns bunch spacing is described below. The filling procedure is sketched in Fig. 5.5. Following the bunch pattern notation

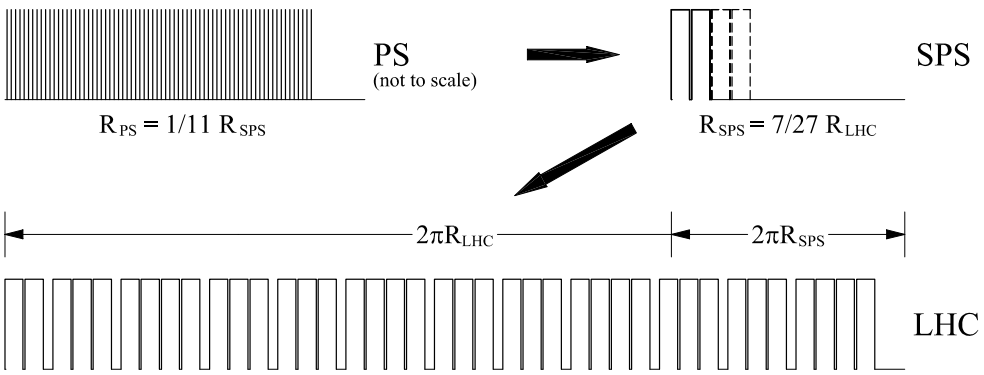

Fig. 5.5: Nominal filling scheme from PS to LHC for luminosity production with 25 ns bunch spacing. The bunch patterns in SPS and LHC are drawn to scale whereas the PS bunch pattern is magnified.

in [173, 174] where b denotes a populated bucket and e an empty bunch position, the filling scheme in the PS can be simply written as

$$\mathrm{fs_{PS}} \oplus 4 \otimes e = (72 \otimes b \oplus 8 \otimes e) \oplus 4 \otimes e\,,$$

so that $\mathrm{fs_{PS}}$ denotes the PS bunch pattern that reappears in SPS and LHC (see Fig. 5.5, top left). The operators marked by a circle can be regarded as non-commutative additions and multiplications. The pattern in the SPS can be composed of a string of PS patterns and of padding with empty buckets to end up with 924 possible bunch positions.

The full bunch pattern in the LHC can be described by the a sequence of digits defining the number of PS batches per SPS cycle, namely

$$\{234\}\ \{334\}\ \{334\}\ \{334\}\,.$$

Resolving this pattern according to the notation introduced above, the full nominal filling scheme for the LHC becomes

$$\begin{aligned}\mathrm{fs_{LHC}} = \{&2 \otimes \mathrm{fs_{PS}} \oplus 30 \otimes e \oplus 3 \otimes \mathrm{fs_{PS}} \oplus 30 \otimes e \oplus 4 \otimes \mathrm{fs_{PS}} \oplus 31 \otimes e\} \\ &\oplus 3 \otimes \{2 \otimes [\mathrm{fs_{PS}} \oplus 30 \otimes e] \oplus 4 \otimes \mathrm{fs_{PS}} \oplus 31 \otimes e\} \oplus 80 \otimes e\,,\end{aligned}$$

where the curly brackets are set corresponding to the bunch pattern above. The complete filling scheme can thus be written as

$$\begin{aligned}\mathrm{fs_{LHC}} = \{&2 \otimes (72 \otimes b \oplus 8 \otimes e) \oplus 30 \otimes e \\ &\oplus 3 \otimes (72 \otimes b \oplus 8 \otimes e) \oplus 30 \otimes e \oplus 4 \otimes (72 \otimes b \oplus 8 \otimes e) \oplus 31 \otimes e\} \\ \oplus 3 \otimes \{&2 \otimes [3 \otimes (72 \otimes b \oplus 8 \otimes e) \oplus 30 \otimes e] \oplus 4 \otimes (72 \otimes b \oplus 8 \otimes e) \oplus 31 \otimes e\} \oplus 80 \otimes e\,. \quad (5.1)\end{aligned}$$

By setting b and e to unity it can easily been shown that the total number of bunch positions is 3564. Furthermore, setting $b = 1$, $e = 0$ shows that the number of bunches per LHC ring is 2808.

The bunch pattern can by modified as long as the bunch train structure $\mathrm{fs_{PS}}$ remains unchanged. However, the generation of long bunches in the LHC as described below already requires modifications of the bunch pattern in the PS.

5.1.2 Limitations of the LHC injector chain

Several limitations of the existing accelerator complex may restrict the performance of an upgraded LHC, as the injector chain will already have a hard time providing the protons required for the ultimate scheme.

At low energy, the total beam intensity is limited by the tune shift induced by the transverse self-field of the beam. The space charge force acts incoherently on the individual particles depending on their position inside the beam. A short derivation of the space charge tune shift is given in App. F. Similar to beam-beam tune spread in high energy colliders, the so-called space charge limit is extremely difficult to compensate and, in analogy to the beam-beam limit, it is regarded as the fundamental current limitation for circular hadron accelerators in the low energy regime.

Furthermore, extremely high beam intensities may result in a significant radioactive irradiation of the accelerators if beam losses are not well under control. As most of the uncontrolled

beam losses take place at low energies where lost particles deposit their energy almost completely within the accelerator components, this is of special concern for the injector chain of the LHC.

Various options for increasing the beam intensity as well as reducing the uncontrolled beam losses in the LHC injector chain are under discussion [175] to remove its limitations at low beam energy. Although the maximum bunch intensity within the beam quality requirements for the LHC is presently limited to $1.5 \cdot 10^{11}$ protons per bunch (about 20 % above the bunch intensity needed for the nominal LHC scheme) in the PS, especially the installation of a new high energy injector linear accelerator, the so-called Superconducting Proton Linac (SPL), would increase the available bunch intensity to some $4 \cdot 10^{11}$ protons [175]. This improvement comes from the fact that such a linear accelerator would allow injection into the PS at an energy of 2.2 GeV where the direct space charge limitation is suppressed by a factor of $\beta\gamma^2|_{2.2\,\mathrm{GeV}}/\beta\gamma^2|_{1.4\,\mathrm{GeV}} \simeq 1.9$ compared to the present transfer energy between PSB and PS.

For the further analysis in this report it is assumed that the injector chain does not impose a strict intensity limitation for the LHC, and that it is capable of delivering a beam similar to the nominal LHC beam but with intensities up to three to four times its bunch population at ejection from the SPS.

5.2 Generation of long and flat bunches

Starting from an almost standard LHC beam configuration with 25 ns bunch spacing, different schemes to confine batches of nominal bunches to long and flat bunches or even single superbunches per beam have been discussed in Chapter 4.

5.2.1 Direct approach

A straightforward approach to form long and flat bunches at flat-top energy in the LHC would be the merging of each PS batch with its length of 72 bunches at a time distance of 25 ns each into one long bunch held by barrier buckets [176]. According to the total number of PS batches in the LHC, 39 long and flat bunches would finally remain. It should be mentioned that synchrotron radiation is assumed to be properly compensated at 7 TeV by a dedicated RF installation during the manipulations described below.

Fig. 5.6 illustrates the longitudinal phase space during the subsequent steps of the scheme. Before the generation of long and flat bunches, the beam is injected and accelerated according to the scheme for the nominal LHC beam. At the injection flat-top, barrier buckets are positioned in the $9 \cdot 25\,\mathrm{ns} = 225\,\mathrm{ns}$ long gaps between two adjacent PS batches in a first step. In a second step the amplitude of the harmonic RF system holding the beam is decreased adiabatically so that the bunch trains are debunched to the barrier bucket placed around the batch. This debunching procedure can be performed either directly starting from the 400.8 MHz RF system, or the bunches could be handed over to an RF system at 40.08 MHz. An RF system at 40.08 MHz would be compatible with the nominal bunch spacing of 25 ns and could serve as a mediator between the 400.8 MHz RF buckets and the RF barriers pulses whose pulse length corresponds to a frequency of some 10 MHz.

After debunching, coasting beam-like flat bunches with a length of approximately 1.8 μs are confined by the barrier pulses (Fig. 5.6, center). It is worth mentioning that debunching with 400.8 MHz would lead to a much reduced longitudinal density because only every tenth bucket at an RF frequency is occupied in the nominal scheme so that less than 10 % of the batch length

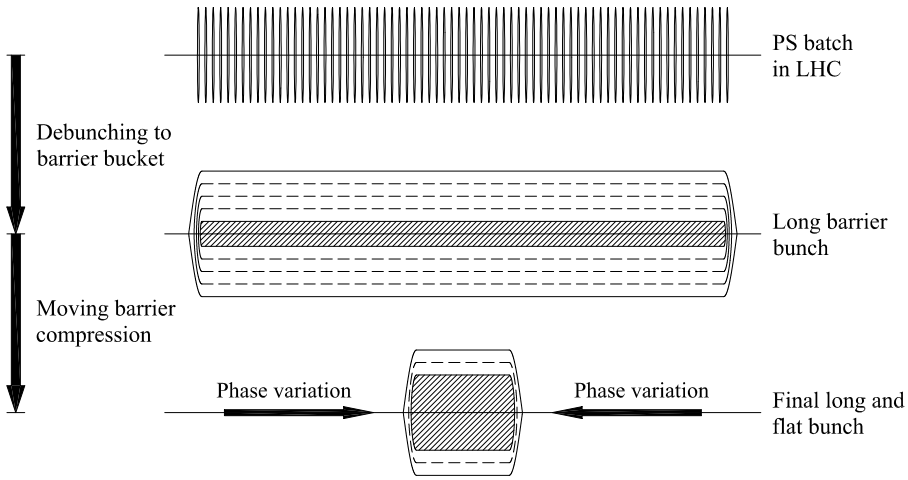

Fig. 5.6: Overview of the simple scheme which combines a batch of 72 initial bunches to a single long and flat bunch. The batch is debunched to a barrier bucket and the long bunch is finally compressed by moving barriers.

is populated with particles. The collision of such long and low density bunches cannot deliver reasonable luminosity.

To preserve the longitudinal particle density, debunching should rather be done with 40.08 MHz. Bunch compression is performed in a third step. As has been introduced in Sec. 3.4.1, the length of a barrier bucket can be manipulated by adiabatically moving the barriers in phase with respect to each other. This phase motion compresses the bunch in between, while the longitudinal particle density and momentum spread increase simultaneously. The barrier bucket compression is applied in the LHC until the original momentum spread of the initial bunches is re-established, which also corresponds to the restoration of the original longitudinal density.

Although the scheme described above seems to promise a simple creation of long and flat bunches, it has several inherent drawbacks which nearly exclude its application to a high intensity beam in the LHC [176]:

Firstly, the adiabatic bunch compression by moving RF barriers would take a time in the order of several ten minutes to keep the longitudinal emittance dilution within reasonable limits. Following the adiabaticity criterion introduced in Sec. 3.4.1 the compression would diminish the integral of the luminosity over time by lengthening the filling and beam preparation time so that the luminosity gain due to the long and flat bunches would be reduced significantly.

Secondly, assuming barrier pulses at frequencies around 7.5 . . . 10 MHz, which represents the upper technical limit of inductively loaded broad band RF cavities, the final bunches would have a considerable fraction of their particles within the tails, and the luminosity gain obtained by crossing such bunches is below the theoretical limit of $\sqrt{2}$ (see Chapter 4).

Thirdly, the beam is accelerated to the collision energy of 7 TeV by the superconducting RF system at 400.8 MHz and this RF system will be also present and influence the beam during the generation of the long and flat bunches. However, especially the very long coasting beam-like bunches are prone to perturbing RF voltages after debunching into the barrier buckets. Even though the superconducting RF system will be equipped with an efficient vector feedback to suppress transient beam loading [177], it will not be capable to reduce the RF voltage reliably enough as required for the generation of long and flat bunches.

Fourthly, the effect of the average energy loss of the particles at collision energy caused by synchrotron radiation must be compensated. This requires an RF system generating a constant voltage of some 6.7 kV along the full PS batch length of 1.8 μs. As the RF systems have to be free from of DC components, the long positive pulse must be followed by a short negative pulse of large amplitude which is generated within the gap of two PS batches. Such a compensation, which is necessary in addition to the barrier bucket system to confine the long bunches, presents a challenging and expensive task.

Finally, the momentum spread after debunching to the barrier bucket is small compared to the spread of the nominal LHC bunches. The thresholds for the microwave instability (see Chapter 6) are therefore much below the estimated longitudinal impedance in the LHC. As a result, the beam is unstable during the creation of the long and flat bunches.

These major disadvantages of the straightforward scheme of long bunch generation in the LHC demand new approaches to perform the necessary RF manipulations. A more promising scheme is therefore presented below.

5.2.2 Overview of the long bunch generation scheme

The RF gymnastics to generate long and flat bunches, about one order of magnitude longer than the nominal LHC bunches, mainly consists of three ingredients. Two of them, batch compression and bunch pair merging, have been briefly introduced in Chapter 3. The third ingredient, the final formation of the long and flat bunch, is very similar to a bunch pair merging with three or more harmonics which is just stopped in the middle of the process.

Batch compression serves to increase the harmonic number in a circular accelerator from h_1 to h_2. The difference of the two harmonics is chosen small enough so that the bunches can follow the buckets during the harmonic hand-over (see Sec. 3.2.3). The bunch spacing decreases and it is therefore used to push the batches of bunches together more closely. In the nominal LHC scheme, only every tenth bucket is a possible bunch position. Starting the batch compression at the nominal RF harmonic of $h = 35640$ would be inconvenient, because the number of empty buckets between two bunches remains the same. Therefore, the generation of long and flat bunches starts from an RF system at ten times lower RF harmonic $h = 3564$ (40.08 MHz), where every bucket serves as a bunch position. Stepwise increase of the harmonic number up to $h = 7128$ (80.16 MHz) causes the bunch spacing to shrink by a factor of two to 12.5 ns, whereas the number of bunches stays constant throughout the procedure.

To re-establish the original bunch spacing and to reduce the number of bunches, the complementary procedure, bunch pair merging, is applied where the RF amplitude at $h = 7128$ is adiabatically decreased while simultaneously increasing the amplitude at $h = 3564$. The bunch spacing increases again to 25 ns but the number of bunches is halved with respect to the initial state.

Repetitive application of this sequence of batch compression and bunch pair merging allows to progressively confine dense bunches as illustrated in Fig. 5.7. It is obvious that the number of initial bunches must be a power of two so that the confinement is restricted to $4, 8, 16, 32, 64 \ldots 2^n$ bunch batches. A reasonable choice of this batch length is explained in what follows.

Choice of batch length

Two main arguments determine the number of initial bunches to be combined to one long and flat bunch in the LHC:

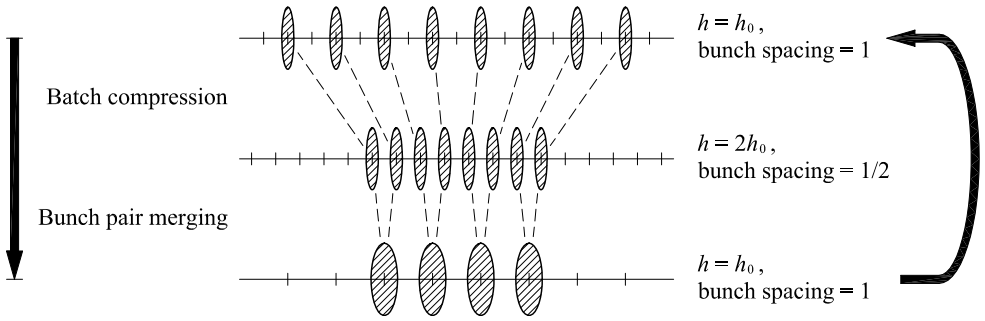

Fig. 5.7: Subsequent application of batch compression and bunch pair merging gradually reduces the number of bunches and increases the intensity per bunch.

Firstly, assuming a constant emittance per bunch, the required RF voltage for the creation and the storage of the long and flat bunches is proportional to the square of the number of combined bunches. The absolute voltages necessary to store the final bunches after the combination of batches of 16 bunches can be found in Tab. 4.3. A reasonable RF voltage providing sufficient bucket area during the creation of these bunches is somewhat larger, namely about 1.5 MV.

Secondly, the number of remaining bunches, multiplied by their bunch length, can be considered as an effective beam length. Following the derivations in Sec. 4.2.5, this effective beam length $n_b l_b$ should be chosen so that the maximum beam-beam tune shift is reached with the maximum available average beam current (see Fig. 4.3).

The relevant beam parameters for different numbers of bunches confined to one long bunch are given in Tab. 5.3.

Number of initial bunches per long and flat bunch		1	4	8	16	32	64
Total number of bunches, n_b		2808	624	312	156	78	39
Effective beam length, $n_b l_b$ (rectangular equivalent, 3 harmonics)	[m]	531	2613	1306	653	327	163
Average current for $\Delta Q = -0.01$, I_0 (alternate beam crossings)	[A]	0.94	12.8	6.4	3.2	1.6	0.8
RF voltage for the generation of long bunches, U_{RF}	[MV]		0.1	0.4	1.5	6	24

Tab. 5.3: Parameters for the choice of the number of initial bunches to generate a long and flat bunch. The longitudinal emittance per initial bunch is taken to be 1 eVs at the LHC injection flat-bottom. The total number of long and flat bunches per beam is based on the empty to occupied bucket factor 2808/3564 of the nominal LHC beam.

As already pointed out in Sec. 4.3.6, a very high luminosity could be achieved with options confining less than 16 initial bunches, but at the expense of excessively high and unpractical total beam currents.

On the other hand, compressing more than 32 LHC bunches requires a considerable RF voltage to generate the long bunches, and the beam-beam limit restricts the beam intensity in the range of the intensity of the ultimate LHC scheme (see Tab. 4.2). However, it will be very difficult for the experiments to cope with the event rate associated with this very small number

of superbunches in the LHC.

Therefore, the only remaining two options of combining either 16 or 32 almost nominal LHC bunches to one long bunch are considered realistic and worth being discussed in more detail.

Total batch length in the LHC

Direct batch compression of batches of 16 or 32 bunches close to each other without any gap in between is excluded for two reasons: firstly, because the harmonic number 3564 is neither divisible by 16 nor 32, and secondly because, during batch compression, the effective RF amplitude is modulated along the batch so that at least the edge buckets cannot be populated with particles.

As the harmonic number $h = 3564$ decomposes to $2^2 \cdot 3^4 \cdot 11$, the favorable batch lengths leaving at least one empty bucket at each end are $n_{\mathrm{batch}} = 2 \cdot 3^2 = 18$ for 16 respectively $n_{\mathrm{batch}} = 2^2 \cdot 3^2 = 36$ for 32 bunches. The fundamental harmonic of the batch confinement RF gymnastics is thus 198 or 99 which corresponds to the number of available bunch positions for the final long and flat bunches. Furthermore, the step width in harmonic number of the hand-overs during batch compression is also defined by this step of $\Delta h = 198$ or $\Delta h = 99$.

The complete schedule for the harmonic number changes during batch compression as well as the increase of the number of buckets per batch is illustrated in Figs. 5.8 and 5.9. The bunch

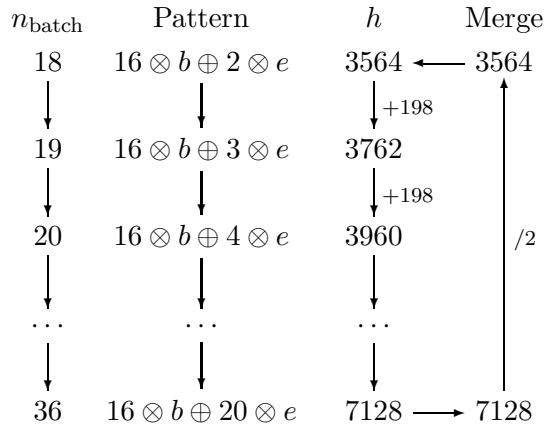

Fig. 5.8: Schedule of harmonic numbers and bunch patterns during long bunch combination of 16 initial bunches.

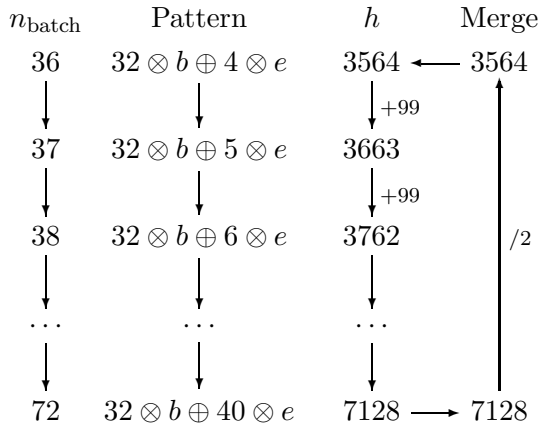

Fig. 5.9: Same harmonic schedule as in Fig. 5.8 but for a batch of 32 initial bunches. The bunch pattern notation is introduced at the end of Sec. 5.1.1.

patterns are given for the first batch compression. For subsequent compressions the number of bunches is less while the number of empty bucket positions is larger.

It can be seen from the harmonic schedule that the RF systems for the batch compression have to cover the frequency range from 40.08 ($h = 3564$) to 80.16 MHz ($h = 7128$), no matter whether 16 or 32 bunches are combined. However, no more than two RF harmonics are acting on the beam simultaneously so that the complete RF gymnastics can be covered by two tunable groups of RF systems. It should be mentioned that the final formation of the long and flat bunches may require additional fixed frequency RF systems if more than two harmonics are applied to flatten the bunch shape.

The new LHC cycle

At the collision energy of 7 TeV, each beam with nominal intensity contains some 362 MJ ($2808 \cdot 1.15 \cdot 10^{11}$ protons), which makes the machine extremely sensitive to any kind of beam losses. At injection energy, the acceptable losses are 15 times larger. As complicated RF gymnastics can cause small beam losses, it is clearly preferable to perform most of the beam gymnastics at the injection flat-bottom of the LHC.

Neglecting the effects of bucket area reduction during batch compression, a change of the harmonic number at constant RF voltage causes the bucket area to shrink according to $1/h^{3/2}$ so that the smallest bucket area occurs at the end of the batch compressions. The bucket area for relevant harmonic numbers together with the bunch emittances are shown in Fig. 5.10. It

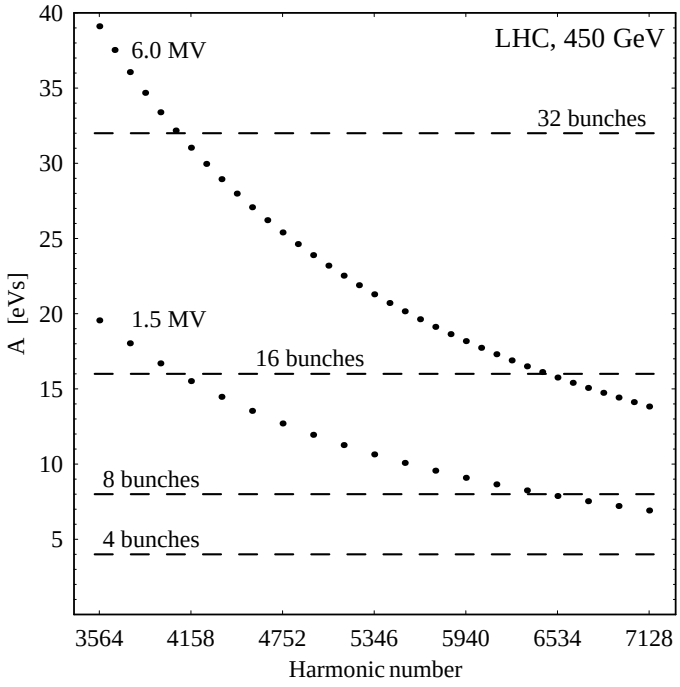

Fig. 5.10: Bucket area versus harmonic number for relevant RF frequencies between 40.08 and 80.16 MHz at constant voltage of 1.5 and 6 MV at the injection flat-bottom in the LHC. The dashed lines show the total emittance of 2^n initial bunches.

becomes clear that in the 16 bunch scheme as well as in the 32 bunch scheme the initial batch can be combined to two remaining buckets held at $h = 3564$ at injection energy.

While the bunch emittance stays virtually constant during acceleration, the bucket area grows proportionally to $\sqrt{E/|\eta|} \simeq \gamma_{\rm tr}\sqrt{E} \propto \sqrt{E}$ so that it is 3.9 times larger at collision energy. Therefore the last batch compression and the final formation of the long and flat bunches must be carried out at the LHC flat-top.

Batches of two bunches according to the bunch pattern of $2 \otimes b \oplus 16 \otimes e$ (16 initial bunches) or $2 \otimes b \oplus 34 \otimes e$ (32 initial bunches) are accelerated with the 40.08 MHz RF system. The moderate average energy gain of 485 keV/turn results in a synchronous phase of $\phi_0 = (180 - 18.8)^0$ respectively $(180 - 4.6)^0$, and the bucket area reduction as sketched in Fig. 2.5 due to the synchronous phase is not critical during acceleration.

It is important to point out that an additional benefit of shifting as much of the RF manipulations to the injection flat-top is offered by the scaling of the synchrotron frequency proportional to $\sqrt{|\eta|/E} \simeq 1/(\gamma_{\rm tr}\sqrt{E}) \propto 1/\sqrt{E}$. To keep the same adiabaticity during the process, the manipulation can be executed four times faster at 450 GeV.

5.2.3 Beam transfer from SPS to LHC

As the batch confinement RF gymnastics is based on RF systems at harmonic numbers between 3564 and 7128, the beam from the SPS is injected into large 40.08 MHz buckets at the LHC flat-bottom. Furthermore, the estimation of the beam loading voltage induced to the superconducting 400.8 MHz cavities (see Sec. 6.5) shows that they even have to be removed for operation with long bunches. Parallel operation of both the standard superconducting RF system and a 40.08 MHz RF installation is impossible with reasonable power capabilities.

The condition for a longitudinally matched bunch to bucket transfer between two circular accelerators has been derived in Sec. 3.5 so that the voltage ratio optimum between SPS and LHC is given by

$$\frac{V_{\mathrm{SPS}}}{V_{\mathrm{LHC}}} = \left(\frac{R_{\mathrm{SPS}}}{R_{\mathrm{LHC}}}\right)^2 \left|\frac{\eta_{\mathrm{SPS}}}{\eta_{\mathrm{LHC}}}\right| \frac{h_{\mathrm{LHC}}}{h_{\mathrm{SPS}}} = 0.38 \cdot \frac{h_{\mathrm{LHC}}}{h_{\mathrm{SPS}}} \,. \tag{5.2}$$

For matched injection into 40.08 MHz buckets the voltage ratio becomes 0.29. However, as an additional constraint, the bucket area must be sufficient in both accelerators.

The bucket area of the 200 MHz SPS buckets at extraction flat-top is plotted in Fig. 5.11 versus the available RF voltage. Assuming a bunch emittance of 0.6 to 0.7 eVs at 450 GeV, the

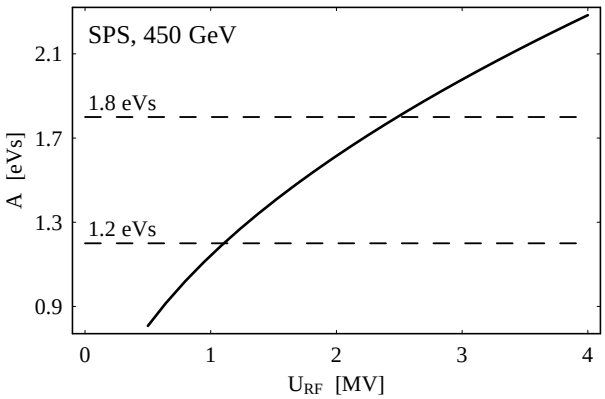

Fig. 5.11: Bucket area of the 200 MHz RF system in the SPS versus its RF amplitude.

bucket area should be at least three times as large as the bunch emittance to keep the bunch within the linear region of the bucket. Therefore, the minimum RF voltage limitation in the SPS for extraction into a 40.08 MHz RF system in the LHC is about 3 MV. The upper voltage limit is simply given by the available RF power, which limits the maximum RF voltage to some 8 MV.

Beam transfer by bunch rotation

Depending on whether 16 or 32 initial bunches should be combined to one long and flat bunch, the available RF voltage at 40.08 MHz in the LHC will be either $2 \cdot 1.5$ MV or $2 \cdot 6$ MV.

In the case of 3 MV, the corresponding RF voltage in the SPS according to Eq. (5.2) is only 0.87 MV so that the bucket area would be insufficient. Therefore, a virtual reduction of the RF voltage by bunch rotation is foreseen, to obtain a ratio of bunch length to energy spread of about 0.87 MV at extraction. The bunches are rotated in the longitudinal phase space in the SPS, and the extraction to the LHC takes place when the bunch length is largest, respectively after a rotation by a quarter of a turn.

Following the analysis in Sec. 3.3.1, the maximum bunch lengthening factor reachable by an instantaneous voltage step down from 8 to 3 MV is 1.63. After rotation in the longitudinal

phase plane, when the bunch is longest, it has similar parameters as a bunch kept in a stationary bucket with 1.1 MV, except that such a bunch would be significantly stretched out in the non-linear regions of the bucket as its emittance is close to the bucket area (see Fig. 5.11).

Tracking calculations of the beam transfer scheme by bunch rotation show that a small but non-negligible emittance blow-up occurs. Starting from a matched bunch of 0.65 eVs longitudinal emittance in the SPS, the RF amplitude is raised adiabatically from 3 MV to 8 MV and then suddenly switched back to 3 MV. After one quarter of a period at the synchrotron frequency, the bunch is transferred to the LHC and tracked for further 0.2 s to observe residual mismatch. The longitudinal emittance blow-up caused by such a transfer between SPS and LHC with optimized parameters is illustrated in Fig. 5.12. As expected, the longitudinal emittance remains

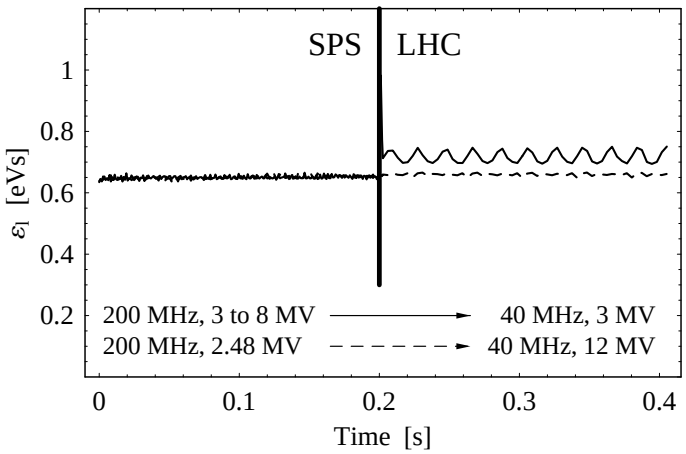

Fig. 5.12: Longitudinal emittance during a bunch transfer from SPS to LHC including bunch lengthening by bunch rotation in the SPS (continuous line). The dashed line represents the transfer to 12 MV at 40.08 MHz in the LHC. The longitudinal emittance is defined as the area of the encircling ellipse containing 99 % of the bunch particles normalized to 0.65 eVs at the beginning of the process.

constant during the adiabatic voltage increase within the first 200 ms. The bunch rotation itself is by far too fast to be visible on the timescale of Fig. 5.12; the bunch is extracted some 2.5 ms after the instantaneous voltage reduction. After injection into the LHC, an oscillation of the effective longitudinal emittance with the synchrotron frequency can be observed. It is caused by the residual longitudinal mismatch of the injected bunch. After filamentation, the final bunch has an emittance of some 0.8 eVs and the transfer blow-up is about 23 %. It should be pointed out that the residual longitudinal mismatch comes from a non-ideal bunch rotation: a significant fraction of particles suffers from the reduced synchrotron frequency at large oscillation amplitudes. Therefore, the optimum rotation time must be $1.25 \cdot \pi/(2\omega_s)$ to obtain minimum transfer blow-up, slightly longer than a quarter period of the linear synchrotron frequency.

Direct transfer

In the case of 32 initial bunches combined to one long and flat bunch, the available RF voltage has to be about $2 \cdot 6$ MV at 40.08 MHz and, according to Eq. (5.2), the corresponding RF voltage in the SPS is about 3.5 MV. It is expected that the matched transfer causes virtually no longitudinal emittance blow-up (see Fig. 5.12, dashed line).

However, the bucket area of a 40.08 MHz RF system in the LHC is much larger than the emittance of the injected bunches resulting in low synchrotron frequency spread and virtually no Landau damping. This might restrict the maximum RF amplitude during injection, and the bunch rotation scheme might be favorable even if more RF voltage would be available.

Albeit the ideal longitudinal emittance after beam transfer to the LHC is estimated to be below 0.8 eVs, an additional blow-up caused by a higher harmonic RF system to re-establish

Landau damping (see Sec. 6.3.6) must be taken into account. Therefore the subsequent analysis of the RF gymnastics assumes a longitudinal emittance of 1 eVs.

It is important to point out that the transfer of nominal bunches from the SPS (8 MV) to the 400.8 MHz RF system (8 MV) also causes a longitudinal emittance blow-up. Instead of stretching the bunches as suggested above, a bunch rotation might be an option to shorten the bunches and to suppress the mismatch [178].

5.2.4 Batch compression

After beam injection, the RF manipulation to generate the long and flat bunches commences. The harmonic number is raised in steps of 198, respectively 99, which corresponds to a step of unity with respect to the local harmonic number of the batch (see Figs. 5.8 and 5.9). The lower harmonic RF amplitude at h_1 is adiabatically decreased while the higher harmonic RF at $h_1 + 198$ or $h_1 + 99$ is increased simultaneously.

When both harmonics are of equal RF voltage, the beat frequency at $h_2 - h_1$ has the same amplitude as the two main carriers so that the effective RF focusing is large at the center of the batch but decreases to nearly zero at the very ends of the batch. This problem is most critical at the beginning of the first harmonic hand-over as only the last (16 initial bunches) or the last two (32 initial bunches) buckets are kept empty at both ends of the batch. An example of the separatrices and bucket areas for the worst case during the first harmonic hand-over of the combination of 32 bunches is shown in Fig. 5.13. In the case of 16 initial bunches, the

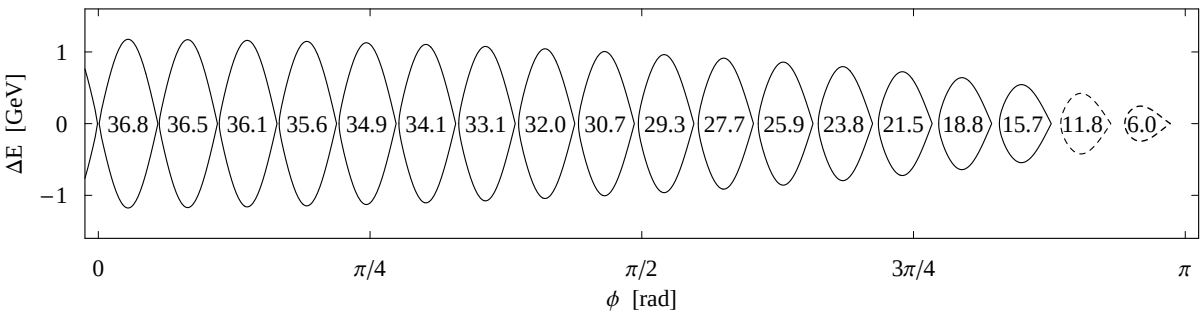

Fig. 5.13: Separatrices in the middle of the first harmonic hand-over from $h = 3564$ to $37/36 \cdot 3564 = 3663$ when both RF voltages are equal and at half of their maximum amplitude, namely 3 MV each. The separatrices of empty buckets are plotted with dashed lines. As the stationary trajectories are symmetric around $\phi = 0$ only one half is shown. The buckets areas (in the center of the separatrices) are given in units of eVs.

situation is similar. The bucket area of the populated buckets varies from 8.1 to 17.9 eVs in this case, and the empty bucket at the end of batch has an area of 4.1 eVs.

The analysis above seems to suggest that the gaps in between the batches are not mandatory. However, despite of their function to make the bunch pattern compatible with the LHC with its global harmonic of 3564, it is important to point out that the bucket area dynamically oscillates from the stationary value as shown in Fig. 5.10 to the minimum value (Fig. 5.13) within each single harmonic hand-over. In the adiabatic limit, the bunch inside the bucket must be able to follow this quadrupole excitation caused be the bucket motion without dilution in the longitudinal phase space. The development of the bucket areas of center (dashed line) and tail buckets is presented in Figs. 5.14 and 5.15. While the area of the center bucket shrinks smoothly, the outer buckets, especially the last one, are strongly modulated. This behaviour

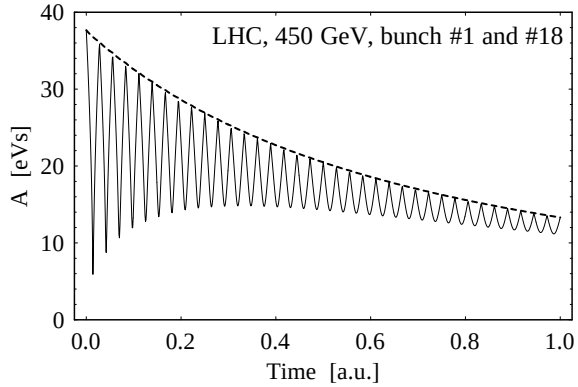

Fig. 5.14: Development of the bucket area during batch compression from $h = 3564$ to 7128 in steps of $\Delta h = 99$. While the center bunch mainly shrinks proportional $1/h^{3/2}$ (dashed line), the last bunch shows a strong modulation of the bucket area with each harmonic hand-over (continuous).

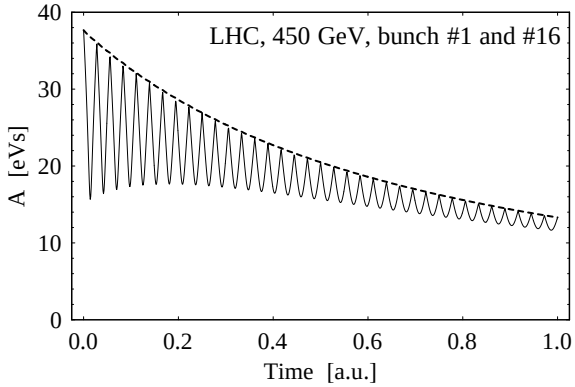

Fig. 5.15: Comparison of the bucket area development of center (dashed line) and last populated bucket (continuous). The bucket area is still strongly modulated, but the variation is already significantly reduced compared to the last, empty bucket (Fig. 5.14).

can cause emittance dilution if the bucket area is modulated so fast that the bunch is not able to follow the rapid changes of the bucket.

For the calculation of Figs. 5.14 and 5.15 the time for each harmonic hand-over was assumed to be constant. Since the degree of modulation is largest for the first sub-steps of the batch compression, they should be lengthened so that the time derivative of the effective RF focusing does not surpass a certain limitation during the batch compression manipulation.

Time optimization

From the analytical calculation of RF potential or separatrices during batch compression, one could get the impression that the RF manipulation is symmetric in the sense that both ends of the batch move to the center simultaneously. However, it should be kept in mind that, above transition, the bunch at the front of the batch must be slightly accelerated while the bunch at the back must be decelerated to initiate their relative phase motion with respect to the batch center.

Therefore a batch compression can also be regarded as sketched in Fig. 5.16. Each

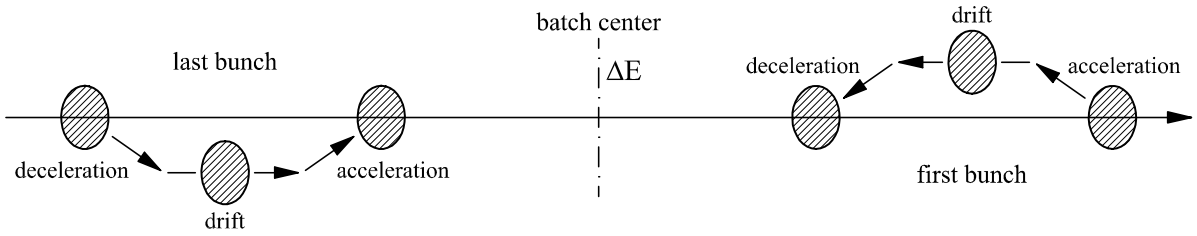

Fig. 5.16: During batch compression, each bunch of the batch has to be slightly accelerated or decelerated to move them towards the center. The offset energy of this acceleration or deceleration increases with the distance of the bunch from the center of the batch.

bunch is slightly displaced in energy where it drifts in phase to reach its new position after the

batch compression. It becomes clear that the bunch motion of the front and the back half are reflections in a point around the batch compression center.

It is worth noting that this view of the batch compression manipulation is not taken into account in the calculations of buckets via the Hamiltonian theory. A simple harmonic hand-over between two harmonics, where the lower harmonic is decreased linearly while the higher harmonic is also increased linearly, the motion of the bucket center switches non-adiabatically from $d\phi_0/dt = 0$ to $d\phi_0/dt \neq 0$. This effect excites a dipole oscillation of the bunch, which causes emittance dilution and thus a blow-up of the effective longitudinal emittance. Especially the bunches at the tails of the batch suffer from this effect.

Therefore, a simple equilibration of the voltage ramps is presented in what follows. This equilibration ensures that the bunches are slowly accelerated and decelerated at the beginning and at the end of the batch compression.

For the optimization, the following parameters are assumed at the beginning and at the end of the batch compression:

	before		after
Harmonic, h	h_0	$\longrightarrow$	$2h_0$
Total batch length, l	l_0	$\longrightarrow$	$l_0/2$
Time, t	0	$\longrightarrow$	τ_{bc}

.

For simplicity it is assumed that the harmonics number does not change stepwise, but that the effective harmonic number varies smoothly with time, namely

$$h(t) = h_0 \left(\frac{t}{\tau_{\mathrm{bc}}} + 1 \right) , \tag{5.3}$$

so that the length of the batch develops according to

$$l(t) = l_0 \Big/ \left(\frac{t}{\tau_{\mathrm{bc}}} + 1 \right) . \tag{5.4}$$

This function has a gradient at $t = 0$ and $t = \tau_{\mathrm{bc}}$ so that the buckets switch from stationary to moving instantaneously, which is strongly non-adiabatic. Especially at the beginning of the process a large energy offset of the tail bunches is required.

An optimized function of the time dependent bunch length $l(t)$ should be smooth and have vanishing derivatives at $t = 0$ and $t = \tau_{\mathrm{bc}}$. Trigonometric functions can fulfill these requirements, and a reasonable choice can be written as

$$l_{\mathrm{opt}}(t) = \left[\frac{3}{4} + \frac{1}{4} \cos \left(\pi \frac{t}{\tau_{\mathrm{bc}}} \right) \right] l_0 \, . \tag{5.5}$$

The improved batch length function is plotted in Fig. 5.17. One can observe that the batch length starts to shrink smoothly.

The time scaling function to achieve the improved batch length shrinkage can be found easily by demanding that $l_{\mathrm{opt}}(t) = l(t_1)$, where t_1 is the new time function which itself depends on the original time t. Finally, this function becomes

$$t_1(t) = \left[\frac{1}{3/4 + 1/4 \cdot \cos(\pi t/\tau_{\mathrm{bc}})} - 1 \right] \tau_{\mathrm{bc}} \, . \tag{5.6}$$

The time function can be used to convert the linear amplitude ramp functions of the batch compression to such amplitude where the end of the batch moves according to Eq. (5.5).

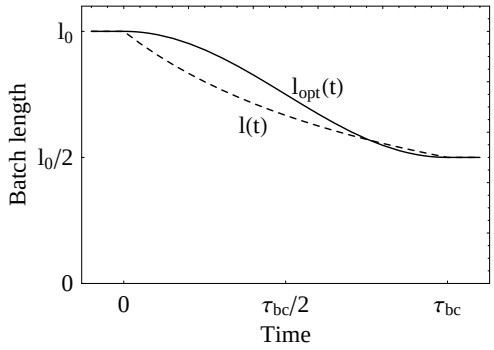

Fig. 5.17: Improved batch length function versus time (continuous line). As a reference, the batch length function of a non-equilibrated batch compression is also shown.

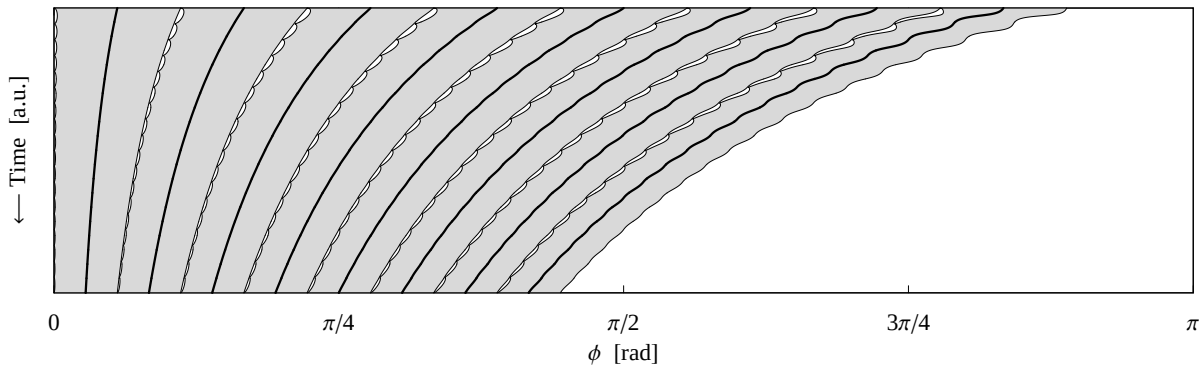

Fig. 5.18: Movement of the bucket centers during the first batch compression for a simple scheme. The thick lines mark the center positions of the buckets while the shaded areas enclosed by thin lines represent the total longitudinal extent of the buckets. Only one half of the batch is shown.

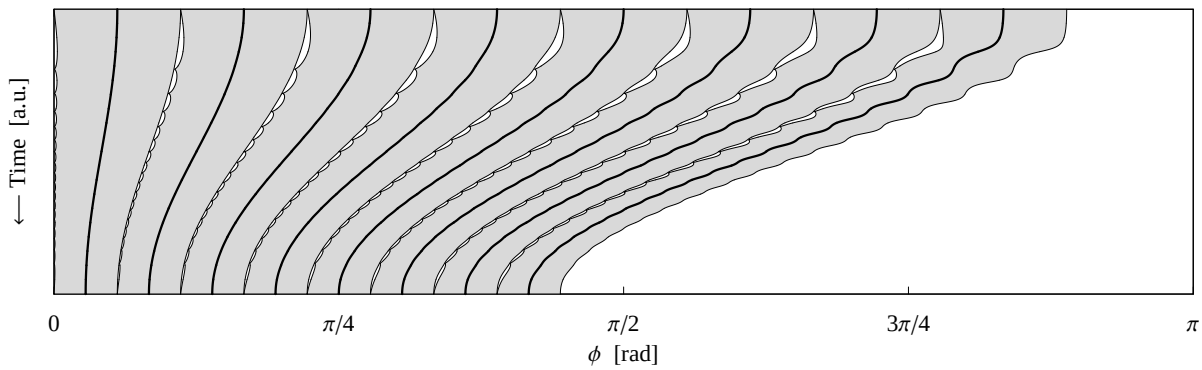

Fig. 5.19: Same representation of bucket centers and bucket lengths as in Fig. 5.18 but for an improved scheme with a batch length variation according to Eq. (5.5).

The resulting movement of the buckets in the case of non-equilibrated voltage ramps during batch compression of 16 bunches is sketched in Fig. 5.18, while the optimized case is presented in Fig. 5.19. Clearly, especially the edge bunches are accelerated respectively decelerated smoothly at the beginning and at the end of the batch compression.

The harmonic program and the RF amplitude ramps for an equilibrated batch compression of a batch of 16 bunches with 2 empty buckets in between are illustrated in Fig. 5.20. Essentially the first and the last harmonic hand-over from $h = 3564$ to $3564 + 198$ and from $h = 7128 - 198$ to 7128 have to be performed with non-linear amplitude ramps because the acceleration and

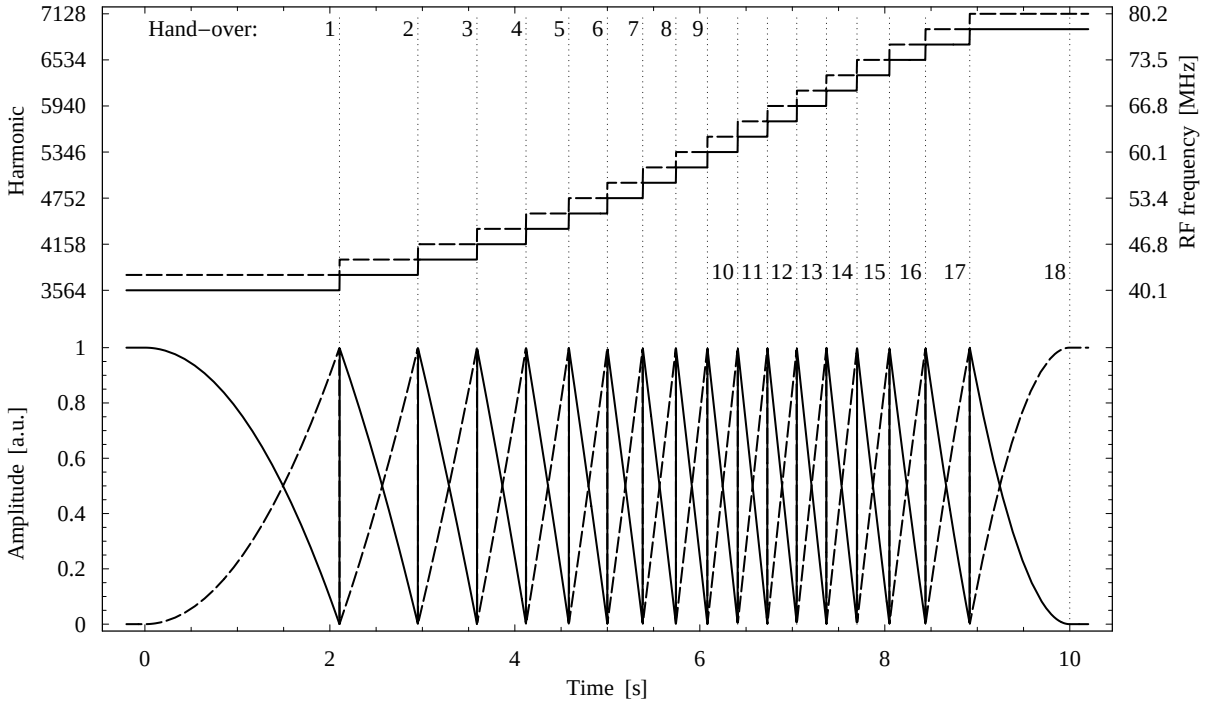

Fig. 5.20: Harmonic and voltage ramps for an optimized batch compression of the bunch pattern $16 \otimes b \oplus 2 \otimes e$ from $h = 3564$ to 7128 by 18 stepwise harmonic hand-overs. The lower harmonic and the related amplitude are plotted as continuous lines while the higher harmonic and amplitude are represented as a dashed line.

deceleration of the tail bunches needs to be initiated. The intermediate harmonic hand-overs still have almost linear variation of the RF amplitudes; they are just shifted together in time.

Tracking studies demonstrate the effect of the equilibration during batch compression on the longitudinal emittance: Figs. 5.21 and 5.22 show the development of the longitudinal RMS emittance during the first batch compression of a batch of 16 bunches with a gap of two empty buckets between adjacent batches. The initial bunches have a parabolic distribution with a total emittance of 1 eVs. Each of them consists of some 2000 macro particles. Collective effects are not taken into account. In the case of a constant time for each harmonic hand-over, the emittance of the tail bunch is diluted significantly due to the non-adiabatic modulation of the RF focusing. It is worth noting that the subsequent bunch mergings become asymmetric even if only the last bunch suffers from this excitation. This leads to additional emittance dilution. However, in the case of the equilibrated batch compression with amplitude ramps according to Fig. 5.20, virtually no longitudinal emittance dilution is visible although the batch compression has the same total duration as assumed in the non-optimized case.

Amplitude modulation

It is shown in Fig. 5.13 that the effective RF focusing is strongly modulated along the batch when the two RF system acting on the beam have the same amplitude. This modulation, from which especially the tail buckets may suffer, has a negative effect on the bunches at the ends of the batch because, as mentioned above, the fast variation in RF focusing can excite a quadrupole oscillations if the RF manipulation is not perfectly adiabatic. The possible benefit of an additional amplitude modulation to counteract the bucket area variation along the batch

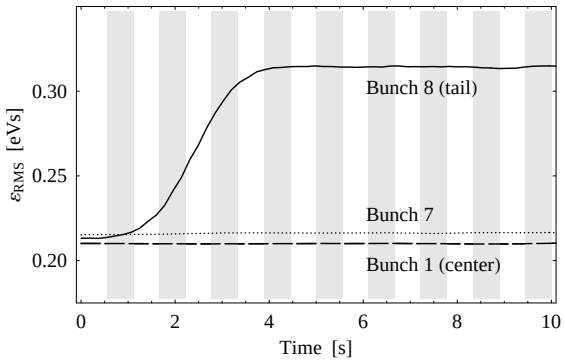

Fig. 5.21: Emittance development of center and tail bunches during batch compression of a 16 bunch batch in the LHC from $h = 3564$ to 7128. Each harmonic hand-over has the same duration. The tracking calculation was performed starting with 1 eVs bunches at an energy of 450 GeV (emittance conversion from total to RMS see Tab. 2.3).

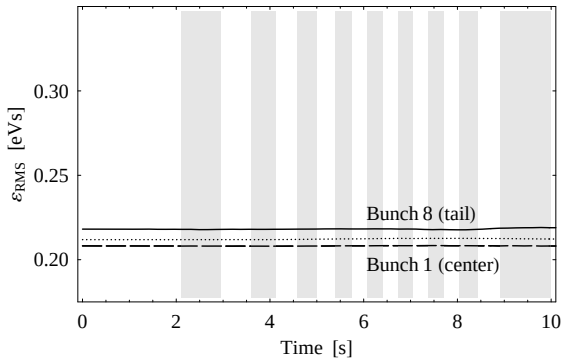

Fig. 5.22: Same representation as in Fig. 5.21 but for the equilibrated batch compression. There is virtually no longitudinal emittance dilution visible anymore although the manipulation takes the same time as in the bare case. The alternating white and gray striped regions indicate the harmonic hand-overs.

is therefore analyzed in this paragraph.

Assuming that the bunches are handed over from the harmonic h_1 to h_2, both RF amplitudes are modulated with the batch frequency given by $(h_2 - h_1)\omega_0$. In the frequency domain, an amplitude modulated signal consists of a main carrier at e.g. $h_1\omega_0$ with the batch frequency ω_0 and of two carriers which are just $(h_2 - h_1)\omega_0$ apart. RF cavities with a high quality factor do not have sufficient bandwidth to follow the fast amplitude modulation at the batch frequency with reasonable drive power, and additional RF systems would have to be installed to generate the modulation side bands. The technical implementation would thus be an approach in the frequency domain, too.

Adding the side band amplitudes U_{s1} and U_{s2} to the unmodulated combination of two RF carriers at h_1 and h_2 as stated in Eq. (3.7) results in a total RF amplitude which can be written as

$$\begin{aligned} U(t) = &- \underbrace{U_{s1}\sin\left[(2h_1 - h_2)\omega_0 t\right]}_{\text{lower side band of } h_1} + \underbrace{(U_1 - U_{s2})\sin(h_1\omega_0 t)}_{\text{main carrier } h_1 \text{ and lower side band of } h_2} \\ &+ \underbrace{(U_2 - U_{s1})\sin(h_2\omega_0 t)}_{\text{main carrier } h_2 \text{ and upper side band of } h_1} - \underbrace{U_{s2}\sin\left[(2h_2 - h_1)\omega_0 t\right]}_{\text{upper side band of } h_2}, \end{aligned} \tag{5.7}$$

where the terms are given in the order of ascending frequency. The upper side band of the carrier at h_1 coincides with the carrier at h_2. The lower side band of the main carrier at the harmonic h_2 has the same frequency as the carrier at h_1. Finally, only two additional RF systems operating on the harmonics $2h_1 - h_2$ and $2h_2 - h_1$ are required to generate the amplitude modulation of both carriers at the batch frequency.

The modulation amplitude of the side bands $U_s = U_{s1} = U_{s2}$ is calculated numerically from the condition that the center and the last occupied bucket have identical areas. In analogy to the bucket area distribution along the batch as sketched in Fig. 5.13 for the first harmonic hand-over, Fig. 5.23 illustrates the same situation, but with additional side bands according to Eq. (5.7). The areas of center and tail bucket are equal by definition. However, center and tail buckets now have the smallest areas while the largest buckets are situated in the center of each half of the batch.

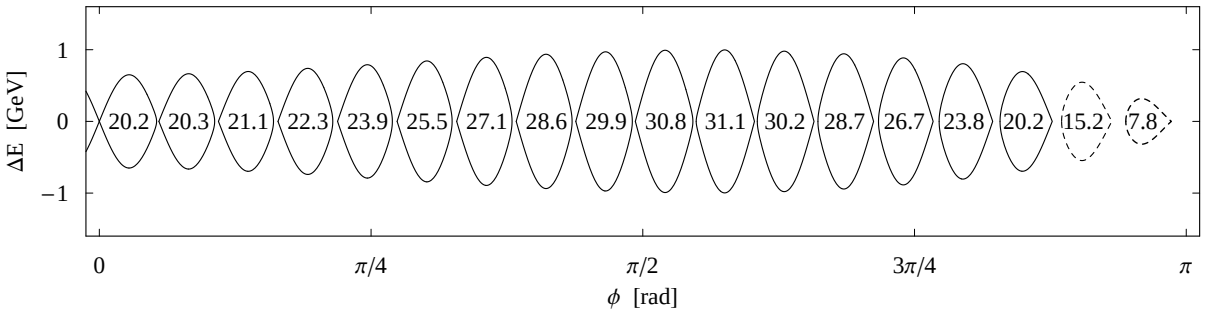

Fig. 5.23: Separatrices and bucket areas as in Fig. 5.13, but with amplitude modulation of both RF amplitudes so that the bucket area of the center and the tail bunches is identical. Again only one half of the 32 buckets of the batch is shown. The optimum voltage ratio is $U_{s1}/U_1 = U_{s2}/U_2 = 0.348$.

The maximum modulation amplitude is only needed at the instant when both RF amplitudes are equal during a harmonic hand-over. It must be zero in between, when the beam is held by one RF frequency only. The modulation side bands are therefore increased during each harmonic hand-over until both main RF amplitudes are equal. Then the modulation amplitude reaches its maximum to equilibrate the bucket areas as shown in Fig. 5.23. The side band amplitudes are decreased again towards the end of the harmonic hand-over so that they vanish when a higher harmonic main RF carrier holds the beam.

Analyzing the development of the longitudinal emittance with numerical tracking calculations shows that the additional amplitude modulation has a positive effect on the longitudinal dilution of the tail bunches (see Fig. 5.24). Even though the additional amplitude modulation

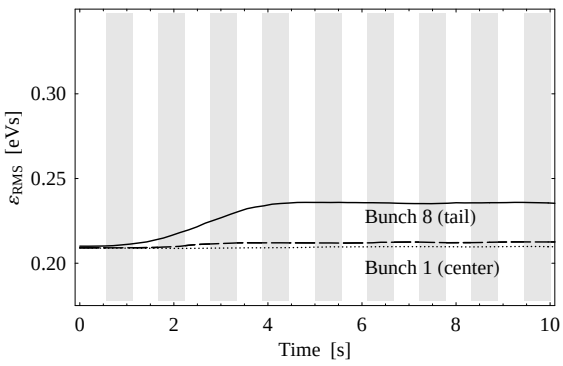

Fig. 5.24: Emittance development of center and tail bunches during batch compression as shown in Fig. 5.21 but with additional amplitude modulation during the harmonic hand-over. The center bunches are not affected significantly by the quadrupole oscillations of their buckets.

causes a variation of the effective RF focusing of the center buckets during each harmonic hand-over, no significant dilution of the bunches in those buckets can be observed. However, when the batch has a total length of four bunches and the remaining bunches have large emittances, all bucket areas are equal with amplitude modulation but slightly smaller than the bucket areas without modulation. The tracking calculations show that this results in a bucket area limitation so that particles get lost during the last batch compression with four remaining buckets at 450 GeV.

Keeping in mind that two additional RF systems with non-negligible voltage demands of some 40 % of the two main RF system would have to be installed, amplitude modulation might be an option when the batch compression is limited by insufficient area of the tail buckets. As this is not the case for analyzed batch compressions which are performed during the long and flat bunch combination scheme in the LHC (see Fig. 5.13), amplitude modulation is not

necessary. The reduced blow-up of the tail bunches as illustrated in Fig. 5.24 is not significant as it is compensated by the time optimization scheme anyway.

Modified amplitude functions

For all schemes considered so far (see also Sec. 3.2.3) it was assumed that the higher harmonic amplitude would be increased while decreasing the lower harmonic amplitude simultaneously. In this case, both amplitudes are equal and have half of their maximum value at the middle of each harmonic hand-over.

An increase of the minimum bucket area during the harmonic hand-overs of $\sqrt{2}$ is achieved by the voltage ramps as sketched in Fig. 5.25 [81]. It should be mentioned that it is not mandatory that the amplitude ramps are linear. Time equilibration of the procedure for smooth acceleration and deceleration of the tail bunches can be reached as in the case of bare batch compression. Firstly, the RF amplitude at the larger harmonic h_2 is increased while the

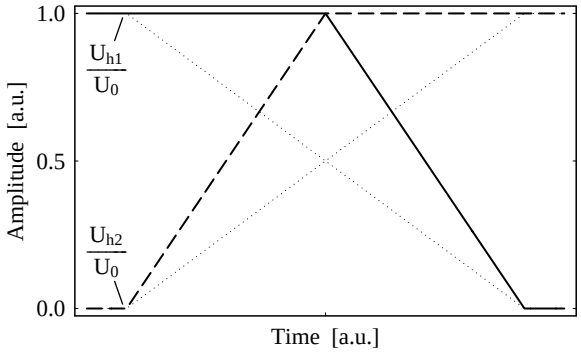

Fig. 5.25: Amplitude ramps (continuous and dashed) for harmonic hand-overs with increased bucket area during the process. The linear voltage functions (dotted) are shown for comparison only.

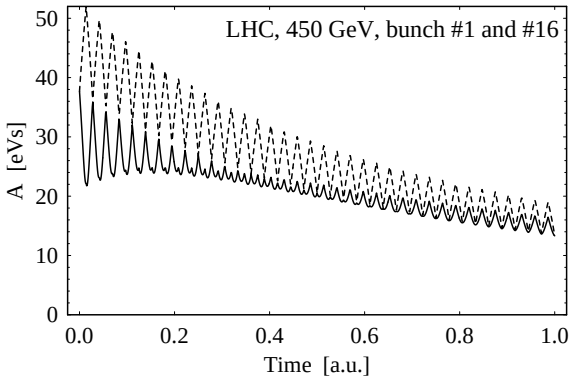

Fig. 5.26: Comparison of the bucket area development of center (dashed) and last populated bucket (continuous). Each of the 36 harmonic hand-overs is performed by voltage curves as shown in Fig. 5.25. Compared to Fig. 5.15 both buckets have a strongly modulated effective RF focusing.

amplitude at h_1 stays constant. In the middle of the process, both voltages are equal and at their maximum values. Secondly, the amplitude at the lower harmonic is decreased to zero so that the bunches are held by the RF system at h_2 alone.

Fig. 5.26 presents the modulation of center (dashed) and tail (continuous) bucket for a complete compression of 32 bunches with four empty buckets between the batches. In direct comparison to Fig. 5.15 one can clearly see that the bucket area modulation of the tail buckets is reduced by a factor of $\sqrt{2}$. However, the area of the center buckets is now also modulated significantly. Even if only at reduced strength, all other buckets are additionally modulated by the special amplitude ramps as shown in Fig. 5.25.

Batch compression with the amplitude ramping scheme discussed above has been in operation for the preparation of the primary proton beam in PS for antiproton production at CERN [73, 82]. As the bunch emittance becomes close to the bucket area limitation, one can profit from the increased effective RF focusing. For the batch combination scheme proposed for the LHC, the buckets are sufficiently large compared to the small bunch emittance at the beginning of the procedure so that the application of these modified amplitude functions during harmonic hand-over is not necessary. The bunches would even suffer from increased longitudinal

emittance dilution.

Summary of batch compression options

Several possible options to improve the batch compression manipulation are analyzed in the preceding sections. Tab. 5.4 gives an overview of these options with the bare batch compression as reference. While the standard batch compression with harmonic hand-overs having linear

	Bucket area	Long. Emittance	Add. Hardware
Bare scheme	reference	reference	none
Time optimization	unchanged	reduced blow-up of tail bunches	none
Amplitude modulation	first and last bucket equilibrated	reduced blow-up of tail bunches	two additional RF systems
Modified amplitude functions	bucket area increased	slight blow-up of center bunches	none

Tab. 5.4: Benefits of different optimization options of the long and flat bunch combination RF gymnastics.

RF amplitude ramps results in reasonable performance with respect to the dilution of the longitudinal emittance, the effect can be reduced significantly by time optimization. It is important to point out that this optimization requires no additional hardware installations.

Adding amplitude modulation during each sub-step of the harmonic increment also reduces the longitudinal dilution of the tail bunches. However, a supplementary RF system capable of generating some 40 % of the amplitude of the RF systems for the main carriers must be installed to generate the amplitude modulation side bands.

The choice of a special amplitude function during each harmonic hand-over has a negligible effect on the longitudinal emittance of the beam. As the bucket areas generated by a 40.08 MHz long and flat bunch combination RF system in the LHC are sufficiently large compared to the bunch emittance during the first steps of batch compression, there are no strong arguments to apply it for the proposed scheme to gain the factor of $\sqrt{2}$ in bucket area. However, it might be an option if the RF amplitude must be kept small for beam stability reasons during the first batch compression.

5.2.5 Bunch pair merging

After each compression, the batch is held by an RF system operated at 80.16 MHz ($h = 7128$). To reduce the number of bunches by a factor of two and to re-establish the initial RF frequency of 40.08 MHz ($h = 3564$), bunch pair merging is applied (see. Figs. 5.8 and 5.9). This type of RF manipulation has already been introduced as an example for an adiabatic procedure in Sec. 3.2.2. An improvement option to optimize the voltage ramps with respect to adiabaticity during the process analogous to the optimization of the batch compression is discussed in what follows.

Time optimization of bunch pair merging

An equivalent time optimization as presented for the batch compression in the preceding section can be performed for bunch pair merging because the initial bunches have to be accelerated

and decelerated towards the common center of gravity. According to Eq. (3.5) and (3.6), the RF potential during bunch pair merging is given by

$$W(\phi) = \frac{1}{h_0}\left[\frac{t}{\tau_{\mathrm{bm}}}\sin h_0\phi + \frac{1}{2}\left(1-\frac{t}{\tau_{\mathrm{bm}}}\right)(\cos 2h_0\phi - 1)\right], \tag{5.8}$$

where τ_{bm} denotes the time duration of the bunch merging. The position of the bucket centers is derived from the minima of the potential, namely

$$\phi_0\left(\frac{t}{\tau_{\mathrm{bm}}}\right) = \begin{cases} \pm\dfrac{1}{h_0}\arccos\dfrac{t/\tau_{\mathrm{bm}}}{2(t/\tau_{\mathrm{bm}}-1)}, & t/\tau_{\mathrm{bm}} < 2/3 \\ 0, & \text{elsewhere} \end{cases} \tag{5.9}$$

The motion of the bucket centers is illustrated in Fig. 5.27 (thick lines). After two thirds

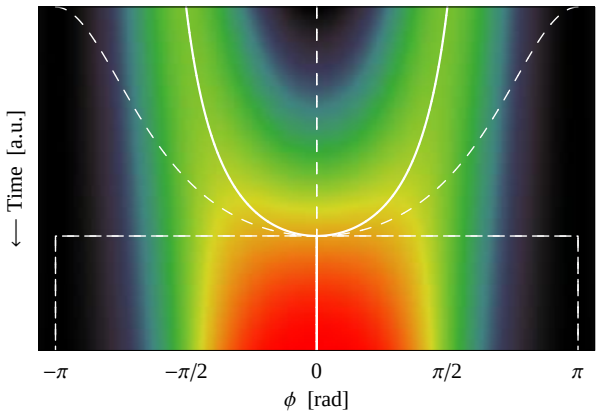

Fig. 5.27: Phase motion of the bucket centers (thick line) and the region of the sub-buckets (enclosed by the thin lines) during bunch pair merging with linear voltage ramps ($h_0 = 1$).

of the process, the separated sub-buckets vanish completely, and a single bucket reaching from $-\pi$ to π remains (Fig. 5.27, thin lines). The positions of the sub-bucket centers vary quickly, resulting in a large energy offset of the particles inside. This energy offset may cause emittance dilution when the phase velocity $d\phi_0/dt$ abruptly decreases to zero at $t/\tau_{\mathrm{bm}} = 2/3$.

Demanding that the motion of the sub-buckets should follow a cosine function so that the bunches are smoothly accelerated and decelerated during the first two thirds of the merging process

$$\phi_{\mathrm{opt}}\left(\frac{t}{\tau_{\mathrm{tm}}}\right) = \pm\frac{\pi}{4h_0}\left[3-\cos\left(\frac{3\pi}{2}\frac{t}{\tau_{\mathrm{tm}}}\right)\right] \tag{5.10}$$

the time function to get the desired bucket motion is obtained as

$$t_1(t) = \frac{\tau_{\mathrm{bm}}}{1-\dfrac{1}{2}\Big/\cos\left\{\dfrac{\pi}{4}\left[3-\cos\left(\dfrac{3\pi}{2}\dfrac{t}{\tau_{\mathrm{bm}}}\right)\right]\right\}} \tag{5.11}$$

by equating Eqs. (5.10) and (5.9). The equilibrated bucket motion is shown in Fig. 5.28; in fact, the buckets are now smoothly accelerated and decelerated toward each other. The time dependent voltage ramps are derived inserting Eq. (5.11) into Eq. (3.6) and can be finally written as

$$U_1(t) = U_0 \cdot \begin{cases} \dfrac{1}{1-\dfrac{1}{2}\Big/\cos\left\{\dfrac{\pi}{4}\left[3-\cos\left(\dfrac{3\pi}{2}\dfrac{t}{\tau_{\mathrm{bm}}}\right)\right]\right\}}, & t/\tau_{\mathrm{bm}} < 2/3 \\ t/\tau_{\mathrm{bm}}, & \text{elsewhere} \end{cases} \quad \text{and} \tag{5.12}$$

$$U_2(1) = 1 - U_1(t).$$

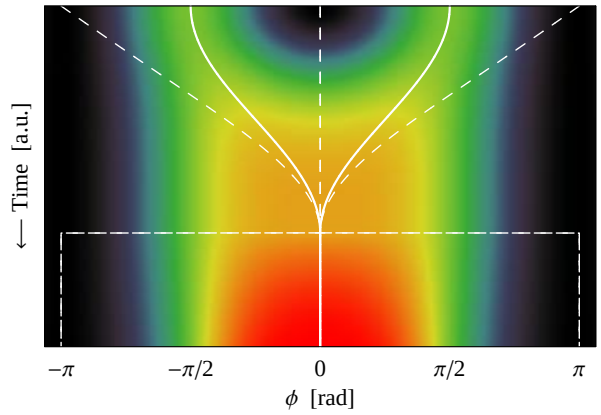

Fig. 5.28: Phase motion of the bucket centers (thick line) and the region of the sub-buckets (enclosed by the thin lines) during bunch pair merging as in Fig. 5.27 but with optimized voltage ramps ($h_0 = 1$).

Fig. 5.29 illustrates these amplitude ramps (continuous) together with the simple, linear

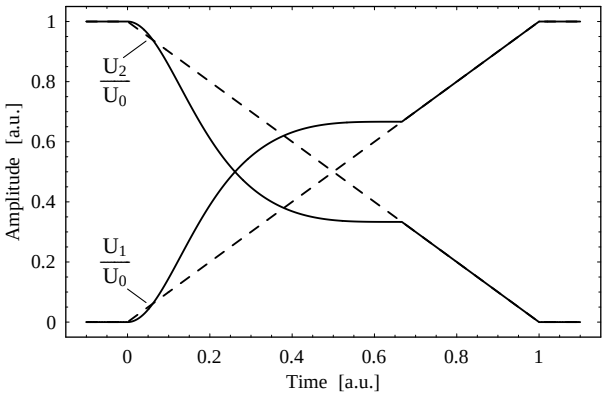

Fig. 5.29: Optimized amplitude ramps during bunch pair merging according to Eq. (5.12) for a smooth bucket motion (continuous, see Fig. 5.28) compared to linear amplitude functions (dashed, see Fig. 5.27).

amplitude functions (dashed). Comparing both functions shows a lack of adiabaticity in the middle of the process which is compensated by the time equilibration. After two thirds of the process, the sub-buckets vanish, and linear amplitude curves can be applied as the bucket center does not move anymore. The scheme has also been checked by numerical tracking calculations but no beneficial effect on the longitudinal emittance is observed. As long as the bunch merging is carried out sufficiently adiabatically, the final emittance of the merged bunch is almost the same for linear and time optimized amplitude ramps. In case of a fast bunch merging for which a longitudinal emittance blow-up is observed, the time optimized amplitude ramps sometimes even have an adverse effect on the longitudinal emittance. Therefore, the linear amplitude functions are kept for the long and flat bunch combination scheme for the LHC.

5.2.6 Final formation of long and flat bunches

The final formation of the long and flat bunch is supposed to be a rather simple RF manipulation with which the last two remaining buckets held at the harmonic 7128 (80.16 MHz) are transferred to a single flattened bucket. In fact, this RF gymnastics is very similar to a bunch pair merging which is halted in the middle of the process, except that more RF systems contribute. For simplicity the optimum final amplitudes as given in Tab. 4.3 are set linearly. Neglecting synchrotron radiation, the final longitudinal phase space of a long and flat bunch held by two respectively three different RF harmonics is illustrated in Fig. 5.30 and 5.31. Even for three RF harmonics, the resulting bunches approximates the rectangular shape reasonably well. It is worth noting that the maximum longitudinal density starting from bunches with a fixed

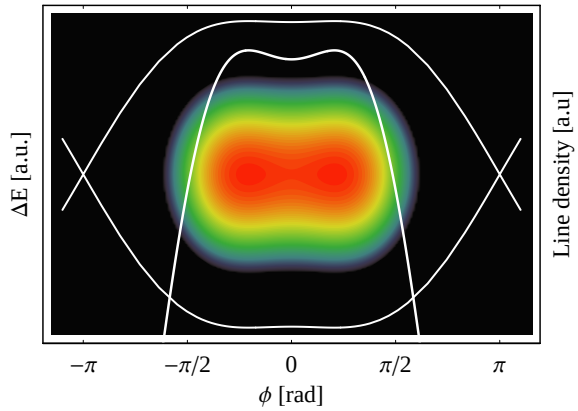

Fig. 5.30: Longitudinal phase space and line density of a final long and flat bunch held by a double harmonic RF system.

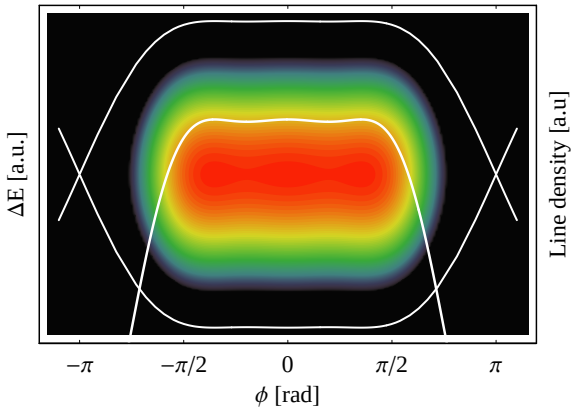

Fig. 5.31: Same representation as is Fig. 5.31 but for three multiple RF harmonics at 40.08, 80.16 and 120.24 MHz. The peak current is lowered for fixed intensity because of the longer bunches.

intensity decreases with increasing number of harmonics due to an increase of the bunch length (see Tab. 4.3).

5.2.7 The complete combination scheme

Arranging the RF manipulations successively results in a complete manipulation scheme to combine 16 or 32 bunches to one long and flat bunch. An overview of the bunch pattern during the procedure is given in Tab. 5.5, while the development of the buckets is illustrated in Figs. 5.32 and 5.33. From the bucket motion the time optimization of the batch compression

Manipulation	16 initial bunches	32 initial bunches	Energy
Initial bunch pattern	$16 \otimes b \oplus 2 \otimes e$	$32 \otimes b \oplus 4 \otimes e$	
Batch compression	$16 \otimes b \oplus 20 \otimes e$	$32 \otimes b \oplus 40 \otimes e$	
Bunch merging	$8 \otimes b \oplus 10 \otimes e$	$16 \otimes b \oplus 20 \otimes e$	
Batch compression	$8 \otimes b \oplus 28 \otimes e$	$16 \otimes b \oplus 56 \otimes e$	
Bunch merging	$4 \otimes b \oplus 14 \otimes e$	$8 \otimes b \oplus 28 \otimes e$	450 GeV
Batch compression	$4 \otimes b \oplus 32 \otimes e$	$8 \otimes b \oplus 64 \otimes e$	
Bunch merging	$2 \otimes b \oplus 16 \otimes e$	$4 \otimes b \oplus 32 \otimes e$	
Batch compression		$4 \otimes b \oplus 68 \otimes e$	
Bunch merging		$2 \otimes b \oplus 34 \otimes e$	
Acceleration	$2 \otimes b \oplus 16 \otimes e$	$2 \otimes b \oplus 34 \otimes e$	
Batch compression	$2 \otimes b \oplus 34 \otimes e$	$2 \otimes b \oplus 70 \otimes e$	7 TeV
Final formation	$1 \otimes b \oplus 35 \otimes e$	$1 \otimes b \oplus 71 \otimes e$	

Tab. 5.5: Bunch pattern during the LHC combination scheme for 16 and 32 initial bunches.

manipulations becomes clearly visible as expected: the buckets are slowly accelerated and decelerated during each process to avoid the excitation of a dipole mode at the transition from stationary to moving bucket.

To check the performance of the RF manipulation, batches of bunches consisting of some 2000 particles each have been tracked in the longitudinal phase space through the complete procedure in the LHC. To save calculation time, the acceleration itself was replaced by a simple

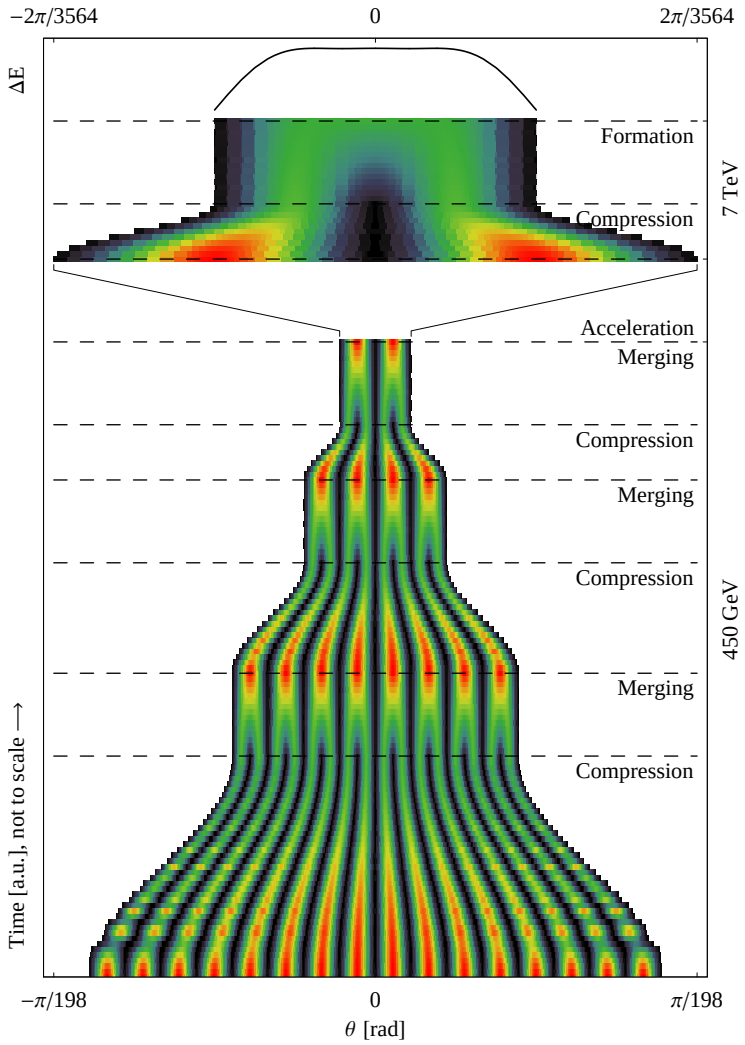

Fig. 5.32: Development of the buckets during the complete combination RF gymnastics of 16 bunches. The color scale is proportional to the height of the separatrix in energy. The final separatrix is shown on the top.

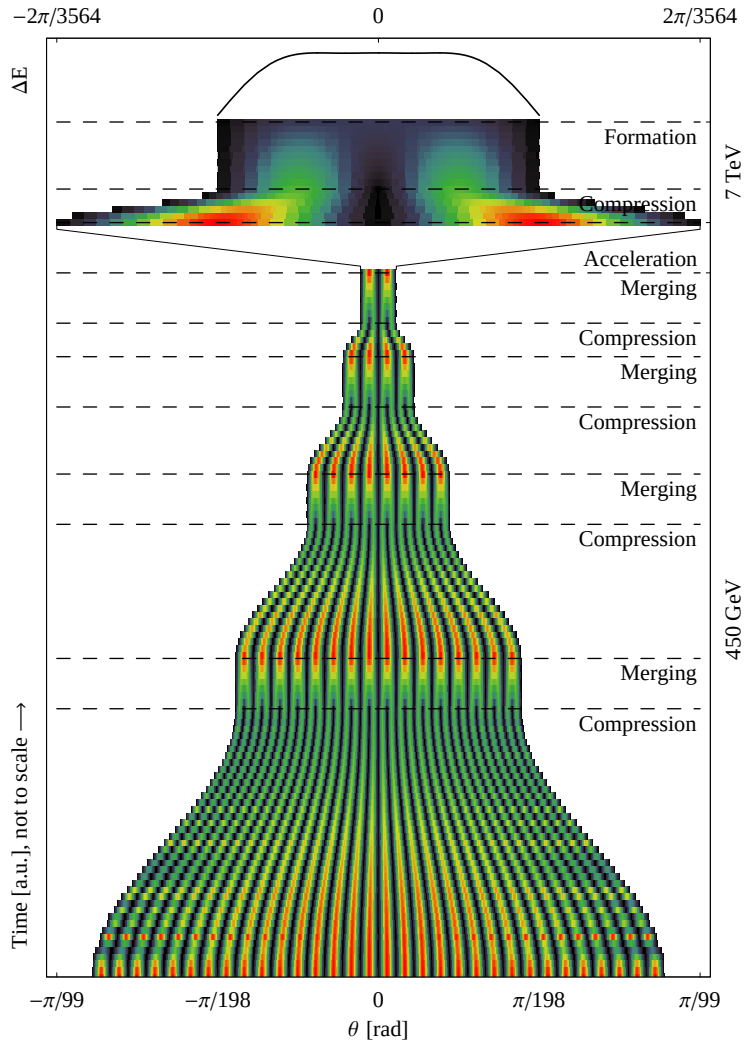

Fig. 5.33: Development of the buckets during the complete combination RF gymnastics of 32 bunches. The representation is equivalent to Fig. 5.32.

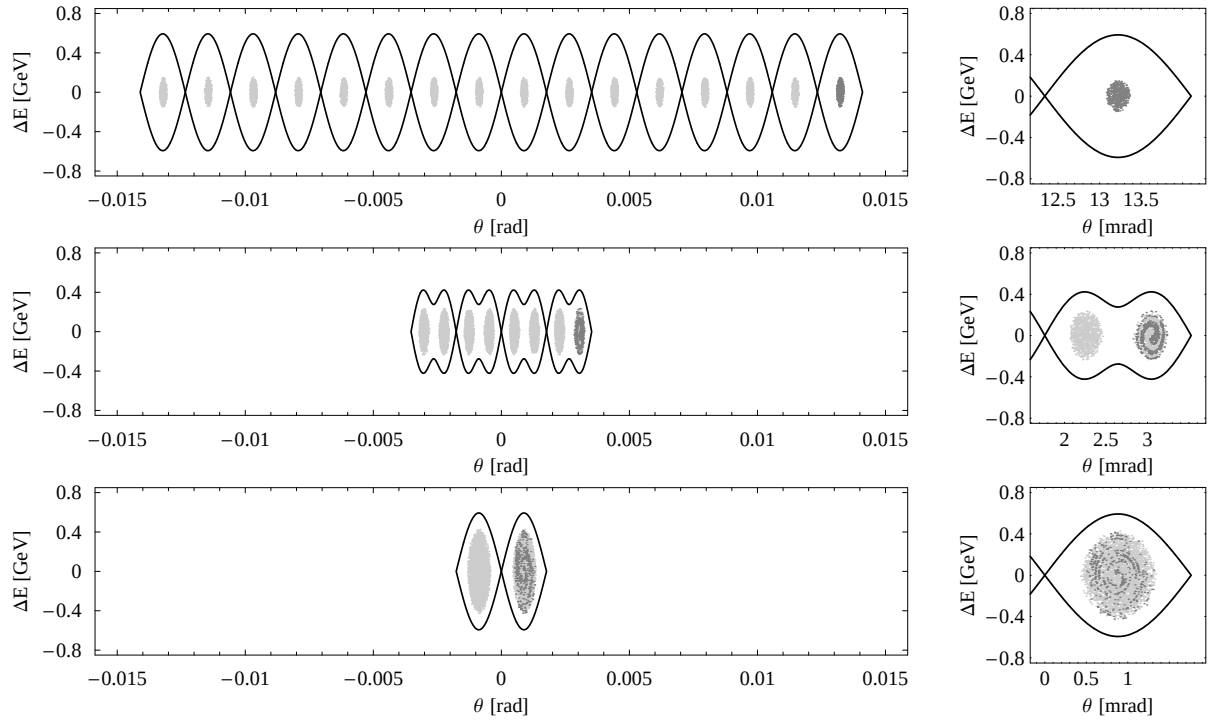

Fig. 5.34: Longitudinal phase space during the generation of a long and flat bunch at the beginning (top), in the middle (center) and at the end of the RF manipulation at the LHC flat-bottom. The last bunch of the batch (dark gray), which suffers most from the RF gymnastics, is magnified in the right plots.

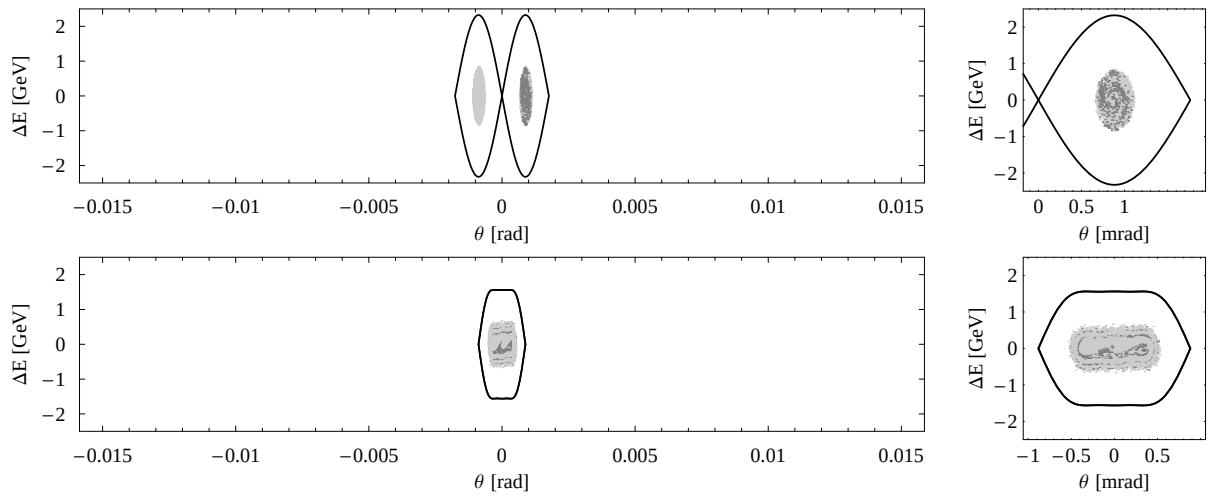

Fig. 5.35: Longitudinal phase space at beginning and end of the RF manipulation at flat-top. It is worth noting that the vertical scale is changed with respect to Fig. 5.34.

energy scaling of all particles. For the same reason, only particles within half of the batch have been taken into account as the second half of the batch is symmetric. The complete time optimized harmonic and RF amplitude program used for tracking is shown in Fig. 5.36. The acceleration in the LHC (represented by the dark gray line) will last some 20 minutes, which is more than an order of magnitude longer than the time needed for the generation of long and flat bunches. Virtually no longitudinal emittance blow-up is expected during acceleration from

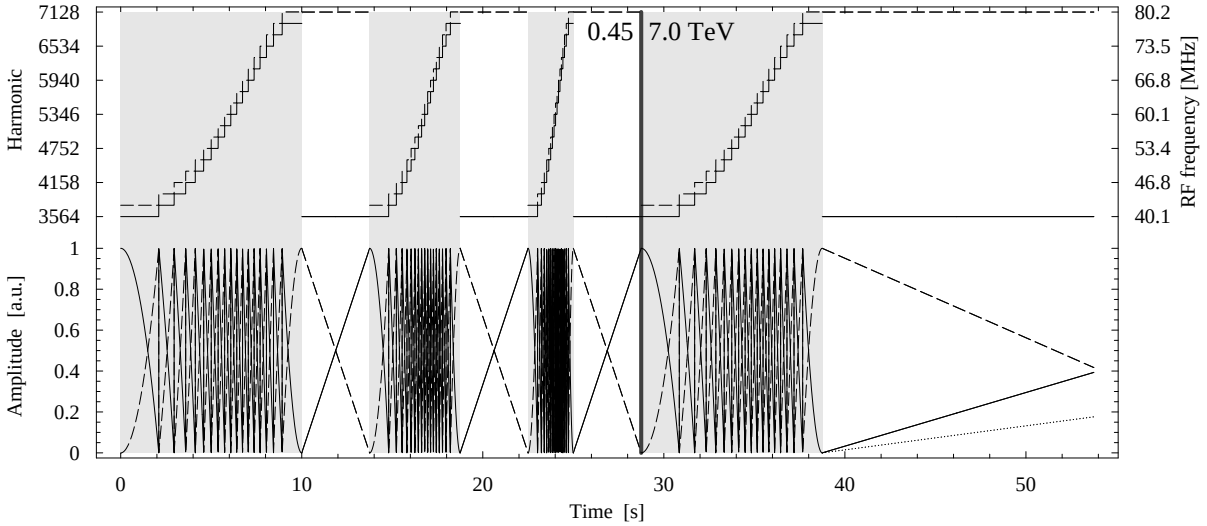

Fig. 5.36: Harmonic and voltage program for the complete long and flat bunch generation scheme. The thick gray line corresponds to acceleration with the 40.08 MHz RF system for about 20 minutes. For a detailed plot of the first batch compression see Fig. 5.20.

injection to collision energy.

To simplify the handling of the multi-bunch systems and sophisticated non-linear RF amplitude and harmonic functions, a dedicated tracking code has been developed. Firstly, this code is extremely flexible with respect to multi-bunch systems, e.g. it allows to logically merge or split bunches. All analysis functions like emittance derivation or bunch position calculation can be applied to the logical bunches individually. Secondly, as the code is implemented as a series of functional packages in Mathematica [179], most of the parameters can be handled as functions, and the full flexibility of Mathematica itself can be employed to construct them. Especially calculations including isolated or barrier buckets in combination with harmonic RF systems can be performed flexibly. Further examples of different RF manipulations which are evaluated with this code are presented in Chapter 3.

5.3 Adiabaticity and longitudinal emittance

Although adiabaticity is not a crucial parameter during the proposed long and flat bunch scheme, as the additional time needed is below 10 % of the acceleration time in the LHC, it is worth analyzing the expected emittance blow-up versus total duration of the RF manipulation.

The development of the longitudinal emittance during the combination of a batch of 32 initial 1 eVs bunches for different durations is shown in Figs. 5.37 to 5.40. Gray shaded areas are periods where batch compression is applied. The regions in between refer either to a bunch pair merging or the final formation of the long and flat bunch. As only half of the batch is tracked in the longitudinal phase space, the total emittance sums up to some 16 eVs. The upper curves in Figs. 5.37 to 5.40 show the encircling elliptic emittance of 99 % of the particles per bunch summed up over the 16 bunches. It has been re-scaled so that the initial emittance is again 16 eVs. The lower curves in the diagrams represent the sum of the RMS emittance being calculated for each bunch independently (see. Sec. 2.5.1).

The total duration has to be equal or larger than 77.5 s for the emittance blow-up to be

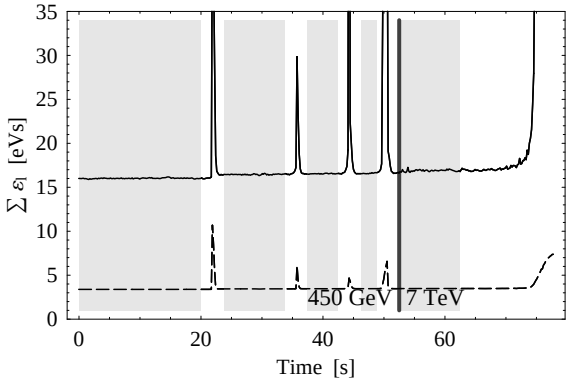

Fig. 5.37: Development of the elliptic (continuous) emittance containing 99 % of the particles and the RMS emittance (dashed) during the combination of batches of 32 bunches. The shaded areas indicate the regions of batch compression.

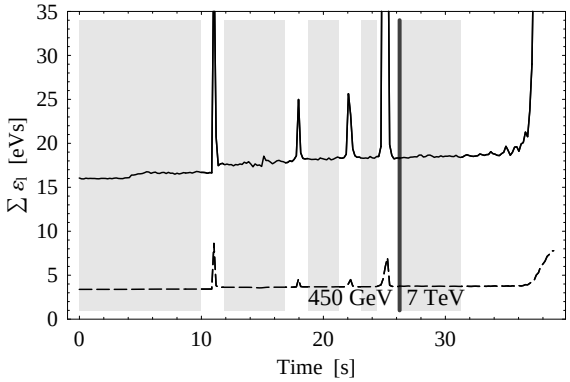

Fig. 5.38: Same representation as Fig. 5.37 but twice faster. An increased blow-up of the effective emittance becomes visible.

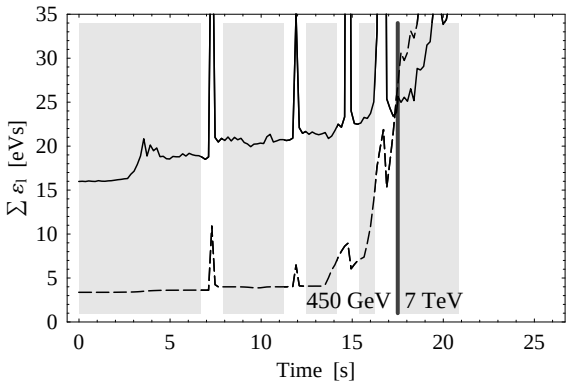

Fig. 5.39: Same representation as Fig. 5.37 but three times faster. The increased emittance growth is significantly stronger than in the figures above. During the last batch compression, particles get lost from their buckets.

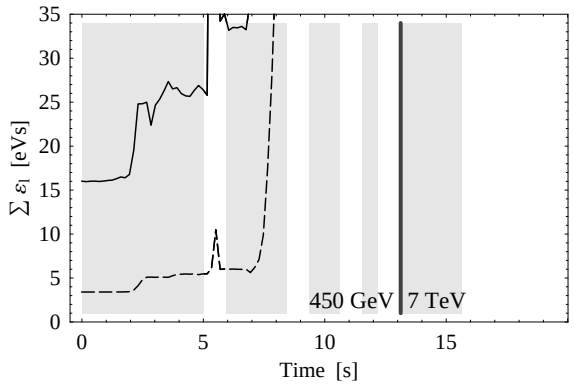

Fig. 5.40: Same representation as Fig. 5.37 but four times faster. Already during the second batch compression, particles get lost from their buckets which virtually leads to an exponential growth of the elliptic emittance because the particle distribution becomes non-elliptic.

negligible and the process quasi-adiabatic. It is worth mentioning that the apparent emittance growth at the end of the final long bunch formation comes from artifacts of the calculation method. As only half of the batch is taken into account for the tracking, the batch is virtually merged with empty bunches. This leads to an artificial blow-up of the RMS emittance by a factor of two whereas the effect on the elliptic emittance is even more severe because the final bunches have a non-elliptic longitudinal distribution.

In Fig. 5.38, where the sequence is executed in less than 39 s, first signs of emittance dilution during the RF manipulations become visible. The situation gets clearly worse when the total duration is reduced to 25.8 s (Fig. 5.39). During the last batch compression at 7 TeV particles start to escape and are lost. In the last case (Fig. 5.40) the result becomes even useless. Particles lost from the buckets cause an enormous emittance dilution, where the bunches are virtually distributed all along the circumference of the LHC and finally lost.

Therefore a total time duration of 77.5 s seems adequate. The first 52.4 s of this duration are spent on the flat-bottom at 450 GeV, while the remaining time is spent on the last batch

compression and bunch merging at 7 TeV. This additional time needed to prepare the beam has a negligible effect on the integrated luminosity.

5.4 Summary

After the detailed analysis of the RF manipulations necessary for the combination of 16 or 32 nearly nominal bunches to a long and flat bunch, the expected performance with respect to the longitudinal emittance is summarized for the 16 bunch scheme in Tab. 5.6.

	RF parameters	Emit., ε_l	$\varepsilon_l/\varepsilon_0$
SPS ejection, 450 GeV	8 MV at 200 MHz (SPS)	0.8 eVs	
Bunch rotation and LHC injection	3 MV at 40 MHz (LHC)	1.0 eVs	25 %
Blow-up by 400.8 MHz RF system	3 MV at 40 MHz	1.1 eVs	10 %
Batch compression to two bunches	2×1.5 MV at 40 ... 80 MHz	12.3 eVs	40 %
Acceleration to flat-top, 7 TeV	3 MV at 40 MHz	12.9 eVs	5 %
Final formation of the long bunch	2×1.5 MV at 40 ... 80 MHz	28.5 eVs	10 %
Collision mode with long bunches	0.8/0.8/0.4 MV at 40/80/120 MHz	28.5 eVs	

Tab. 5.6: Emittance development during the long and flat bunch generation scheme for the LHC ($16 \otimes b \oplus 2 \otimes e$). The last column $\varepsilon_l/\varepsilon_0$ presents the relative blow-up of the effective longitudinal emittance estimated for the manipulation concerned. The necessity of an additional 400.8 MHz RF system causing about 10 % emittance blow-up is due to preservation of Landau damping which is analyzed in Chapter 6.

In case of combining 32 bunches, the emittance growth is expected to be slightly larger as an additional batch compression and bunch pair merging is inserted to the RF gymnastics: the final emittance can be estimated to be around $2 \cdot 28.5\,\text{eVs} \simeq 57\,\text{eVs}$. The RF amplitudes in Tab. 5.6 must be multiplied by a factor of four. The bunch rotation in the SPS to lengthen the bunches before extraction is not required for the combination of 32 bunches, as the RF voltage is sufficient to allow a matched bunch to bucket transfer. The batch combination scheme analyzed in this chapter has several advantages compared to a superbunch scheme with barrier buckets:

Although the RF manipulations are sophisticated, RF amplitudes at no more than two harmonics have to act on the beam simultaneously. The whole scheme can be performed with two or preferably three tunable RF systems in the frequency range of 40.08 to 80.16 MHz delivering about 1.5 MV (16 initial bunches) or 6 MV (32 initial bunches). As the LHC will be filled once or twice per day, a large tuning speed is not required, and it is thus reasonable to propose the use of vacuum cavities with high quality factor tuned by a mechanically moving gap for the large frequency variation. The PS is equipped with RF cavities at 40 MHz [180, 181] and 80 MHz [182] which make use of a special pneumatic gap switch operated in the ultra high vacuum of the beam pipe physically closing the accelerating gap. These cavities are operated very reliably and could serve as a starting point for the design of the cavities needed in the LHC. The large tuning range combined with a mechanical tuning element excludes the construction of superconducting RF cavities.

Furthermore, the two basic ingredients for the batch combination RF manipulation, batch compression and bunch pair merging are well-proven to work with a reasonable performance. Finally, the proposed scheme is fast in the sense that it can be performed adiabatically within less than a few minutes. A decrease of the integrated luminosity due to the long-winded RF gymnastics is thus not expected.

The scheme has been optimized neglecting collective beam effects like instabilities before, during or after the batch combination scheme. This important issue is addressed in the subsequent chapter.

Chapter 6

Collective Effects and Beam Loading

In Chapter 4 the optimum luminosity conditions are calculated under the assumption that no other collective effects than beam-beam interactions limit the longitudinal performance of the LHC. Also the optimization of the RF manipulations to create the long and flat bunches is presented with main focus on single particle dynamics. Therefore, the following chapter addresses two major longitudinal effects provoked by high intensity bunches: collective beam instabilities and beam loading.

During storage and collision of the final long and flat bunches, the region of homogeneous line density is considered as a coasting beam, and consequently the Keil-Schnell criterion is derived from first principles and applied to the expected long bunch parameters in the first part of this chapter. Secondly, criteria for bunched beams are introduced to estimate the beam stability during the injection plateau and during acceleration of the dense bunches by the 40.08 MHz RF system. Counter-measures, like the increase of the synchrotron frequency spread, are basic ingredients to improve longitudinal stability being discussed thereafter. Finally, the influence of steady-state and transient beam loading is analyzed to ensure that the new RF system could be controlled similarly as the superconducting 400.8 MHz cavities.

6.1 Vlasov equation and Keil-Schnell criterion

A simple estimate for the longitudinal stability of a particle beam of given intensity and a well defined momentum distribution is the so-called Keil-Schnell criterion. It has been originally developed from the stability of intense coasting proton beams in the Intersecting Storage Rings (ISR) at CERN [183, 184, 185]. However, if the growth rate of the longitudinal instability is large compared to the synchrotron frequency, the synchrotron motion of particles in a bunched beam can be considered as frozen on the time scale of the instability. The criterion derived in the following section may be applied to a bunched beam as a first guess in such cases.

6.1.1 Vlasov equation and dispersion relation

The longitudinal phase space density in its most general form can be expressed by the distribution function $g = g(\theta, \Delta E/\omega)$. The two independent variables are chosen as a canonically conjugated pair (see Sec. 2.2.2). According to Liouville's theorem each infinitesimal longitudinal density fraction described by g can move in the phase space, but the total time derivative

of the distribution function stays constant:

$$\frac{d}{dt}g\left(\theta, \frac{\Delta E}{\omega}\right) = 0\,.$$

Expanding the total derivatives leads to the general equation of motion

$$\frac{\partial g(\theta, \Delta E/\omega)}{\partial \theta}\dot{\theta} + \frac{\partial g(\theta, \Delta E/\omega)}{\partial(\Delta E/\omega)}\left(\frac{\dot{\Delta E}}{\omega}\right) + \frac{\partial g(\theta, \Delta E/\omega)}{\partial t} = 0\,, \tag{6.1}$$

which is also called Vlasov equation. The dotted variables represent total time derivatives. As the revolution frequencies of the individual particles ω in a high energy beam are close to the average revolution frequency of the beam so that $\omega \simeq \omega_0$, the Vlasov equation reduces to [186]

$$\frac{\partial f(\theta, E)}{\partial \theta}\dot{\theta} + \frac{\partial f(\theta, E)}{\partial E}\dot{E} + \frac{\partial f(\theta, E)}{\partial t} = 0\,, \tag{6.2}$$

where $f = f(\theta, E)$ is the adapted longitudinal distribution function.

To drive the longitudinal instability, a perturbation voltage U_1 at an arbitrary frequency ω_1 is introduced according to $U(t) = U_1 \exp(-i\omega_1 t)$ and an individual particle gains or looses a certain amount of energy per turn given by (see Eqs. 2.2 and 2.6)

$$\Delta\dot{E} = \frac{e\omega U_1}{2\pi}e^{i(n\theta-\omega_1 t)} \simeq \frac{e\omega_0 U_1}{2\pi}e^{i(n\theta-\omega_1 t)}\,, \tag{6.3}$$

wherein n denotes the mode number of the excitation with respect to the revolution frequency. In the case of small perturbations it, can be assumed that the perturbation of the longitudinal density shows the same form as the excitation itself so that

$$f(\theta, E) = f_0(E) + f_1(E)e^{i(n\theta-\omega_1 t)} \tag{6.4}$$

is chosen as an ansatz representing the energy distribution of the unperturbed coasting beam $f_0(E)$ with a corresponding perturbation caused by $U(t)$.

Inserting the derivatives of Eq. (6.4) into the Vlasov equation under the assumption that the perturbation amplitude f_1 is much smaller than f_0, the unperturbed distribution can be written as

$$i(n\omega - \omega_1)f_1(E)e^{i(n\theta-\omega_1 t)} + \frac{df_0(E)}{dE}\frac{e\omega_0 U_1}{2\pi}e^{i(n\theta-\omega_1 t)} = 0\,. \tag{6.5}$$

Separation of the perturbation and energy integration of Eq. (6.5) gives

$$\underbrace{\int f_1(E)\,dE}_{I_1/(e\omega_0)}\; e^{i(n\theta-\omega_1 t)} = -\frac{ie\omega_0 U_1}{2\pi}e^{i(n\theta-\omega_1 t)}\int \frac{df_0(E)/dE}{\omega_1 - n\omega}\,dE\,, \tag{6.6}$$

where the left side is identified by the perturbing beam current. It is worth noting that the normalization of $f(\theta, E)$ is chosen according to

$$\int_0^{2\pi}\int_{-\infty}^{\infty} f(\theta, E)\,dE = N\,.$$

The integral on the right side of Eq. (6.6) can be written in a more convenient form by considering that

$$f_0(E) = \frac{d\omega}{dE}f_0^*(\omega) = -\frac{\eta}{\beta^2}\frac{\omega_0}{E}f_0^*(\omega)\,,$$

and the Vlasov equation becomes

$$I_1 e^{i(n\theta-\omega_1 t)} = \frac{ie^2\omega_0^3\eta}{2\pi E\beta^2} U_1 e^{i(n\theta-\omega_1 t)} \int \frac{df_0^*(\omega)/d\omega}{\omega_1 - n\omega}\, d\omega\,. \tag{6.7}$$

The term on the right side contains in fact the spectral component of the beam transfer function of a coasting beam at ω_1. Introducing a complex longitudinal coupling impedance between beam current $U_1 = -Z_\parallel I_1$ to feedback the beam current perturbation as an excitation, the dispersion relation of the coasting beam reduces to [61, 187]

$$1 = -\frac{ie^2\omega_0^3\eta Z_\parallel}{2\pi E\beta^2} \int \frac{df_0^*(\omega)/d\omega}{\omega_1 - n\omega}\, d\omega\,. \tag{6.8}$$

This dispersion relation is used as a starting point to derive a criterion for longitudinal beam stability.

6.1.2 Stability diagrams

For the calculation of stability diagrams and algebraic conditions for longitudinal beam stability the transformation of the dispersion relation to normalized variables is convenient. The width of one half of the half maximum frequency spread is defined by $S = -\eta\omega_0\Delta p/p$, where $\Delta p/p$ is referred to as half momentum spread at half maximum height[1]. Furthermore, the normalized frequency deviation of beam harmonic and excitation frequency from the average harmonic of the revolution frequency are defined by

$$\left.\begin{array}{rc} & n\omega - n\omega_0 = xnS \\ \text{and} & \omega_1 - n\omega_0 = x_1 nS \end{array}\right\} \; \omega_1 - n\omega = (x_1 - x)nS\,.$$

The distribution in revolution frequencies $f_0^*(\omega)$ is converted according to

$$F_0(x) = \frac{2\pi S}{N} f_0^*(x)\,,$$

which is then normalized properly. For energy distributions $F_0(x)$ being symmetric around $x = 0$, the normalization conditions can be written as [189]

$$\int_{-\infty}^{\infty} F_0(x)\, dx = 1 \qquad \text{and} \qquad F_0(x = \pm 1) = \frac{1}{2} F_0(x = 0)\,. \tag{6.9}$$

Finally, the normalized dispersion relation Eq. (6.8) in the new variables x, x_1 becomes

$$1 = \frac{ieI_0 Z_\parallel}{2\pi E\beta^2\eta(\Delta p/p)^2 n} \int \frac{dF_0(x)/dx}{x - x_1}\, dx\,, \tag{6.10}$$

where I_0 denotes the average beam current. As the longitudinal impedance $Z_\parallel$ is complex in general, Eq. (6.10) can be also represented in terms of a normalized impedance:

$$1 = (U' - iV') \int \frac{dF_0(x)/dx}{x - x_1}\, dx \quad \text{and}$$

$$U' - iV' = -\frac{eI_0}{2\pi E\beta^2\eta(\Delta p/p)^2} \left(\mathrm{Im}\{Z_\parallel/n\} - i\mathrm{Re}\{Z_\parallel/n\}\right)\,. \tag{6.11}$$

[1] Some authors define $\Delta p/p$ as full momentum spread at half height [188] which is e.g. more convenient for the analysis of stacked beams.

This relation couples the normalized impedance $U' - iV'$ to the normalized complex frequency shift x_1 induced by the perturbation. The regions of impedances where the beam is stable or unstable can be explored by expressing the perturbing part of the beam distribution $f(\theta, E)$ in terms of this induced frequency shift x_1. As this contribution is proportional to $\exp[i(n\theta - \omega_1 t)]$, its frequency can be written as $n\dot{\theta} = n\omega - \omega_1 = nx_1 S$ so that

$$\exp[i(n\theta - \omega_1 t)] = \exp\left(i\mathrm{Re}\{x_1\} n\eta\omega_0 \frac{\Delta p}{p} t\right) \cdot \exp\left(-\mathrm{Im}\{x_1\} n\eta\omega_0 \frac{\Delta p}{p} t\right) .$$

In fact, the real part of the complex frequency shift x_1 leads to a frequency displacement, while the imaginary part of x_1 defines whether the excitation is damped ($\mathrm{Im}\{x_1\} < 0$ for $\gamma > \gamma_{\mathrm{tr}}$) or exponentially excited ($\mathrm{Im}\{x_1\} > 0$ for $\gamma > \gamma_{\mathrm{tr}}$). The trajectory in the complex impedance plane, for which the imaginary part of x_1 is zero, defines the limitation of longitudinal stability. Frequency shift and growth rate are given by

$$\Delta\omega_1 = -\eta\omega_0 \frac{\Delta p}{p} \mathrm{Re}\{x_1\} \quad \text{and} \quad \frac{1}{\tau} = -\eta\omega_0 \frac{\Delta p}{p} \mathrm{Im}\{x_1\} . \tag{6.12}$$

The full stability diagram of a given distribution is generated by evaluating the parameters $U'(x_1)$ and $V'(x_1)$ from Eq. (6.11) for different complex normalized frequency shifts x_1; preferably the parameter x_1 is chosen so that either its real or imaginary part is held constant. An example for such a stability diagram of a quartic distribution

$$F(x) = \frac{15a}{16}(1 - a^2x^2)^2 \quad \text{for} \quad |x| < \frac{1}{a} \quad \text{and} \quad a = \sqrt{1 - 1/\sqrt{2}}$$

is given in Fig. 6.1. The gray shaded area is the region of normalized impedances $U' - iV'$,

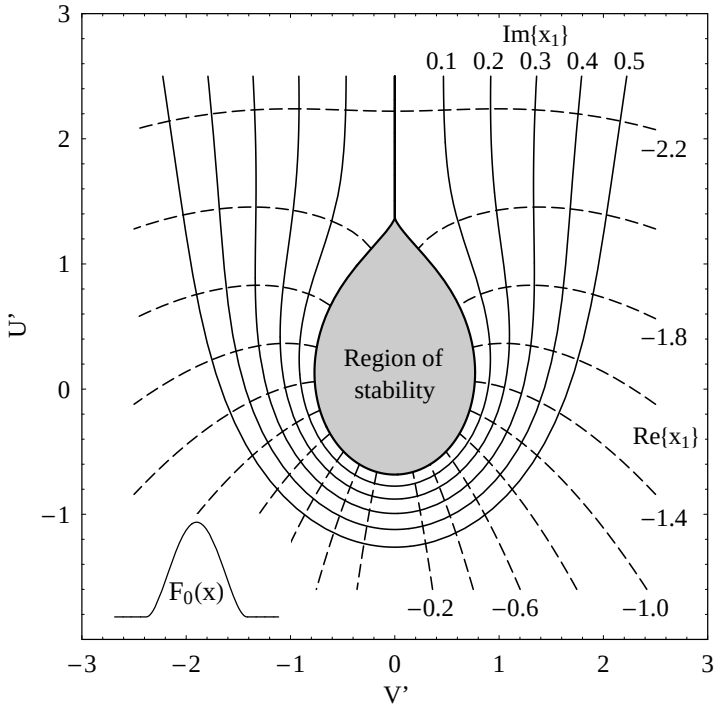

Fig. 6.1: Stability diagram of a coasting beam with a quartic energy distribution, $F_0(x) \propto (1 - a^2x^2)^2$. The gray shaded area represents the region of stability as $\mathrm{Im}\{x_1\}$ is negative ($\gamma > \gamma_{\mathrm{tr}}$) and an excitation of the beam is thus damped. The imaginary part of x_1 is kept constant along the continuous lines, while the real part remains unchanged along the dashed lines.

which are tolerable for a stable beam. To simplify the calculation of stability diagrams, the

dispersion integral from Eq. (6.11) can be integrated partially for distribution functions $F_0(x)$ which vanish at $x = \pm\infty$ so that

$$U' - iV' = 1 \Big/ \int \frac{dF_0(x)/dx}{x - x_1}\, dx = 1 \Big/ \int \frac{F_0(x)}{(x - x_1)^2}\, dx \ . \tag{6.13}$$

As the integral from Eq. (6.11) contains a singularity within its integration limits are furthermore split into real and imaginary part according to

$$\int \frac{dF_0(x)/dx}{x - x_1}\, dx = \mathrm{PV} \int \frac{dF_0(x)/dx}{x - x_1}\, dx + \mathrm{sign}\left(\mathrm{Im}\{x_1\}\right)\, i\pi\, \frac{\partial F_0(x)}{\partial x}\bigg|_{x=x_1} \tag{6.14}$$

so that a numerical computation of the stability diagrams can be performed straightforward. The principal value is defined according to

$$\mathrm{PV} \int_{-\infty}^{\infty} \frac{dF_0(x)/dx}{x - x_1}\, dx = \lim_{\epsilon \to 0} \left[\int_{-\infty}^{x_1 - \epsilon} \frac{dF_0(x)/dx}{x - x_1}\, dx + \int_{x_1 + \epsilon}^{\infty} \frac{dF_0(x)/dx}{x - x_1}\, dx \right] .$$

6.1.3 Keil-Schnell criterion

Although the explicit form of the region of beam stability is different for each distribution function $F_0(x)$, it is essentially centered around the origin of the stability diagram for reasonable distributions. The stability limitation being defined by $\mathrm{Im}\{x_1\} = 0$, as shown for a quartic distribution in Fig. 6.1, is illustrated for different functions $F_0(x)$ in Fig. 6.2 [189, 190, 191]. A common, stable region which is shared by most of the momentum distribution functions is

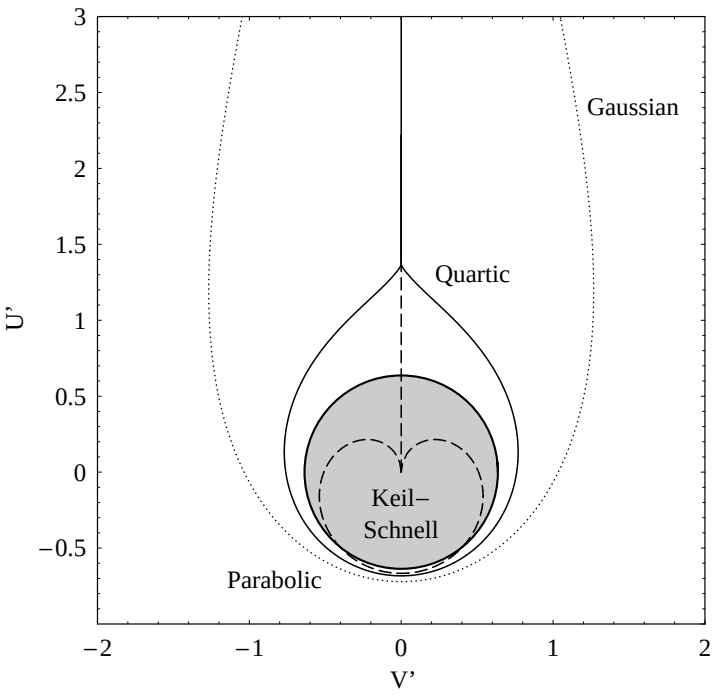

Fig. 6.2: Stability limitation for different momentum distributions in the complex impedance plane. The stable region of a Gaussian beam (dotted) is significantly larger than that of a beam with quartic distribution (continuous). The parabolic distribution shows the smallest area of stability. The gray shaded circle illustrates the stability assumption for the Keil-Schnell criterion.

represented by a simple circle (gray shaded area), whose radius can be described by $F \cdot 2/\pi$, where F is a from factor of the order of unity and the circle in Fig. 6.2 has a radius of $2/\pi$. It is important to point out that the tails of the momentum distribution $F_0(x)$ have a significant

influence on the longitudinal beam stability. The stability region shrinks for distributions without tails like parabolic or elliptic compared to Gaussian or quartic beams.

By replacing the inverse of the dispersion integral in Eq. (6.11) by the circular approximation leads to a stability limitation for the absolute tolerable impedance, namely [192]

$$\left|\frac{Z_\parallel}{n}\right| \leq F\frac{4E\beta^2|\eta|(\Delta p/p)^2}{eI_0}\,. \tag{6.15}$$

Originally published to estimate the beam stability in the ISR [188], this criterion has been proven to be very useful and is therefore known as Keil-Schnell criterion. In fact, the stability limitation depends inversely on the total beam current, and it is proportional to the square of the momentum spread. Beams with a sharp momentum spread are therefore prone to longitudinal instabilities.

Although the Keil-Schnell criterion has been derived for coasting beams only, its range of validity can be extended by considering the stability criterion as a local condition applied to a local fraction of the beam. If the growth rate of the instability (see Eq. 6.12) is much faster than the synchrotron motion, the external RF forces can be neglected and, as a first estimation, it may even be applied to bunched beams [193, 194, 195]. Consequently, the average beam current I_0 as well as the momentum spread $\Delta p/p$ have to be exchanged by their local values. This effect of a very fast growing bunch excitation is referred to as microwave instability as its presence is accompanied by a bunch signal in the microwave range above several hundred MHz, well above the bunch frequency [196]. It is worth noting that the term microwave instability is also used for several other instabilities having a high frequency bunch signal as its characteristic signature.

6.1.4 Stability of the LHC beam during long and flat bunch collision

By definition, the long and flat bunches or superbunches in collision mode have a region of nearly homogeneous line density with a length of at least some 10 ns. This coasting beam section can be treated as such if the inverse instability growth rate is faster than the drift time of the particles between the two bunch ends and if the coasting beam section is excited at frequencies well above 100 MHz.

The effective threshold impedance according to the Keil-Schnell criterion for coasting beams from Eq. (6.15) is illustrated in Fig. 6.3 for the long and flat bunches and compared to the maximum longitudinal density of nominal and low emittance nominal bunches. The total longitudinal impedance in an accelerator is evaluated by summing up all contributing elements installed in the vacuum chamber, each of which is analyzed by means electromagnetic field calculations for its specific geometry. A complete table of impedance estimations for the contributing elements is given in [197] and the total longitudinal impedance is estimated to $|Z_\parallel/n| = 0.076\,\Omega$.

Compared to the instability thresholds in Fig. 6.3, even the case of a superbunch with a longitudinal density at the beam-beam limit corresponding to a local current of some 131 A is stable with respect to the Keil-Schnell criterion. The limit is found to be around $|Z_\parallel/n| = 0.165\,\Omega$. It is worth noting that the local density of the nominal bunches as well as those of the low emittance nominal bunch has more than one order of magnitude of safety margin.

6.2 Landau damping

The so-called Landau damping is an effect of apparent natural damping which occurs when an ensemble of oscillators with slightly different resonant frequencies is excited by a coherent

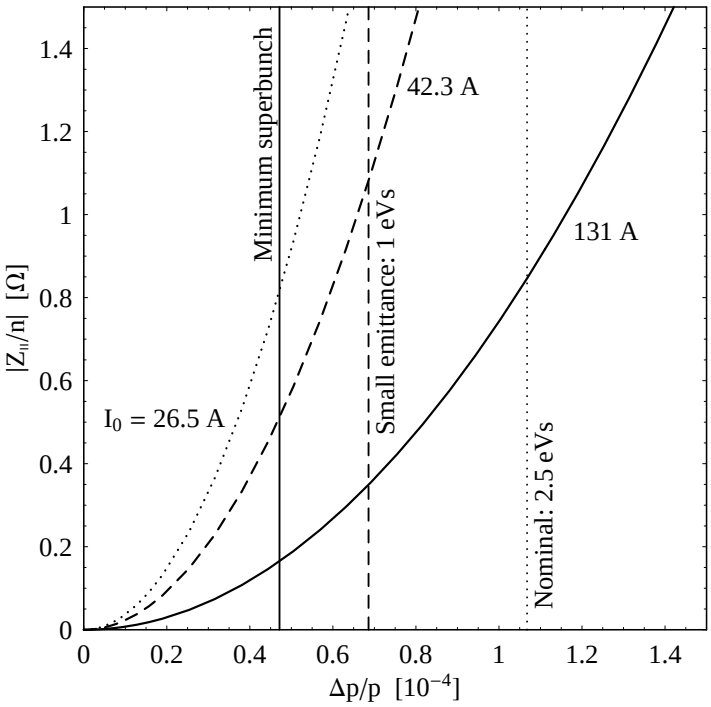

Fig. 6.3: The graphs represent the Keil-Schnell limit of the tolerable, effective longitudinal broad band impedance to preserve the stability of the coasting beam section of a long and flat bunch or a superbunch at collision energy. It is given for a local beam current of 26.5 (dotted), 42.3 (dashed) and 131 A (continuous) which corresponds to the local density of the nominal, the low emittance nominal (see Tab. 5.2 and the minimum emittance long or superbunch (see Tabs. 4.5 and 4.6). The momentum spread as half width half maximum of the corresponding parabolic distribution is indicated by the vertical lines.

signal [198]. In fact, a particle bunch treated in the longitudinal phase space plane is such a system: the individual particles oscillate around the center of gravity of the bunch while their individual oscillation frequencies vary with their maximum phase deviation from the center. This distribution of frequencies is calculated in Sec. 2.2.6 and in App. D. As becomes clear from Fig. 6.4, the beam behaviour of the individual particles depends on the RF configuration, even though the bunch projections might be identical. Therefore, only a small fraction of the particles in a bunch with a large synchrotron frequency spread (Fig. 6.4) are excited by an harmonic excitation, whereas a bunch with a small synchrotron frequency spread may be excited easily as a whole.

Landau damping of the longitudinal dipole motion can be investigated by calculating the average bunch motion from the subset of individual particles within the bunch [199]. The synchrotron oscillation of a single particle driven by a harmonic excitation is described by

$$\ddot{\phi} + \omega_s^2 \phi = e^{-i\omega t}\,, \tag{6.16}$$

where ϕ denotes the phase deviation from the bucket center and ω is the frequency of the driving term. The driving amplitude is arbitrarily normalized to unity. The single particle solution of Eq. (6.16) proportional to the driving term can be written as

$$\phi(t) = \frac{\hat{\phi}}{\omega_s^2 - \omega^2} e^{-i\omega t}\,.$$

The distribution of resonance frequencies of N particles in the bunch is represented by the function $G(\omega) = 1/N\, dN/d\omega_s$ and is normalized so that the integral over all frequencies gives unity. It is worth mentioning that this frequency distribution is also symmetric with respect to negative frequencies: $G(\omega_s) = G(-\omega_s)$. In fact, $G(\omega_s)\, d\omega_s$ is the fraction of individual oscillators having a resonance frequency between ω_s and $\omega_s + d\omega_s$.

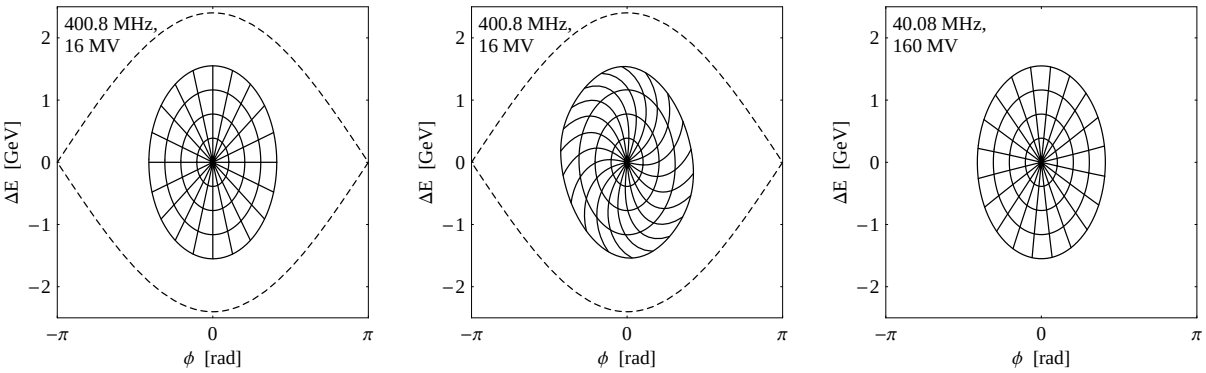

Fig. 6.4: Tracking of particles on a net to illustrate a stationary bunch during one period of the linear synchrotron frequency. The left phase space shows the initial bunch. After one synchrotron period in a 400.8 MHz bucket with an RF voltage of 16 MHz (center) it becomes obvious that the synchrotron frequency in the outer regions of the bunch is reduced. The right phase space shows the same bunch in a matched 40.08 MHz bucket. The separatrix is not visible as it is far away from the bunch. The whole bunch can be considered to be within the linear region of the bucket so that no dispersion is visible. It is important to point out that the RF amplitude of 160 MV has only been chosen as an example to obtain matched bunches under the same conditions as for the 400.8 MHz system.

The average dipole motion of the whole ensemble of oscillators is expressed by

$$<\phi(\omega)>=\left[\int_{-\infty}^{\infty}\frac{G(\omega_s)}{\omega_s^2-\omega^2}\,d\omega_s\right]e^{-i\omega t}\,, \tag{6.17}$$

where the integration over negative frequencies is included for convenience. Part of the integrand can be expanded according to [200, 201]

$$\frac{1}{\omega_s^2-\omega^2}=\frac{1}{2\omega}\left(\frac{1}{\omega_s-\omega}-\frac{1}{\omega_s+\omega}\right)$$

so that the average bunch motion Eq. (6.17) reduces to

$$<\phi(\omega)>=\frac{1}{2\omega}\left[\int_{-\infty}^{\infty}\frac{G(\omega_s)}{\omega_s-\omega}\,d\omega_s-\int_{-\infty}^{\infty}\frac{G(\omega_s)}{\omega_s+\omega}\,d\omega_s\right]e^{-i\omega t}=\left[\frac{1}{\omega}\int_{-\infty}^{\infty}\frac{G(\omega_s)}{\omega_s-\omega}\,d\omega_s\right]e^{-i\omega t}\,. \tag{6.18}$$

The singularity of the integrand at $\omega=\omega_s$ leads to a complex solution of the integral in Eq. 6.18 which can be split into real and imaginary part according to

$$<\phi(\omega)>=\frac{1}{\omega}\left[\mathrm{PV}\int_{-\infty}^{\infty}\frac{G(\omega_s)}{\omega_s-\omega}\pm i\pi G(\omega)\right]e^{-i\omega t}\,, \tag{6.19}$$

where PV is again the principal value excluding the singularity. From the velocity variation of the bunch center, namely

$$\frac{d}{dt}<\phi(\omega)>=-i\omega<\phi(\omega)>=\left[\pi G(\omega)-i\mathrm{PV}\int_{-\infty}^{\infty}\frac{G(\omega_s)}{\omega_s-\omega}\,d\omega_s\right]e^{-i\omega t}\,, \tag{6.20}$$

it becomes clear that the first term is in phase with the initially applied driving term (see Eq. 6.17), whereas the second term always has a phase deviation of $\pi/2$. Therefore, the in phase contribution absorbs energy from the driving force and leads to a virtual damping of

the average dipole motion of the bunch. However, only the average motion of the ensemble of oscillating particles is damped and individual particles may be excited enormously. It is interesting to note that the damping term is proportional to the value of the density function at the excitation frequency and that it vanishes once the excitation frequency is outside of the synchrotron frequency spread so that $G(\omega) = 0$. The preservation of Landau damping is therefore mandatory to prevent particle beams from exciting themselves due to self-induced perturbations. Comparing Eq. (6.20) with the dispersion integral Eq. (6.8) for coasting beams reveals that coasting beam stability is based on Landau damping.

6.3 Longitudinal bunched beam stability in the LHC

There are two different classes of longitudinal bunched beam instabilities. On the one hand, single bunch instabilities are based on the excitation of longitudinal oscillations of the particle distribution within the bunch. On the other hand, multi-bunch instabilities arise because of a coupling between different bunches within a batch so that different bunches oscillate in phase with respect to each other. The order of the single bunch oscillation mode is identified by the mode number m whereas the mode along the bunch train of M equal bunches in the accelerator is denoted as $n = 1 \dots M$ [202]. The phase advance between two bunches is described by $2\pi\, n/M$. Considering that the bunch shape oscillation is in fact a rotation of the perturbed longitudinal distribution with the synchrotron frequency and that the coupled bunches circulate with the revolution frequency, the excitation frequency for all possible modes can be written as

$$\omega = h\omega_0 \pm m\omega_s \pm n\omega_0 = \omega_{\mathrm{RF}} \pm m\omega_s \pm n\omega_0\,. \tag{6.21}$$

The following analysis of bunched beam stability is limited to equidistant bunches held by single harmonic RF system and is not applicable to the bunches during RF gymnastics, where more RF systems act on the bunches simultaneously.

6.3.1 Bunch shape oscillations

The first six single bunch modes are illustrated in Fig. 6.5. One can observe that the number of nodes in the line density plots corresponds to the mode number. The oscillation frequencies of the modes are directly given by $\omega = m\omega_s$, which becomes obvious considering that a distorted distribution of the mode m just needs to be rotated by $2\pi/m$ to reproduce itself.

6.3.2 Coupled bunch oscillation modes

The second kind of possible oscillations of a bunch train in a circular accelerator are coupled bunch modes. These modes are mostly excited by resonators with a high quality factor, and therefore a narrow bandwidth, which are coupled to the beam. The long time constant of the field decay in the resonators bridges the time distance between two or even more bunches. In fact, the cavity is excited by a bunch passing through and the excited electromagnetic fields act back on the subsequent bunch train. The number of possible oscillation modes is identical to the number of bunches in the accelerator. An illustration of the four longitudinal coupled bunch modes of a bunch train consisting of four bunches is given in Fig. 6.6. For the mode number n the phase position of the M bunches is calculated according to [203]

$$\Delta\phi_i(t) = \Delta\phi_0 \cos\left(\omega t - 2\pi\frac{n}{M}i\right)\,, \tag{6.22}$$

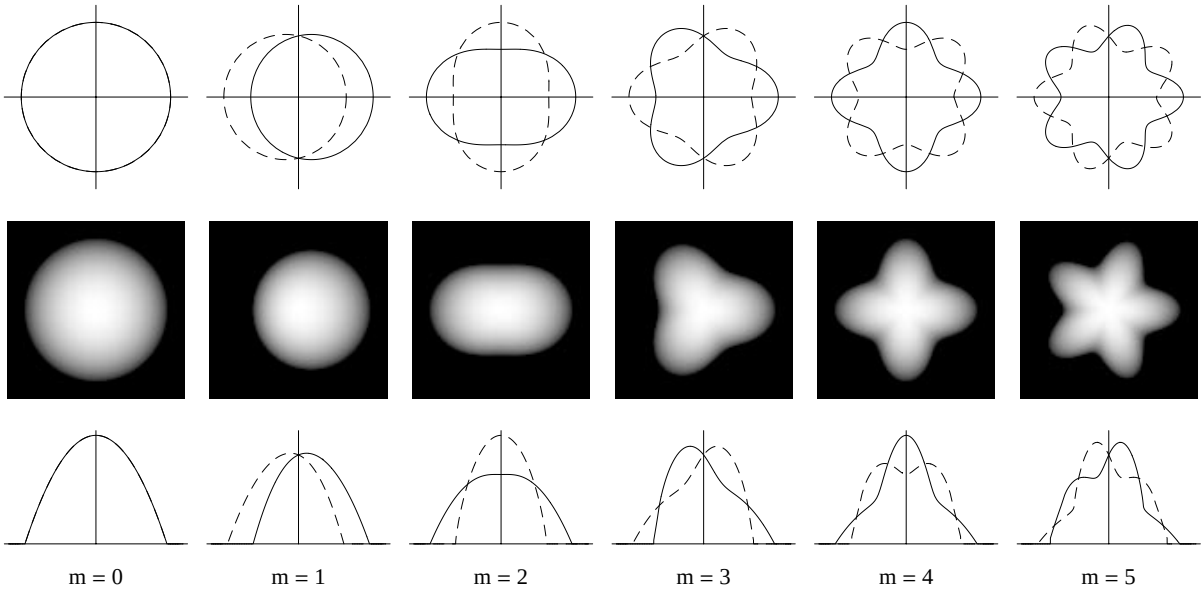

Fig. 6.5: Illustration of the single bunch oscillation modes $m = 0 \ldots 5$. Whereas the upper row shows the bunch outline for two different phases of the oscillation, the center row presents the longitudinal distribution assuming parabolic bunches. The resulting line density is sketched in the bottom row. The zeroth mode just results in a stationary parabolic bunch.

where i is the number of the bunch and $\Delta\phi_0$ its maximum phase excursion. The Landau damping time constant of single bunch higher order oscillation modes as well as coupled bunch modes can be larger or smaller as their inverse growth rate resulting in stable, damped or exponentially growing oscillations.

6.3.3 Narrow band resonator impedances

The complex synchrotron tune shift for bunched beams and finally a criterion for the longitudinal stability of bunched beam can be derived similarly to the calculation of the Keil-Schnell criterion for coasting beams as shown in Sec. 6.1. However, adding the synchrotron motion introduces considerable complexity to the calculation so that only the basic ideas shall be given in this report. The full derivations and the underlying theory can be found in [204, 205, 206, 207]. The procedure to derive longitudinal bunched beam instabilities is summarized as follows [208]:

As shown for the case of a coasting beam, a reasonable unperturbed beam distribution is chosen firstly and a small perturbation is added to it. Secondly, the local density $f(\tau, E, z)$ is derived and inserted into the Vlasov equation, wherein the external force due to the synchrotron motion is also taken into account. The ansatz for the perturbed local density function, namely

$$f(\tau, \Delta E, z) = f_0(\tau, \Delta E) + f_1(\tau, \Delta E, z)\,, \tag{6.23}$$

is chosen in such a way that only the perturbed part depends on the longitudinal position z. The unperturbed part is not influenced by the excitation caused by preceding beam particles, however is contributes to the excitation of subsequent beam. It is worth noting that the coordinate system can be defined so that the unperturbed synchrotron motion of the single particles is transformed to circles in a normalized longitudinal phase space. This allows an easy separation

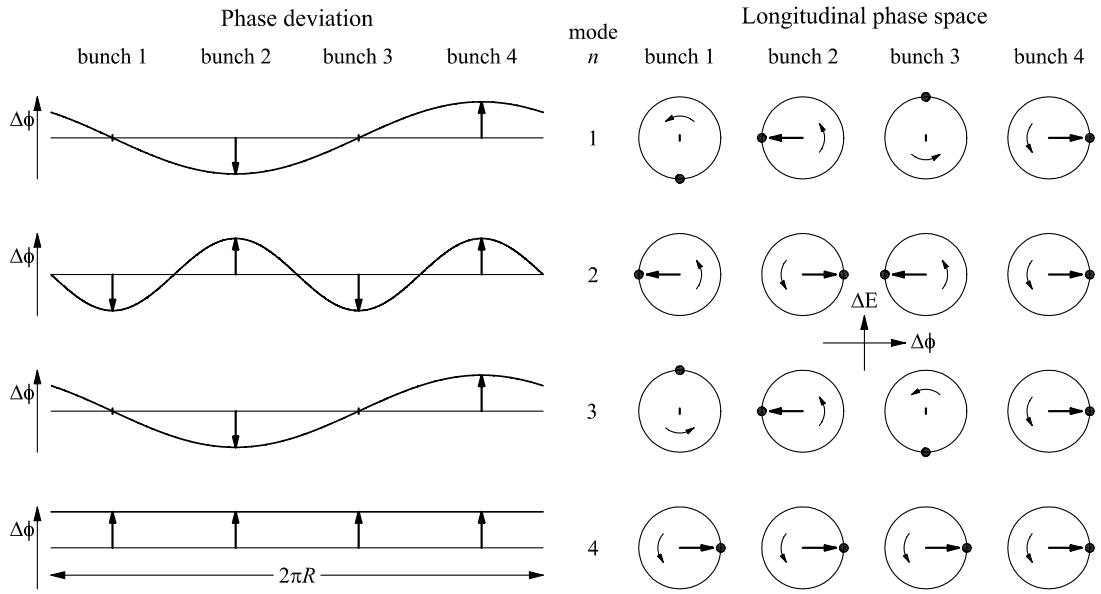

Fig. 6.6: Illustration of the possible coupled bunch modes of four bunches in a circular accelerator. Besides of a phase difference of π, the first and the third mode are identical in this case.

of the radial modes (illustrated in Fig. 6.5), and the local density can be written as

$$f_0(r)\, d\tau\, dE = N g_0(r) r\, dr\, d\phi \tag{6.24}$$

where $g_0(r)$ is the radial distribution normalized according to

$$\int_0^{2\pi} \int_0^{\infty} g_0(r) r\, dr\, d\phi = 1\,. \tag{6.25}$$

It should be pointed out that the radius is defined in time units $[r] = [\text{time}] = \text{s}$. Finally one ends up with a dispersion relation similar to the dispersion relation of coasting beams but including a general longitudinal force. This force must be expressed in such a way that the influence of preceding on subsequent particles passing through the accelerator is incorporated.

The dispersion relation for a perturbation excited by a narrow band cavity with the shunt impedance R_s at the resonance frequency ω_r can be written as [207]

$$1 = -i \frac{e^2 N R_s m M \eta \omega_0^2}{2\pi E \beta^2 \omega_s \omega_r} D(\alpha \tau_{\text{sep}}) \int_0^{\infty} \frac{dg_0(r)}{dr} \frac{J_m^2(\omega_r r)}{\omega - m\omega_s(r)}\, dr\,, \tag{6.26}$$

where J_m denotes the m-th Bessel function of the first kind. The parameter α represents the inverse filling time $\omega_r/(2Q)$ of the cavity and the function

$$D(\alpha \tau_{\text{sep}}) = -i 2\alpha \tau_{\text{sep}} \sum_{k=0}^{\infty} e^{2\pi i k n/M - k(\alpha - i\omega)\tau_{\text{sep}}} \sin(k\omega_r \tau_{\text{sep}})$$

describes the coupling between the bunches and the resonator, taking the bunch spacing field decay within the bunch spacing into account [202]. In case of a small relative synchrotron frequency spread $[\omega_s(r) - \omega_s]/\omega_s \ll 1$, the complex synchrotron frequency shift is expressed by

$$\Delta\omega = \omega - m\omega_s = i \frac{e^2 N M R_s \eta \omega_0^2}{8\pi^2 E \beta^2 \omega_s \hat{\tau}} D(\alpha \tau_{\text{sep}}) F_m(2\omega_r \hat{\tau}) \tag{6.27}$$

with

$$F_m(2\omega_r\hat{\tau}) = -\frac{4\pi m\hat{\tau}}{\omega_r}\int_0^\infty \frac{dg_0(r)}{dr}J_m^2(\omega_r r)\,dr\,.$$

The form factor F_m is plotted for a parabolic (left) and quartic (right) distribution in Fig. 6.7. The bunches have a total length of $2\hat{\tau}$. It is worth noting that Eq. (6.27) is consistent with the

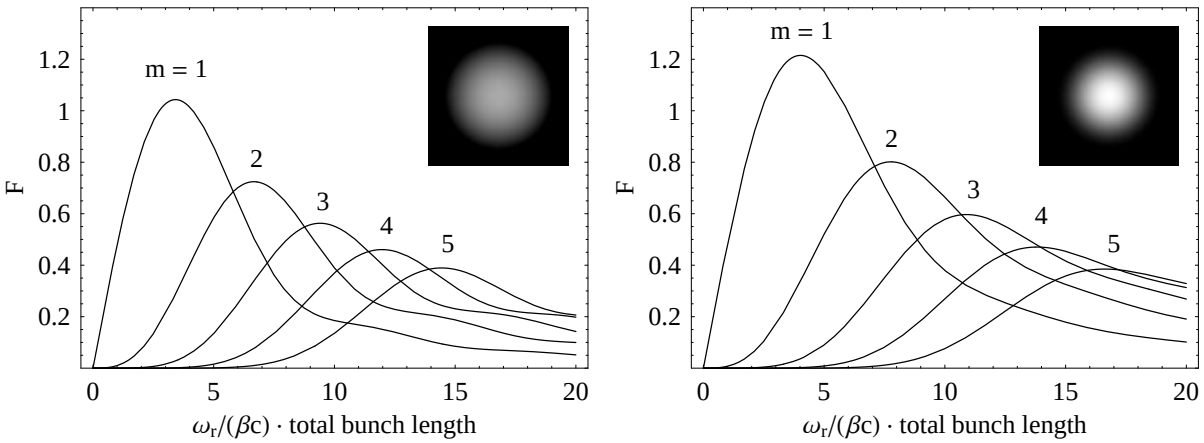

Fig. 6.7: Form factor $F(2\omega_r\hat{\tau})$ for parabolic (left) and quartic (right) radial distribution function $g_0(r)$.

synchrotron tune shift given in [202].

In analogy to the calculations for coasting beam stability a simple stability criterion based on circles in the complex stability diagram can be given from the analysis of the dispersion integral in Eq. (6.26). Landau damping is preserved as long as [202]

$$\frac{1}{\tau} < \frac{\sqrt{m}}{4}\Delta\omega\,, \tag{6.28}$$

and the excited mode of coupled bunch oscillations remains stable. This means for dipole oscillations that the tune spread in synchrotron frequency should be four times wider than the tune shift due to the narrow band resonance.

For a first estimation of longitudinal stability considering the most sensitive mode, the coupling function $D(\alpha\tau_{\rm sep})$ can be replaced by its maximum value as illustrated in Fig. 6.8. Clearly, the coupling function becomes small for driving impedances having small field decay

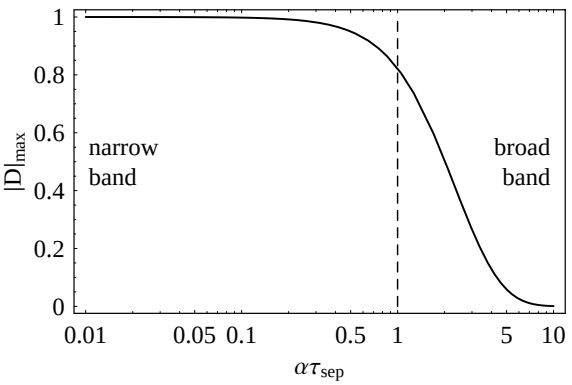

Fig. 6.8: Maximum of the coupling function versus $\alpha\tau_{\rm sep} = \pi\omega_r/(QM\omega_0)$. The number of equally distributed bunches is defined by M.

durations compared to the bunch frequency. Consequently, a preceding bunch has almost no

influence on the subsequent particles. However, for resonators with a large quality factor, as it is mostly the case for higher order mode resonances of RF cavities or parasitic resonance in metallic objects within the accelerator like pumping slots, the coupling function $D(\alpha\tau_{\mathrm{sep}})$ can be approximated to unity.

Following the stability criterion imposed by Landau damping from Eq. (6.28), the maximum tolerable narrow band impedance is derived considering that the growth rate is defined as the inverse imaginary frequency shift (see Sec. 6.1.2). Landau damping is thus preserved as long as the shunt impedance of the driving resonance fulfills the relation

$$R_s \lesssim \sqrt{m}\frac{U_0\cos\phi_0\omega_0}{2I_0}\frac{\hat{\tau}h}{M}\frac{\Delta\omega_s}{\omega_s}\Bigg/\left[D\left(\frac{\pi\omega_r}{QM\omega_0}\right)F(2\omega_r\hat{\tau})\right]\,, \tag{6.29}$$

where $I = NMe\omega_0/(2\pi)$ denotes the total beam current, and where M equidistant bunches are assumed. The total bunch length is given by $2\beta c\hat{\tau}$. The azimuthal dipole mode $m = 1$ is most prone to a coupled bunch instability due to a narrow band excitation as the tolerable threshold impedance increases proportionally to $\sqrt{m}$, and also the maximum height of the bunch form factor $F_m(2\omega_r\hat{\tau})$ as shown in Fig. 6.7 decreases with the mode number.

6.3.4 Broad band impedance

In the preceding section, the narrow band resistive impedance driving the coupled bunch instability is assumed to be the only impedance present in the accelerator. However, in real machines a so-called broad band impedance, which is in fact the contribution of all components, like bellows, monitors or kicker magnets seen by the beam, is modeled as broad band resonance. This broad band resonator directly has a negligible effect on the coupled bunch instabilities, as the fields in this virtual resonator decay much faster than the bunch spacing (see Fig. 6.8). However, it contributes to the synchrotron tune shifts, displacing them in such a way that Landau damping can be lost for coupled bunch modes which would be well damped according to Eq. (6.28) neglecting the broad band impedance.

Following the analysis in [205, 206], the absolute tune shift due to the longitudinal broad band impedance can be written as

$$\Delta\omega = -i\frac{\pi^3 I_0}{3\hat{\tau}^3\omega_0^3 U_0\cos\phi_0}\frac{1}{Mh}\frac{m\omega_s}{m+1}\underbrace{\sum_{p=-\infty}^{\infty}\frac{Z(p)}{p}h_{\mathrm{mm}}(p)\Bigg/\sum_{p=-\infty}^{\infty}h_{\mathrm{mm}}(p)}_{(Z_\parallel/n)_{\mathrm{eff}}}\,, \tag{6.30}$$

where the coefficients $h_{\mathrm{mm}}(p)$ denote the relative spectral power of the bunches at the frequency $p\omega_0$. It is convenient to define an effective longitudinal impedance $(Z_\parallel/n)_{\mathrm{eff}}$ including the spectral distribution [209]. Landau damping for the m-th mode is preserved as long as

$$\frac{1}{\tau} = -\mathrm{Im}\{\Delta\omega\} < \frac{1}{2}\frac{m}{m+1}\Delta\omega_s\,.$$

It is worth noting that longitudinal coupled bunch modes are driven by the imaginary part of the effective impedance only. The threshold impedance can be derived by inserting Eq. (6.30) into the criterion for Landau damping, namely[2]

$$\left(\frac{\mathrm{Im}\{Z_\parallel\}}{n}\right)_{\mathrm{eff}} \lesssim \frac{3}{2\pi^2}\frac{Mh^3U_0\cos\phi_0}{I_0}\frac{\Delta\omega_s}{\omega_s}\hat{\tau}^3\omega_0^3\,. \tag{6.31}$$

[2] A different derivation of the criterion finally ends up with the same result as Eq. (6.31) for $\pi \simeq 3$ [210].

It should be pointed out that the instability threshold criteria for longitudinal narrow as well as broad band impedances are, due to the formulation of the Landau damping criterion, proportional to the synchrotron frequency spread of the bunch. An artificial increase of the spread normally results in improved bunched beam stability.

6.3.5 Stability of the LHC beam during long and flat bunch scheme

The longitudinal stability of the nominal LHC beam during injection flat-bottom, acceleration and collision mode held by the superconducting RF system operated at 400.8 MHz has been analyzed in detail by several authors [209, 211, 212, 213, 214, 215, 216]. Basically, the stability criteria introduced above have been applied to the relevant beam parameters. However, during the RF manipulation at injection and collision energy, multiple RF harmonics act on the beam simultaneously and the criteria are not strictly valid anymore. They may only give a first estimation of stability as the bunches are held by a single harmonic RF in between the substeps of the batch combination scheme.

The longitudinal stability during the long and flat bunch generation scheme presented in Chapter 5, as well as during acceleration of partly combined bunches with a 40.08 MHz RF system, is estimated in this section.

The longitudinal beam parameters during acceleration in the LHC are derived on the basis of the realistic magnetic cycle [217] of the LHC dipole magnets, which is assumed to remain unchanged with respect to the nominal scheme. The magnetic dipole induction corresponding to the particle energy and its first derivative are sketched in Fig. 6.9. The ramp rate is varied

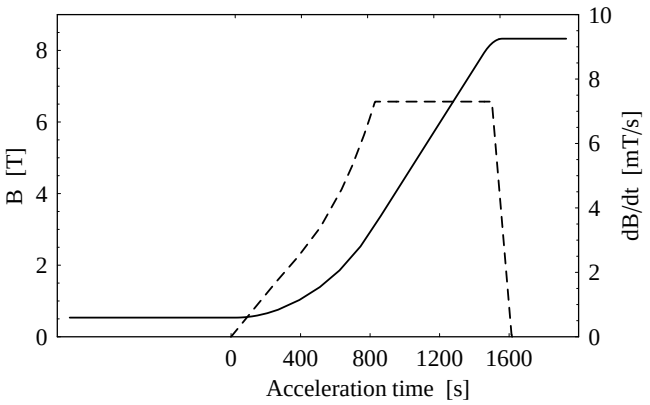

Fig. 6.9: Magnetic cycle of the LHC dipole magnets during acceleration (continuous). The first derivative is shown as a dashed line.

smoothly at the beginning as well as at the end of the acceleration. The maximum ramp rate of 7.3 mT/s is limited by the voltage capabilities of the main power converters. It is important to point out that the average energy gain of the particles during acceleration does not exceed 485 keV/turn.

Fig. 6.10 shows the longitudinal emittance development during the cycle according to Tab. 5.6 as well as the available bucket area. The bucket area during acceleration is presented for a constant RF amplitude of 3 MV throughout the cycle. In fact, $2 \cdot 1.5$ MV would be available in a scheme where 16 bunches are combined to one long and flat bunch. At the injection flat-bottom, a linear increase from about 1 eVs to the emittance of the combined bunches of 12.9 eVs is assumed for simplicity. During this linear increase, the time scale in Fig. 6.10 has no validity, as the combination scheme is performed within one minute, too fast to be visible in the plot. Furthermore, the longitudinal emittance does not increase linearly due to the re-combination of bunches but rather stepwise with each bunch pair merging.

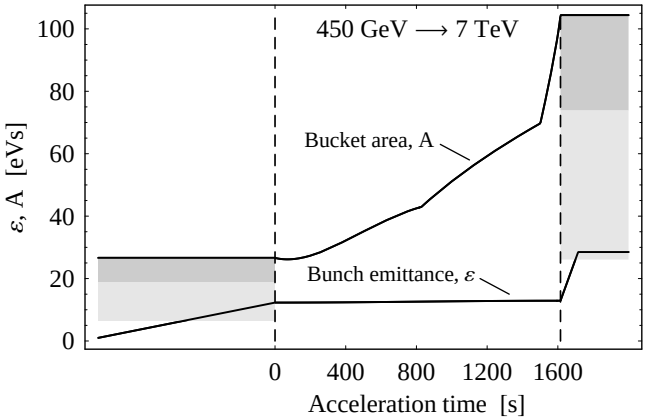

Fig. 6.10: Bucket area (upper curve) and bunch emittance (lower curve) during the LHC acceleration cycle including the combination scheme of 16 initial bunches to a long and flat bunch. The area shaded in dark gray represents possible bucket areas at 40.08 MHz ($h = 3564$) for an RF amplitude between 1.5 and 3 MV. The light gray shaded area below shows the bucket area for 1.5 MV RF voltage in the frequency range from 40.08 to 80.16 MHz that means during the combination RF gymnastics (see also Fig. 5.10).

The qualitative behaviour of bucket area and beam emittance of the second long and flat bunch option combining 32 bunches is equivalent to the graphs shown in Fig. 6.10. The quadrupled RF voltage of 2·6 MV results in twice the bucket area, and the longitudinal beam emittance is assumed to grow to some 26 eVs; twice the bunch emittance of the 16 bunch scheme due to the further bunch merging at flat-bottom. At collision energy one also finally ends up with twice the bunch emittance. It is however worth mentioning that the filling factor, the ratio between bunch emittance and bucket area, remains constant for the 16 and the 32 bunch combination option.

Tolerable narrow band impedance

For a worst-case estimation of the tolerable resonator impedances to preserve Landau damping of coupled bunches bunch modes in the LHC, the form factors in Eq. (6.29) can be substituted by their maximum values: according to Figs. 6.8 and 6.7 the coupling function $D(\pi\omega_r/[QM\omega_0])$ is set to unity and the form factor $F(2\omega_r\hat{\tau})$ is approximated to 1.05 for the dipole mode $m = 1$.

Evaluating Eq. (6.29) according to these simplifications, and with respect to the set of beam parameters introduced above, results in the development of the impedance threshold during the LHC cycle as plotted in Fig. 6.11. Even though the bunch intensity was assumed to be only

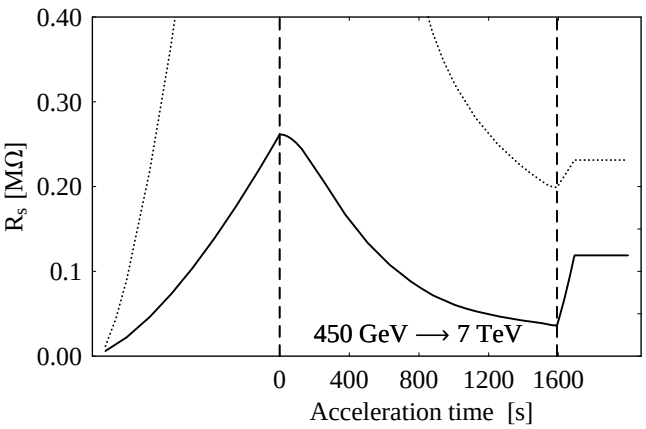

Fig. 6.11: Worst case estimation of the tolerable narrow band impedance along the LHC cycle for a constant RF amplitude of 3 MV at 40.08 MHz (16 bunch scheme, continuous) and $4 \cdot 3$ MV (32 bunch scheme, dotted). The initial bunch intensity is assumed to be nominal in both cases: $1.15 \cdot 10^{11}$ ppb. The stability criteria can be only applied rigorously during acceleration, as multiple harmonic RF systems act on the beam otherwise.

$1.15 \cdot 10^{11}$ ppb, the minimum threshold impedance is more than an order of magnitude below the threshold for operation with the 400.8 MHz RF system [212]. In fact, two problematic regions can be determined: firstly, during injection, when the bunches with a small emittance are injected to the huge buckets at 40.08 MHz. Secondly, when approaching the collision energy

due to the energy dependence of the threshold impedance. A potential cure for the former is proposed in Sec. 6.3.6. Analyzing the scaling of the threshold impedance indicates the main reason for the severe stability limitations of the beam held by a 40.08 MHz RF system. For energies well above transition, so that the phase slip factor η remains constant and for ultra-relativistic beams, it scales according to

$$R_s \propto \frac{\varepsilon_l^{3/2} h^{9/4} U_0^{1/4}}{E^{3/4}} \propto U_0 \left(\frac{\varepsilon_l}{A}\right)^2 ,$$

where ε_l/A denotes the bucket filling factor. Consequently the bunches are prone to become unstable if the buckets are sparsely filled. This is the case for the tiny bunches at injection and at the end of the acceleration, when the bucket area increases proportional to $\sqrt{E}$ times the area reduction factor due to the non-zero synchronous phase (see 2.2.5). Furthermore, the threshold scales as $h^{9/4}U^{1/4}$ so that higher harmonics of the revolution frequency are preferable to hold and accelerate low longitudinal emittance bunches.

Tolerable broad band impedance

A similar analysis can be performed to estimate the threshold of the longitudinal broad band impedance as derived in Eq. (6.31). Fig. 6.12 shows this threshold $(\mathrm{Im}\{Z_\parallel\}/n)_{\mathrm{eff}}$ along the acceleration cycle. The graph looks qualitatively similar to the narrow band impedance

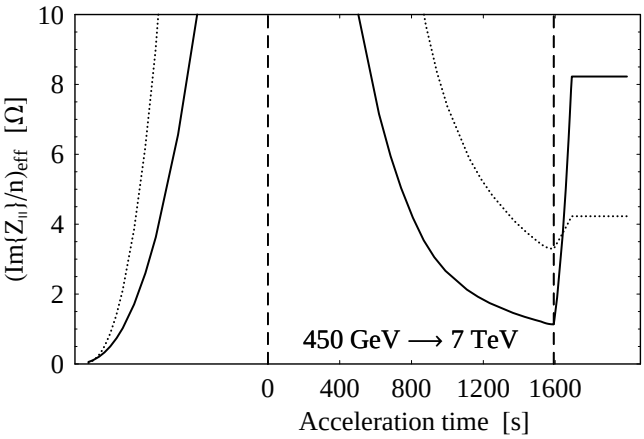

Fig. 6.12: Worst case estimation of the tolerable broad band impedance along the LHC cycle for a constant RF amplitude of 3 MV at 40.08 MHz (16 bunch scheme, continuous) and $4 \cdot 3$ MV (32 bunch scheme, dotted). The bunch intensity is assumed to be nominal.

limitation as illustrated in Fig. 6.11. The problematic phases can again be identified during injection and at the end of the injection cycle. The former region during injection would impose a severe limitation of $(\mathrm{Im}\{Z_\parallel\}/n)_{\mathrm{eff}} \simeq 0.0058\,\Omega$ for the nominal bunch intensity to the tolerable broad band impedance so that bunches would certainly become unstable without counter measures. As soon as the longitudinal emittance increases during the combination procedure, the threshold stays well above the estimated broad band impedance of $0.076\,\Omega$ in the LHC. The scaling of the threshold impedance can be written as

$$\left(\frac{\mathrm{Im}\{Z_\parallel\}}{n}\right)_{\mathrm{eff}} \propto \frac{\varepsilon_l^{5/2} h^{7/4}}{E^{5/4} U_0^{1/4}} \propto \frac{U_0}{h^2} \left(\frac{\varepsilon_l}{A}\right)^{5/2} ,$$

wherein the strong dependence on the bucket filling factor becomes apparent. Furthermore, the threshold decreases rapidly with growing beam energy.

The reduced threshold is partly attributed to the small synchrotron frequency spread of low emittance bunches in large RF buckets. Applying means to increase the synchrotron frequency

spread avoiding unreasonable blow-up, the longitudinal emittance improves the stability threshold for broad band as well as for narrow band impedances directly proportionally (see Eqs. 6.29 and 6.31). This counter measure is discussed in the subsequent section.

The installation of an additional RF system to capture and hold the beam during the filling procedure of the LHC rings could be envisaged as a second counter measure; e.g. a capture RF system operated at 200.4 MHz in the LHC has already been considered and designed [218] up to the construction of the required normal conducting cavities, but has been finally postponed [219, 220]. This system would be potentially available for the upgrade. Filling the two LHC rings by injecting into 200.4 MHz bucket would provide stable beams until the hand-over to the 40.08 MHz RF system. The bunch combination scheme to generate long and flat bunches could commence immediately and the sojourn time of the small emittance bunches in the large buckets could be reduced to the order of a few seconds. This might be sufficient if the instability cannot grow fast enough during this period.

6.3.6 Increase of the synchrotron frequency spread

Both narrow band and broad threshold impedances for longitudinal bunched beam stability are directly proportional to the relative spread of the synchrotron frequencies within the bunch. In the case of bunches in stationary buckets (see Eq. 2.43), the relative synchrotron frequency spread in the single harmonic RF system is expressed in terms of the longitudinal emittance ϵ_l as

$$\frac{\Delta\omega_s}{\omega_s} = \frac{1}{16}\sqrt{\frac{2|\eta|\omega_0^2 h^3}{\pi E\beta^2 e U_0}} \cdot \varepsilon_l \,, \tag{6.32}$$

where the emittance is given in units of $\mathrm{eV}\cdot s$. In fact, decreasing the RF harmonic by one order of magnitude from $h = 35640$ to 3564, as proposed for the long and flat bunch generation scheme, and decreasing the RF voltage by a factor of approximately another order of magnitude, reduces the synchrotron frequency spread by a factor of ten. This results in an unstable beam during the generation of long and flat bunches. Inserting the stationary bucket area into Eq. (6.32) reduces it to $\Delta\omega_s/\omega_s = 1/\sqrt{\pi}\cdot\varepsilon_l/A_{\mathrm{eVs}}$ so that the spread is actually proportional to the relative filling factor of the bucket. Consequently, the synchrotron frequency spread of bunches in 40.08 MHz buckets is lowest during the injection of the small bunches from the SPS, where the bucket area is large compared to the tiny bunch emittance in the range of 1 eVs. After the combination of several of these bunches, the situation becomes less critical. Adding some higher harmonic RF amplitude is a well known technique to increase the synchrotron frequency spread of a bunch [168, 169], which shall be analyzed in what follows.

Synchrotron frequency spread including a higher harmonic RF system

For an arbitrary RF amplitude function, the synchrotron frequency of a particle oscillating on a closed trajectory can be written in integral form according to Eq. (2.41), and analytic approximations for a stationary as well as for an accelerating harmonic bucket are given in Sec. 2.2.6 and App. D.

The influence of increasing the synchrotron frequency spread of the low emittance bunches to the large RF buckets at 40.08 MHz can be analyzed numerically. The following assumptions for the higher harmonic RF system have been made: firstly, the synchrotron frequency spread of a 1 eVs bunch should be increased by at least one order of magnitude. Secondly, the higher harmonic RF systems should be compatible with the RF manipulations so that it can stay active also during the first combination steps of the long and flat bunch generation procedure. This

implies that the increase in synchrotron frequency must be sufficient for any phase relation between main RF focusing. The longitudinal emittance dilution due to the additional RF system should be below 25 % to keep the degradation of the longitudinal beam quality within reasonable limits.

The frequency of the higher harmonic has be chosen so that it results in a significant slope variation of the effective RF focusing along the bunch. Considering that the initial bunch length in the LHC is of the order of 4 ns, the use of 200.4 MHz and 400.8 MHz is investigated. The relative synchrotron frequency versus single particle emittance is plotted in Figs. 6.13 and 6.14. It is interesting to note that the influence on particles with a certain emittance is compensated

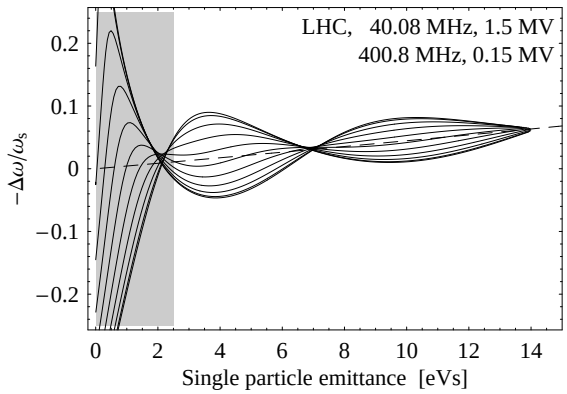

Fig. 6.13: Relative synchrotron frequency deviation versus single particle emittance for a combination of 40.08 and 400.8 MHz RF amplitude in the LHC at injection flat-bottom. The ensemble of continuous curves is calculated for phase relations between the two RF systems, varying from 0 to π in steps of $\pi/10$. The dashed line shows the unperturbed relative synchrotron frequency of the 40.08 MHz RF system alone.

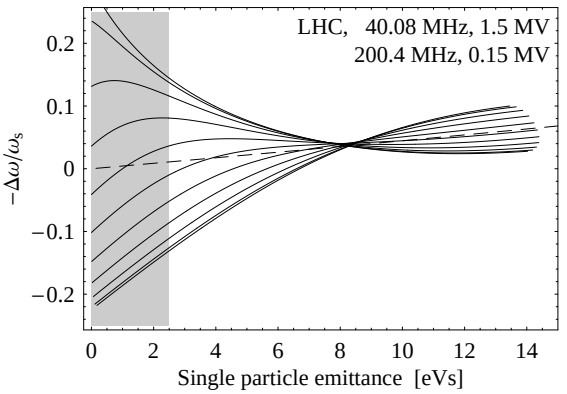

Fig. 6.14: Same representation as in Fig. 6.13 but for the combination of 40.08 and 200.4 MHz. The relative spread for bunches with an emittance smaller than 1.5 eVs is significantly reduced compared to the higher harmonic RF system operated at twice 200.4 MHz. The gray shaded area represents the nominal bunch emittance.

so that they oscillate with the single harmonic synchrotron frequency, unaffected by the phase of the higher harmonic RF.

As shown in Fig. 6.13, only some 150 kV at 400.8 MHz would suffice to restore a relative synchrotron frequency spread comparable to $\Delta\omega_s/\omega_s = 0.1$ of the nominal LHC bunch. However, the large frequency ratio between the main and the higher harmonic system is mandatory to obtain large synchrotron frequency spreads within small bunches, independent from the phase relationship of the two RF amplitudes (see Fig. 6.13). It is important to point out that the superconducting 400.8 MHz RF installations cannot be employed directly as higher harmonic RF system. Due to their large shunt impedance, the beam induces too much voltage in the eight cavities to control the RF amplitude down the level of 150 kV (see Sec. 6.5).

Emittance blow-up

Following the analysis in the preceding section, the synchrotron frequency spread of small bunches in large buckets can be increased significantly by adding some higher harmonic RF voltage to the main bucket. However, bunches with in elliptic boundary injected to such a double harmonic RF system are not perfectly matched anymore, resulting in emittance blow-up depending on the frequency and the amplitude of the higher harmonic system. After some initial emittance dilution, the bunch matches itself to the perturbed trajectories of the bunch so

that virtually no further emittance increase is expected after a few periods of the synchrotron frequency.

The emittance blow-up of a bunch held in a 40.08 MHz bucket caused by some RF voltage at 400.8 MHz is presented in Fig. 6.15. It can be obtained by tracking a parabolic bunch with

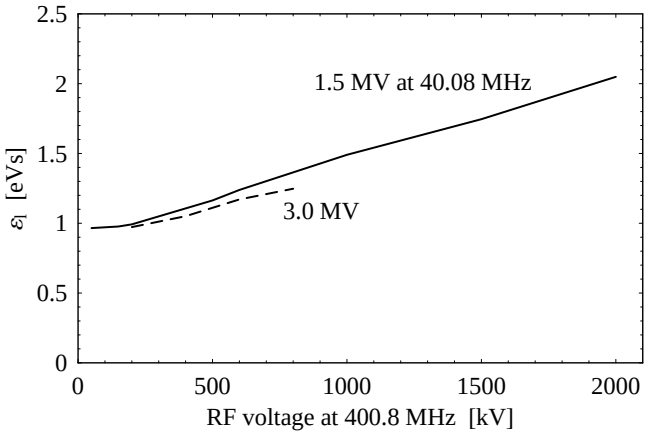

Fig. 6.15: Blow-up after full dilution of a parabolic bunch injected into a double harmonic RF system 40.08/400.8 MHz, where the higher harmonic RF amplitude increases the spread of synchrotron frequencies within the bunch. The main RF voltage is set to 1.5 and 3 MV.

an initial elliptic contour under the influence of the two RF systems. The emittance dilution increases proportionally to voltage at 400.8 MHz and up to some 0.5 MV it remains well below 25 %. Under these conditions, it is therefore justified to assume an increase of the synchrotron frequency spread by one order of magnitude for the longitudinal stabilization at the cost of some 25 % in emittance (see Tab. 5.6).

Non-harmonic RF system

Up to now the ratio of fundamental and higher harmonic RF system has been assumed to be whole numbered so that both contributions to the RF buckets are symmetric to the reference energy. Setting the higher harmonic system to a non-integer harmonic shifts the energy of the sub-buckets with respect to the average beam energy in the main RF buckets. In fact, the frequency offset causes a phase slippage of main and sub-bucket, leading to a continuous variation of the local synchrotron frequency within the bunch.

However, as can be seen in Fig. 6.16, the application of such a scheme can introduce parametric resonances due to the phase slippage of the higher harmonic RF system, which moves in the same direction as individual particles in spheres of influence of the off-energy sub-buckets.

Tracking calculations like the example above show that the development of the effective longitudinal emittance is very sensitive to energy offset and amplitude of the higher harmonic. During batch compression, the RF focusing of the individual bunches varies along the batch so that also the coupling between main and higher harmonic RF system changes continuously. Therefore, such a scheme cannot be applied straightforward in combination with the long and flat bunch generation scheme in the LHC.

6.4 Synchrotron frequency distribution with respect to RF phase stability in long bunch collision mode

The synchrotron frequency distribution during storage of the final long bunches in bucket generated by multiple RF harmonics is of special interest as the bunches are stored in this mode for

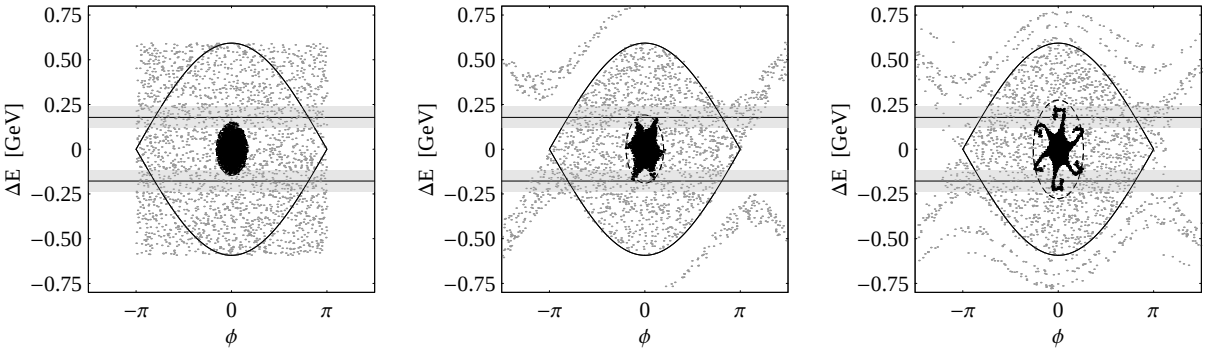

Fig. 6.16: Development of a 1 eVs bunch held by an RF voltage of 1.5 MV at 40.08 MHz under the influence of two additional higher harmonic RF systems at 400.8 MHz. The higher harmonic RF systems have an amplitude of some 150 kV. They are operated symmetrically slightly below and above the integer harmonic. Their center energy is indicated by the continuous horizontal lines, and their bucket height is illustrated as gray stripes. The gray shaded macro-particles are tracked for reference only. The dashed emittance ellipse contains 99 % of the particles. The phase space on the left shows the initial phase space while center and right plot illustrate the bunch after 0.64 and 2.1 periods of the synchrotron frequency.

several hours. Studies in the SPS with bunches held by a double harmonic RF bucket generated by the 200 and 800 MHz have shown that the phase stability between both RF systems must be kept within tight tolerances if the bunches should be stretched [168].

The synchrotron frequency distribution for the final long bunches held by two, three and four multiples of 40.08 MHz is illustrated in Fig. 6.17. The synchrotron frequencies of particles with

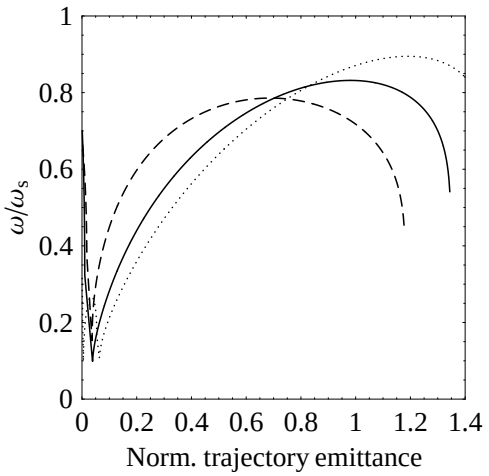

Fig. 6.17: Relative synchrotron frequency versus single particle emittance normalized to bucket area of the single harmonic bucket for the voltage ratios given in Tab. 4.3. The distribution for three RF harmonics is represented by the continuous line while dashed and dotted lines show the case for two and four RF harmonics. The phase relation between the different harmonics is assumed to be ideal.

large oscillation amplitudes are very similar to those of an ideal barrier bucket (see Fig. 2.12, graph for $\phi_0 = 0$). However, few particles in the bunch center may be captured in the sub-buckets so that their synchrotron frequency increases. This effect causes the increase of the synchrotron frequency distribution for small single particle emittances.

The phase relation between different RF systems is not perfectly defined in a real accelerator environment. Transient beam loading due to gaps in the bunch pattern of the LHC may cause small phase variations from bucket to bucket. The effect of such phase variations on the synchrotron frequency distribution for a bunch held by three RF harmonics is presented in Figs. 6.18 and 6.19. The lowest curves are consistent with the continuous line shown

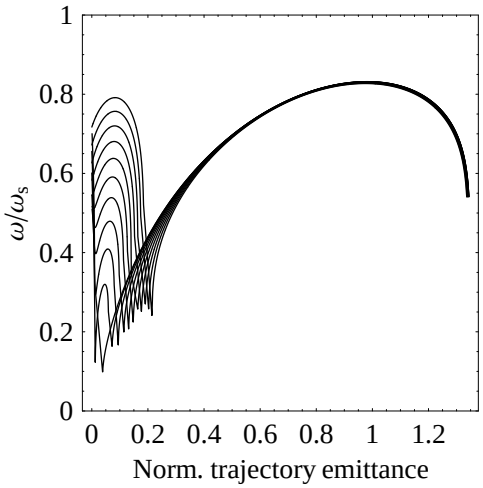

Fig. 6.18: Ensemble of frequency distributions versus single particle emittance normalized to the single harmonic bucket area in a three harmonic RF system according to Tab. 4.3. The phase of the two RF systems at $h = 3564$ and $h = 10692$ is kept constant, while the phase of the harmonic $h = 7128$ is varied up to 20^0 from its ideal value in steps of 2^0.

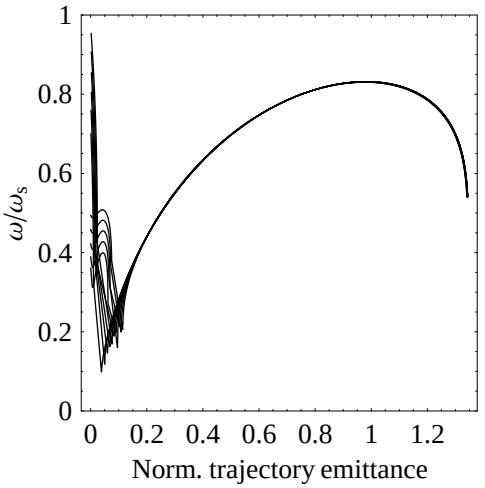

Fig. 6.19: Same representation as in Fig. 6.18 but for the variation of the third harmonic at $h = 10692$ while the phase relation between $h = 3564$ and $h = 7128$ is kept constant. The distributions are calculated for the phase of largest bucket height. The phase units are defined with respect to the RF harmonic whose phase is varied.

in Fig. 6.17. For the phase shift under consideration the synchrotron frequency distribution changes significantly for particles in the center of the bunch. For particles in the outer regions with a normalized single particle emittance above 0.2, the phase deviations between the different RF harmonics are not critical in this case.

6.5 Beam loading

As discussed above, the bunches in an accelerator can communicate via narrow band impedances, which may cause excitation of coupled bunch modes. Not only the succeeding bunches suffer from the field induced by particles before them, but also the element representing the impedance, mostly a cavity, is obviously influenced and this phenomenon is called beam loading. As the RF cavities couple the beam to an RF power source, their impedance is intentionally made as large as possible and they are thus most prone to beam induced voltage.

In fact, there are two resulting effects: firstly, the cavity is detuned by a long chain of equal bunches and secondly, transient RF voltages may be induced by an asymmetric bunch pattern including gaps or intensity variations from bunch to bunch. After comparing the effect of stationary beam loading in the LHC for the 400.8 MHz and a 40.08 MHz RF system under basic assumptions, calculations on transient beam loading during generation and storage of long and flat bunches in the LHC shall be presented. It is shown that the transient voltages in the superconducting 400.8 MHz cavities cannot be suppressed effectively enough so that the RF manipulation to generate long and flat bunches would be severely deteriorated. Consequently, the superconducting RF system must be removed for the LHC operation with long bunches.

6.5.1 Stationary beam loading: steady state

Neglecting transients due to gaps in the bunch pattern or intensity variations of the individual bunches, a simple RF system, consisting of an RF amplifier as power generator and the cavity to couple the RF power to the beam (Fig. 6.20), can be represented as sketched in Fig. 6.21 by a circuit of lumped elements to model its behaviour. As the large stored energy of a high

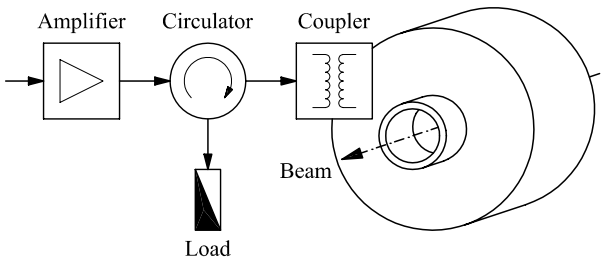

Fig. 6.20: Simple RF system consisting of an RF amplifier protected by a circulator and an RF cavity. The coupler matches the high impedance of the cavity to the low impedance of the amplifier.

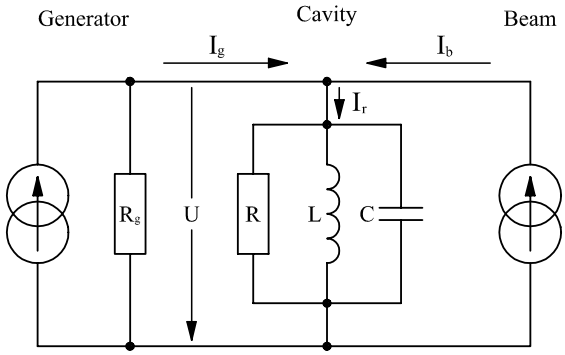

Fig. 6.21: The right part of Fig. 6.20 sketched as a lumped element circuit. The coupler is already included in the generator impedance R_g [221].

intensity beam can create enormous instantaneous RF power compared to the capabilities of the power amplifier, it is approximated as a pure current generator. The cavity is replaced by its parallel resonant circuit and the power generator by a current source having a finite internal resistance. It is important to point out that its internal resistance is already converted by the transformation ratio of the coupling system in the lumped element circuit in Fig. 6.21 .

To optimize the effective generator power needed to drive the beam, the generator current must be decomposed into a forward component I_g^+, flowing from the generator to the cavity, and a reflected component I_g^- in the opposite direction. Minimizing the reflected power $P_g^- = 1/2R|I_g^-|$ back to generator assures that most of its power drives the combination of cavity and beam.

In the following analysis all voltages and currents are assumed to oscillate with the excitation frequency ω defined by the generator. According to Fig. 6.21 the relation between currents is expressed by

$$I_g + I_b - I_r = 0 \qquad \text{or} \qquad I_g^+ - I_g^- + I_b - I_r = 0\,.$$

Application of Ohm's law to the generator as well as to the resonant circuit, assuming that its resonant frequency is given by $\omega_0^2 = 1/(LC)$ and the loss resistor is large so that the resonant circuit has a small bandwidth compared to ω_0, the current relation can be written as [222]

$$2I_g^+ + I_b = \left[\left(\frac{1}{R} + \frac{1}{R_g}\right) + 2i\Delta\omega\, C\right] U\,, \tag{6.33}$$

where $\Delta\omega = \omega - \omega_0$ denotes the frequency difference between generator and resonant frequency of the lumped element resonator. The lumped elements L and C still have to be exchanged by their equivalent cavity parameters, the resonant frequency ω_0 and the so-called R/Q, a geometrical parameter of the cavity, namely

$$C = \frac{1}{\omega_0(R/Q)} \qquad \text{and} \qquad L = \frac{(R/Q)}{\omega_0}\,.$$

Eq. (6.33) is thus transformed to

$$2I_g^+ + I_b = \left[\left(\frac{1}{Q_0} + \frac{1}{Q_g}\right) + 2i\frac{\Delta\omega}{\omega_0}\right]\frac{U}{(R/Q)}\,, \tag{6.34}$$

where Q_0 and Q_g are defined to give the resonator shunt impedance R and the internal resistance of the generator R_g respectively, when multiplied by the geometry parameter R/Q.

Keeping in mind that all current and voltage vectors rotate in the complex plane, the current phase ψ is chosen so that the center phase of the bunch coincides with a real voltage at the synchronous phase ϕ_0:

$$Ue^{i\omega t} \quad \longleftrightarrow \quad I_b e^{i\omega t}e^{i\psi} \tag{6.35}$$

$$Ue^{i\omega t}\sin\phi_0 = Ue^{i\omega t}(\cos\psi - i\sin\psi) \quad \longleftrightarrow \quad I_b e^{i\omega t}\,. \tag{6.36}$$

The current phase is determined by the relation $\sin\phi_0 = \cos\psi$ so that the current can be written as $I_b = |I_b|(\sin\phi_0 + i\cos\phi_0)$. It is worth noting that the synchronous phase at constant energy is defined as $\phi_0 = 0$ below and $\phi_0 = \pi$ above transition. Additionally, I_b denotes the Fourier component of the beam current at the RF frequency as this spectral line represents the only component which can excite the narrow band impedance. Its absolute value may be replaced by $2I_0 f_b$, where the form factor f_b becomes unity for infinitely short bunches and decreases with increasing bunch length.

Finally, the forward and reflected generator currents are expressed by [223]

$$I_g^+ = \left\{\left[\frac{1}{Q_g} + \frac{1}{Q_0}\right]\frac{U}{2(R/Q)} - I_0 f_b\sin\phi_0\right\} + i\left[\frac{\Delta\omega}{\omega_0}\frac{U}{(R/Q)} - I_0 f_b\cos\phi_0\right]\,, \tag{6.37}$$

$$I_g^- = \left\{\left[\frac{1}{Q_g} - \frac{1}{Q_0}\right]\frac{U}{2(R/Q)} + I_0 f_b\sin\phi_0\right\} - i\left[\frac{\Delta\omega}{\omega_0}\frac{U}{(R/Q)} - I_0 f_b\cos\phi_0\right]\,, \tag{6.38}$$

and the RF power reflected back to the generator is now derivated easily according to $P_g^- = 1/2(R/Q)Q_g|I_r^-|^2$. In fact, there are two parameters to reduce the reflected power: the detuning $\Delta\omega$ of the cavity and the external load Q_g of the generator. The former acts on the imaginary part of the generator current and the latter on its real one so that the conditions for minimum RF power requirements can be written as

$$\frac{\Delta\omega}{\omega} = -\frac{I_0 f_b\cos\phi_0(R/Q)}{U} \qquad \text{and} \qquad \frac{1}{Q_g} = \frac{2(R/Q)I_0 f_b\sin\phi_0}{U} - \frac{1}{Q_0}\,. \tag{6.39}$$

It is interesting to note that both the optimum detuning as well as the optimum generator Q_g depend on beam current and RF voltage. It is thus desirable to operate the RF system with variable power couplers as foreseen for the superconducting RF system in the LHC [224].

As the superconducting resonators have an unloaded Q_0 in the order of 10^9 being much larger than the external generator Q_g, the second condition reduces to

$$Q_g = \frac{U}{2(R/Q)I_0 f_b\sin\phi_0}\,.$$

In case of constant particle energy so that the synchronous phase is either 0 or π, the optimum external Q_g should be infinite so that there is negligible coupling between generator and cavity. However, this represents only an idealized solution if no transient beam loading is present because virtually small changes of the RF amplitude in the cavity would take infinitely long.

Therefore, superconducting cavities are generally coupled much stronger so that the power amplifier can act against transient effects within reasonable time.

The situation changes for a normal conducting RF system, operated at 40.08 MHz foreseen for the long and flat bunch scheme in the LHC. At constant beam energy, the cavity must be theoretically coupled critically to the power generator by choosing $Q_0 = Q_g$ so that the generator just compensates the resistive losses in the resonator. However, as in the case of the superconducting RF system, more power must be installed coupled more strongly to compensate for transient effects, whose influence is discussed in the subsequent section.

The steady state beam loading parameters neglecting all gaps in the LHC bunch pattern is summarized in Tab. 6.1 to illustrate their order of magnitude. Even though the superconducting

RF frequency, $\omega/(2\pi)$	[MHz]	400.8	40.08	
RF amplitude, U	[MV]	16	1.5	6
Characteristic impedance, R/Q	[Ω]	$8 \cdot 44.5$	$2 \cdot 5 \cdot 30$	$2 \cdot 20 \cdot 30$
Unloaded quality factor, Q_0		$> 10^9$	$2 \cdot 10^4$	$2 \cdot 10^4$
External quality factor, Q_g		10^5	$2 \cdot 10^4$	
Beam induced voltage per bunch (short bunch limit, $f_b = 1$)	[kV]	-16.5	-1.4	-5.6
Cavity detuning, $\Delta\omega/(2\pi)$	[kHz]	6.6	6	

Tab. 6.1: Comparison of the steady state beam loading parameters of the superconducting 400.8 MHz and a normal conducting 40.08 MHz. Gaps in the bunch train are neglected. The assumptions for the cavity parameters of the RF system at 40.08 MHz, twice 5 or 20 cavities per beam, is based on simple extrapolation of similar RF systems operational the PS [180, 182]. The estimations assume the nominal bunch intensity, but can be scaled proportionally to a higher beam current.

cavities are compared to a completely normal conducting RF system, the detuning by the beam is rather similar as the total quality factor of the former RF system is determined by the external quality factor contributed by power amplifier and coupler.

6.5.2 Transient beam loading

It is shown above that in the absence of transient effects, corresponding to a machine filled by a uniform chain of equal bunches, the generator would just have to compensate losses in the normal conducting RF cavities. As the suggested long and flat bunch scheme is based on batches of 16 or 32 bunches with gaps in between, transient effects cannot be avoided.

A charge passing through an RF cavity induces a certain amount of voltage and thus deposits energy inside the cavity. According to the so-called fundamental theorem of beam loading, it can be proven in general [225] that the deposited energy is given by

$$\Delta W = \frac{1}{2} q U_b \,.$$

Consequently, the charge q experiences half of the RF voltage induced by itself. Due to the finite quality factor of the combination of cavity and power amplifier, the induced energy decays exponentially. For the case of short bunches compared to the RF wavelength, it is justified to replace the cavity by its lumped element capacity (see Sec. 6.5.1) so that the induced amplitude becomes $U_b = R\omega_0 q/Q$.

The simple analysis is not restricted to a single charge passing through the resonator but can be generalized easily to a complete chain of point-like bunches with arbitrary distances in

between the bunches. The resulting RF amplitude is composed of the contribution from the power generator plus the summed up contributions of all bunches having passed the cavity until that instant.

This can be formulated by a tracking like algorithm [177, 226], where the bunches are consecutively moved through the cavity, while calculating the voltage for the subsequent bunch, starting at the passage of the previous one. Additionally, the generator counteracts the induced beam induced voltages. The total voltage at the gap of the RF cavity is derived starting from the real part of

$$U(t) = U_g e^{i\omega t} + \text{const.} \cdot e^{i(\omega-\Delta\omega)t} e^{-(t-t_0)/\tau}\,, \tag{6.40}$$

where $\tau = 2Q/\omega_0$ denotes the characteristic field decay time in the cavity, and the constant represents a parameter defined by the initial condition given by the instantaneous gap voltage U_0 at the previous bunch passage t_0. Replacing the constant in Eq. (6.40) results in the general bunch-to-bunch tracking equation:

$$U(t) = \underbrace{U_0 \left[e^{i(\omega-\Delta\omega)(t-t_0)} e^{-(t-t_0)/\tau} \right]}_{\text{beam and generator}} + \underbrace{U_0 e^{i\omega t} \left[1 - e^{-i\Delta\omega(t-t_0)} e^{-(t-t_0)/\tau} \right]}_{\text{generator}}\,. \tag{6.41}$$

The free parameters, generator voltage U_g, generator frequency ω and cavity detuning $\Delta\omega$, are chosen as input variables including a set of initial conditions for bunch positions and energies.

It is important to point out that the extension of the algorithm to multiple RF system can be performed straightforward: the chain of bunches is tracked sequentially through the ensemble of RF systems.

Some examples of the time variation of the gap voltage $U(t)$ are sketched in Fig. 6.22. The

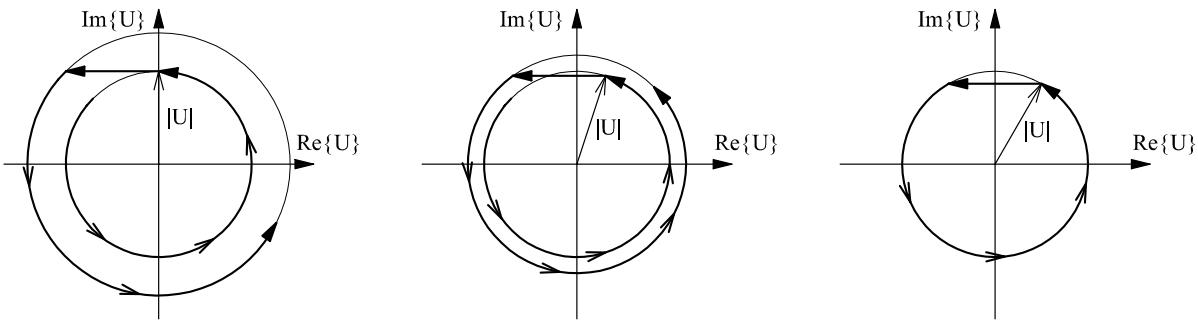

Fig. 6.22: Illustration of the effective voltage vector in the cavity. On the left, the cavity is exactly tuned to the harmonic of the revolution frequency, causing a jump in the absolute RF voltage during each bunch passage [227]. The center diagram represents a partly compensated situation, where the absolute beam induced jump is already reduced. The completely compensated and thus steady state case is shown on the right. The cavity is detuned so that the passing bunch causes a phase jump but the absolute voltage remains constant. Above transition, the unperturbed synchronous phase is located at the positive to negative zero crossing of the U, respectively at $\text{Re}\{U\} = 0$ and $\text{Im}\{U\} = |U|$.

right plot shows a periodic solution, where the beam induced jump of the voltage vector is compensated by a cavity detuning so that the absolute value of the vector remains constant. For small beam induced voltages compared to the contribution of the generator, this result reproduces in fact the steady state solution for beam loading compensation by cavity detuning as introduced by the first relation of Eq. (6.39).

Furthermore it becomes obvious from Fig. 6.22 (right) why small RF amplitudes in order of magnitude of the beam induced voltage can be hardly produced with a reasonable amount of RF power. An enormous detuning is required even in the steady state case, which is mostly outside the tuning range of the cavities. Although the steady state beam-loading can be compensated theoretically, this becomes unfeasible in the presence of beam gaps causing large transients as in the case of the LHC. The maximum tolerable residual voltage at 400.8 MHz during the long and flat bunch generation is limited to some 50 . . . 100 kV, which would lead to a cavity detuning of 6.4 . . . 3.2 MHz to compensate for steady state beam loading, by far out of the tuning range of the superconducting cavities. Furthermore, any beam gap induces huge transients which cannot be compensated. As presently no technique to compensate the transients is available, the 400.8 MHz RF cavities have to be removed or short-circuited for the operation for the creation and storage of long bunches. Transients induced by beam gaps also represent an important issue for the 40.08 MHz alone, however stable periodic solutions can be found for realistic bunch patterns:

An averaged cavity detuning as from Eq. (6.39) can be taken as a starting point for the numerical calculation. Then, the full bunch train is shifted sequentially through the RF system and the influence of the combination between generator and beam induced voltage is applied to the passing bunch according to Eq. (6.41). The average bunch energy is adjusted according to its energy loss or gain while traversing the cavity. Finally, this tracking scheme is repeated multiple times and the bunch positions are memorized for each turn. Actually, the bunches perform synchrotron oscillations around their optimum positions, which can be reconstructed from the synchrotron oscillations seen on the simulated bunch position data.

The optimum bunch phase deviation with respect to its nominal position is shown in Fig. 6.23, for a bunch train having nominal LHC filling pattern (see Sec. 5.1.1) held by the superconducting RF system at 16 MV. The result of the analogous simulation, for the same bunch pattern held by a 1.5 MHz RF system at 40.08 MHz, is found in Fig. 6.24. The param-

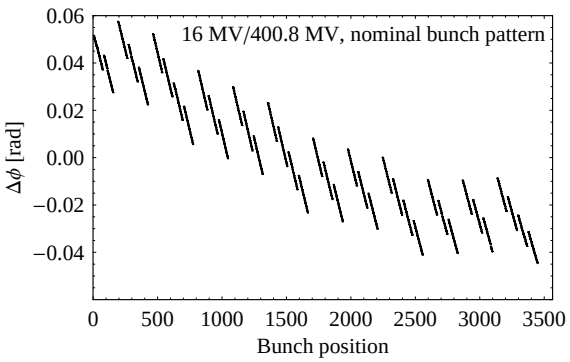

Fig. 6.23: Periodic solution of the steady state phase position for the nominal LHC bunch pattern held by the superconducting RF system with 16 MV. The external quality factor Q_g is assumed to be 10^5.

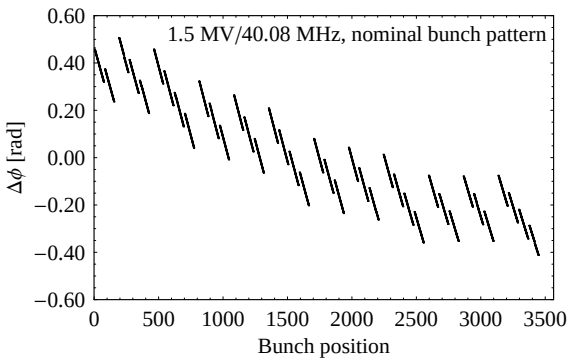

Fig. 6.24: Periodic solution of the steady state phase position for the nominal LHC bunch pattern as in Fig. 6.23 but for a normal conducting 40.08 MHz RF system with 1.5 MV. The phase deviation is given in radians with respect to 400.8 MHz.

eters of the 40.08 MHz system have been set according to Tab. 6.1. The operation of the LHC with such an RF system results in almost ten times larger phase deviations of the bunches. If this causes too large jitter of the collision point of a pair of bunches, it could be compensated by stronger coupling of the generator to the cavity at the expense of an increase in instantaneous RF power [227].

The corresponding RF amplitude is, for the 400.8 as well as for the 40.08 MHz system, nearly constant and the residual variation together with the bunch pattern is plotted in Figs. 6.25 and 6.26. It should be pointed out that both RF systems show a very similar time dependence

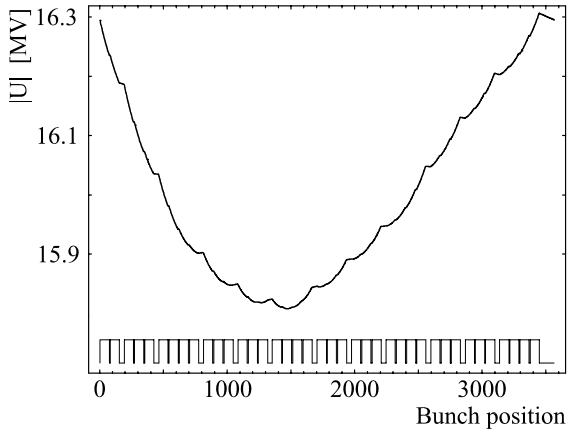

Fig. 6.25: Residual RF amplitude variation at 400.8 MHz along one turn due to beam loading according to the bunch position deviations shown in Fig. 6.23.

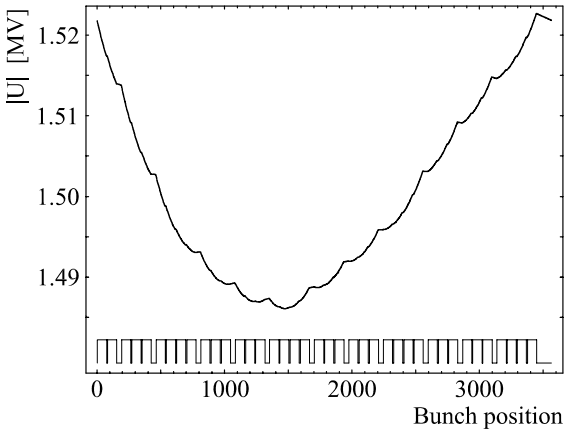

Fig. 6.26: Same representation as in Fig. 6.25 but for the normal conducting RF system at 40.08 MHz. The beam dump kicker gap is located from bunch position 3446 to 3564.

concerning beam loading. This can be attributed to the fact that both RF systems have an almost identical filling time of some 50 μs. This time constant is of the order of half the revolution time which explains in fact the periodicity of the RF voltage illustrated in Figs. 6.25 and 6.26.

The analysis of transient beam loading effects therefore shows that the behaviour of an LHC operated with normal conducting 40.08 MHz cavities would be similar to the nominal situation. The requirements for beam loading compensation are comparable and no special problems are expected. However, the operation of the superconducting 400.8 MHz during the RF manipulations to create and store long and flat bunches causes intolerable transient RF voltages, which cannot be compensated with present technology, and the superconducting cavities will have to be removed from the ring. Although it is clear that the cavities will be of coaxial type, no detailed design is available so far and the beam loading parameters certainly have to be revised according to more elaborated cavity parameters.

Chapter 7

Summary and Outlook

The choice of the longitudinal beam parameters, such as bunch length or bunch form, has a considerable influence on the final performance of the high energy proton-proton collider LHC. Various upgrade options to improve the luminosity of the LHC have been considered so far. This study presents an analysis of the possibilities to operate the collider with long and flat bunches.

After an introduction of the fundamentals of longitudinal beam dynamics, a survey of the large variety of longitudinal beam manipulations is made. This overview includes classical, well established beam manipulation techniques, but also RF gymnastics with barrier buckets, short RF pulses commonly generated in broadband cavities. The conditions for longitudinal matching at beam transfer between two synchrotrons are described.

In the following section, the possibilities of luminosity improvements using long and flat bunches are explored, with respect to the strong beam-beam limit. Three different options are compared. Firstly, short rectangular bunches with a length comparable to nominal LHC bunches intersecting at large crossing angles of some 5 mrad could partially remove the beam-beam limitation far away from any realistic average beam current. However, for a given number of protons per bunch, a large crossing angle is associated with a significant reduction of the luminosity so that the intensity already has to be increased by a large factor to simply recover the nominal and ultimate luminosities. Secondly, long and flat bunches of intermediate length, about an order of magnitude longer than nominal bunches and containing either 16 or 32 nearly nominal bunches each, could push the beam-beam limit by fractional tune spread compensation in the crossing plane. These bunches are held in collision mode by multiples of 40.08 MHz to reproduce a flat line density. Finally, the scenario of operating the LHC with a single superbunch per beam, held by barrier buckets, is investigated for comparison.

The result of these comparisons is that, in terms of beam dynamics, the scheme with bunches of intermediate length has quite competitive performance to the single superbunch case. Additionally, the technical implementation of the former scenario is much more realistic, because of the numerous inherent disadvantages of superbunches, like the need for synchrotron radiation compensation and for broadband cavities.

Based on the final long and flat bunch parameters, a realistic RF manipulation to create them, starting from a nearly nominal bunch pattern, is described and optimized in detail. This manipulation consists of a series of batch compression and bunch pair merging RF gymnastics. Both of these basic ingredients have been amply demonstrated in a real accelerator environment.

Finally, the influence of longitudinal collective effects and beam loading is analyzed. The bunches held by the 40.08 MHz RF system are prone to coupled bunch instabilities, especially

during the period of LHC filling, as their longitudinal emittance is much smaller than the bucket area. The tolerable impedance limitations are at least an order of magnitude more tight than for the storage of the nominal LHC beam. Two cures can be envisaged to suppress longitudinal instabilities: firstly, Landau damping can be improved by superimposing some RF amplitude at a higher harmonic and thus increasing the synchrotron frequency spread within the bunches. The induced emittance growth by such an additional RF system could be kept within reasonable limits. Secondly, a longitudinal coupled bunch feedback, as has been initially considered for the LHC [228, 229], could stabilize the beam. This feedback would have to cover a bandwidth of some 20 MHz since the bunch frequency remains 40.08 MHz during injection.

It is important to point out that the challenge for the detectors of the physics experiments is as large as for the accelerator. However, from the point of view of the experiments, the different scenarios do not have equal interest, even if they can theoretically deliver the same luminosity. Extrapolating from today's detector and data handling technologies, more numerous bunches are clearly preferable in the framework of a first stage LHC upgrade.

In any case, this report shows that long and flat bunches offer potentially valuable solutions for upgrading the LHC luminosity and proposes a challenging but feasible method for creating them.